Supporting Information

A general electrochemical CO_2 fixation to aromatic carboxylic acids *via* the $CO_2^{\bullet-}$ intermediate using a non-transition metal electrode

Baijing Wu[1], Xiaoxue Luo[1], Hongliang Fan[1], Minhua Shao[2,3], Cunpu Li[1*] & Zidong Wei[1]*

[1]State Key Laboratory of Advanced Chemical Power Sources, School of Chemistry and Chemical Engineering, Chongqing University, Chongqing, 400044, China

[2]Department of Chemical and Biological Engineering, The Hong Kong University of Science and Technology, Clear Water Bay, Kowloon, Hong Kong

[3]Guangzhou Key Laboratory of Electrochemical Energy Storage Technologies, Fok Ying Tung Research Institute, The Hong Kong University of Science and Technology, Guangzhou, 511458, China

*Corresponding authors: E-mail: lcp@cqu.edu.cn; zdwei@cqu.edu.cn

Table of Contents

General information

Methods

All reagents were procured from commercial suppliers and used without further purification. The electrochemical synthesis tests were conducted employing a Shanghai Chenhua CHI760E workstation (CH Instruments, Inc. USA). The electrochemistry *in situ* surface-enhanced Raman scattering (SERS) experiment was carried out with a Horiba LabRAM HR Evolution and Labspec software. All Raman spectra were acquired with 785 nm excitation with a spectral range of 100–3200 cm^{-1}. The external standard method was used to quantitatively analyze reactants and products after reaction by high-performance liquid chromatography (HPLC, Shimadzu LC20AD). Nuclear magnetic resonance (NMR) spectra were measured at 400 MHz using an Agilent 400-MR compact NMR system, with DMSO-d_6 serving as the solvent. Chemical shifts (δ) are reported in ppm downfield from tetramethylsilane TMS as an internal standard. X-ray diffraction (XRD) patterns of the samples were recorded on a Rigaku D/max 2200 pc diffractometer, with Cu Kα radiation of wavelength γ = 0.15418 nm, at 40 kV and 40 mA. Scans for 2θ values were recorded at the scan rate of 5 °min^{-1} in the 5–90 °2θ range.

General experimental procedure for electrosynthesis

Electrocatalysis is performed in an undivided cell with aluminum plate (25 mm × 20 mm × 0.80 mm) as anode and graphite (20 mm × 20 mm × 3 mm) as cathode. The Ag/Ag^+ electrode filled with DMF solution prepared using 0.1 mol L^{-1} Bu_4NPF_6 and 0.01 mol L^{-1} $AgNO_3$ is used as a reference electrode. In a 50 mL undivided electrochemical cell equipped with a stirrer, aromatic halides (1 mmol), Bu_4NPF_6 (0.1 mol L^{-1}), and 50 mL DMF were added. After passing CO_2 for half an hour until the solution was saturated, the electrolytic reaction commenced. The electrocatalysis was carried out at a constant potential of −2.5 V (*vs.* Ag/Ag^+) for 10 h at room temperature, with a stirring speed of 700 rpm. CO_2 gas was continuously injected throughout the reaction period. After the reaction completed, the reaction container was opened, and 0.1 mL of the reaction solution was diluted to 1 mL with acetonitrile for HPLC analysis. Subsequently, the reaction mixture was acidified with HCl aqueous (2.0 M) to a pH of approximately 2. The aqueous layer was then extracted with EtOAc (8 × 15 mL), and the combined organic phase was washed with saturated NaCl (4 × 15 mL), dried using anhydrous $MgSO_4$, filtered, and concentrated under vacuum. The crude product underwent purification by column chromatography to furnish the desired product.

Characterization of Products

Quantitative analysis of the reactants and the products after the reaction was performed at 25 ℃ using high-performance liquid chromatography (HPLC, Shimadzu LC20AD) with a Hypersil BDS-C18 column (5 μm, 4.6 mm × 150 mm). The wavelength of the ultraviolet detector (UVD) was set at 254 nm, with the mobile phase consisting of 40% acetonitrile and 60% phosphate buffer (pH = 2), a flow rate of 0.6 mL min^{-1}, and an injection volume of 10 μL.

To illustrate the specific preparation process of the standard solution, we take the preparation of the 2-furoic acid standard solution as an example. First, accurately weigh 50.0 mg of 2-furoic acid standard and transfer it to a 10 mL volumetric flask. Dilute with acetonitrile to the mark to prepare a stock solution with a mass concentration of 5000.0 μg mL^{-1}. Subsequently, accurately transfer a specific volume of 2-furoic acid to prepare a series of standard solutions with mass concentrations of 2.5 μg mL^{-1}, 50.0 μg mL^{-1}, 100.0 μg mL^{-1}, 200.0 μg mL^{-1}, 300.0 μg mL^{-1}, 400.0 μg mL^{-1}, 500.0 μg mL^{-1}, 600.0 μg mL^{-1}, and 700.0 μg mL^{-1} for HPLC analysis.

Electrochemical measurements

The cyclic voltammetry was carried out with a Shanghai Chenhua CHI760E workstation. A glassy-carbon electrode (3mm-diameter, disc-electrode) was used as the working electrode, a Pt plate was used as the auxiliary electrode and an Ag/Ag^{+} electrode was used as a reference electrode. All samples should be bubbled with Ar for 5 min before testing except the cases with CO_2. The measurements were carried out at a scan rate of 100 mV s^{-1} in DMF/Bu_4NBF_6 (0.1 M).

The electron paramagnetic resonance (EPR) experiments

Under standard conditions, electron paramagnetic resonance (EPR) measurements were conducted using a Bruker A300 instrument with 5,5-dimethyl-1-pyrroline N-oxide (DMPO) as the trapping agent. First, a blank test was performed to record an EPR spectrum before the reaction. Subsequently, the electrode was activated using cyclic voltammetry by applying a voltage range of –4.5 V to 0.5 V for 10 cycles, with a scan rate set at 50 mV s^{-1}. After activating the electrode, the EPR of the reaction was measured. CO_2 gas was introduced for at least 30 minutes until saturation was reached before testing began. The reaction was sustained at –2.5 V for 5 hours, and EPR spectra were recorded at 0 h, 0.5 h, 1 h, 2.5 h, and 5 h.

Investigation on the formation of $CO_2^{\bullet-}$ radical anion

The electroreduction was carried out under the standard reaction conditions. After that the reaction mixture was acidized with HCl aqueous (2.0 M). The agueous layer was collected and concentrated in vacuo, and 2.0 ml D_2O was added. The aqueous phase was analyzed by crude ^{1}H NMR and ^{13}C NMR. The formic acid and oxalic acid were detected [1-3].

Density functional theory (DFT) calculations

The DFT calculations were carried out using the Vienna ab initio simulation package (VASP) and Gaussian 16 program [4].

For the VASP calculations, our computational simulations were performed using the projector augmented wave (PAW) pseudo-potentials to describe the interaction between the atomic cores and valence electrons with density functional theory (DFT). The Perdew–Burke–Ernzerhof (PBE) functional within the generalized gradient approximation (GGA) was used to implement DFT calculations [5]. A six layered C(002) slab and Pt(111) slab model were employed to simulate their interaction with CO_2. In all the C(002) slab and Pt(111) slab structure optimization calculations, the atoms at the bottom three layers were fixed, while the other atoms were fully relaxed. The reasonable vacuum layers of the C(002) slab and Pt(111) slab were set around 15 Å in the z-direction for avoiding the interaction between planes, respectively. A cutoff energy of 450 eV was provided. For the well converged energy values of the C(002) slab and Pt(111) slab, the $2 \times 2 \times 1$ Monkhorst Pack kpoint sampling was chosen. Geometry optimizations energies were converged within 10^{-5} eV.

The adsorption energy (ΔE_{ads}) of CO_2 on C(002) and Pt(111) surface was determined by the following expression [6]:

$$\Delta E_{ads} = E_{ads/base} - E_{ads} - E_{base}$$

where $E_{ads/base}$, E_{ads} and E_{base} are the total energy of the adsorbed systems, the isolated CO_2, and base (graphite or Pt), respectively. Accordingly, the negative ΔE_{ads} indicates the energetically favorable (exothermic) interaction between the adsorbate and the graphite or Pt surface.

Moreover, the differential charge density ($\Delta\rho$) of CO_2 on C(002) and Pt(111) surface was determined by the following expression:

$$\Delta\rho = \rho_{ads/base} - \rho_{ads} - \rho_{base}$$

where $\rho_{ads/base}$, ρ_{ads} and ρ_{base} are the global charge density of the adsorbed systems and the individual charge density isolated CO_2, and base (graphite or Pt), respectively.

For the Gaussian calculations, the geometry optimizations were conducted using the M06-2X functional and 6-31G(d) basis set in N,N-dimethylformamide solvent, and the output files were analyzed for wave function using the Multiwfn program [7]. To confirm whether each optimized stationary point was an energy minimum or a transition state, as well as to evaluate the zero-point vibrational energy and the thermal corrections at 298 K, the vibrational frequencies were computed at the same level of theory as for the geometry optimizations. Based on the optimized structures, the M06-2X functional and 6-31G(d) basis set was used to calculate the solvation singlepoint energies to give

more accurate energy information. The solvent effects of geometry optimizations and single-point calculations were considered by the SMD solvation model in N,N-dimethylformamide solvent. Gibbs free Energy (ΔG) is computed by the equation of $\Delta G = \Delta E + \Delta E_{ZPE} - T\Delta S$, where the ΔE is the different energy between each reaction step, ΔE_{ZPE} is the difference of the zero-point energy between each reaction step, ΔS is the difference of vibrational entropy between each reaction step.

Supplementary figures and tables

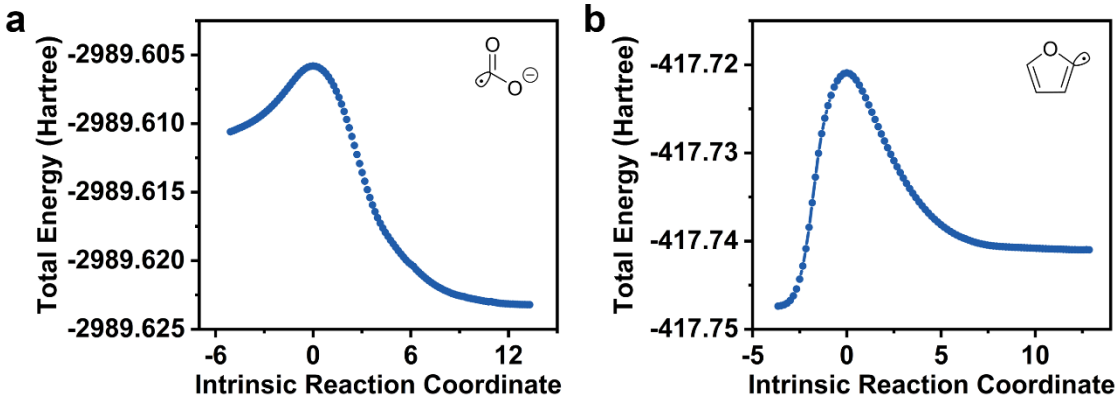

Figure S1. IRC analysis of TS of 2-bromofuran carboxylation reaction based on $CO_2^{\bullet-}$ intermediate (a) and $Ar^{\bullet}$ intermediate (b).

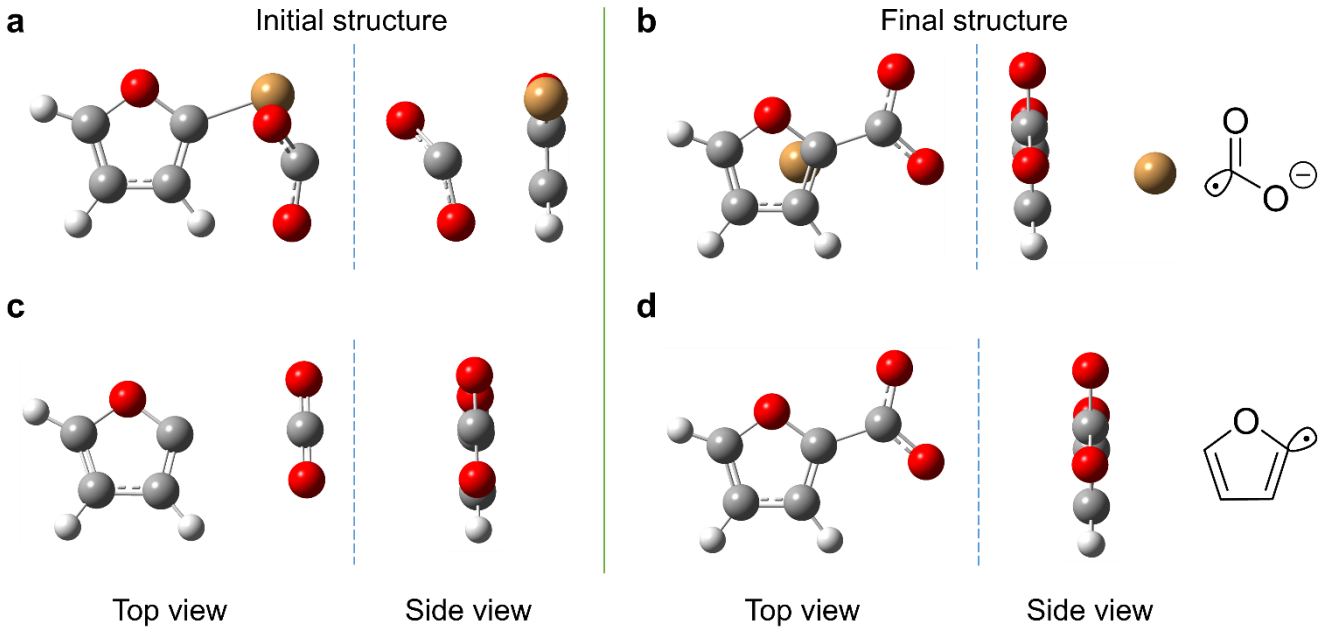

Figure S2. The initial and final structures obtained from the IRC calculation of TS of 2-bromofuran carboxylation reaction based on $CO_2^{\bullet -}$ intermediate (a, b) and $Ar^{\bullet}$ intermediate (c, d).

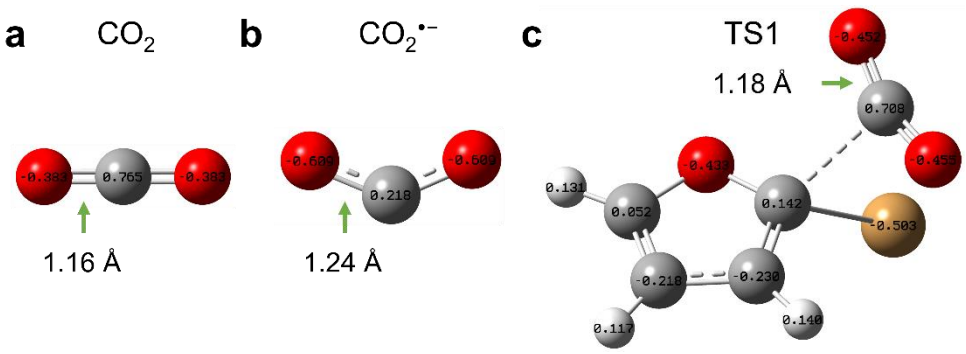

Figure S3. Change of charge density and bond length before and after the interaction between CO_2 and 2-bromofuran. (a) CO_2, (b) $CO_2^{\bullet-}$ intermediate, (c) TS1.

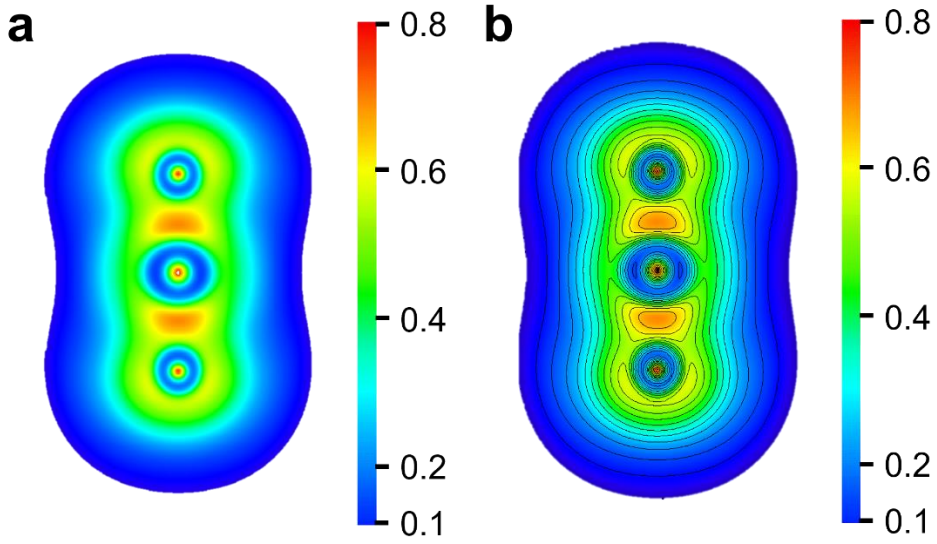

Figure S4. The localized orbital locator of CO_2 molecule.

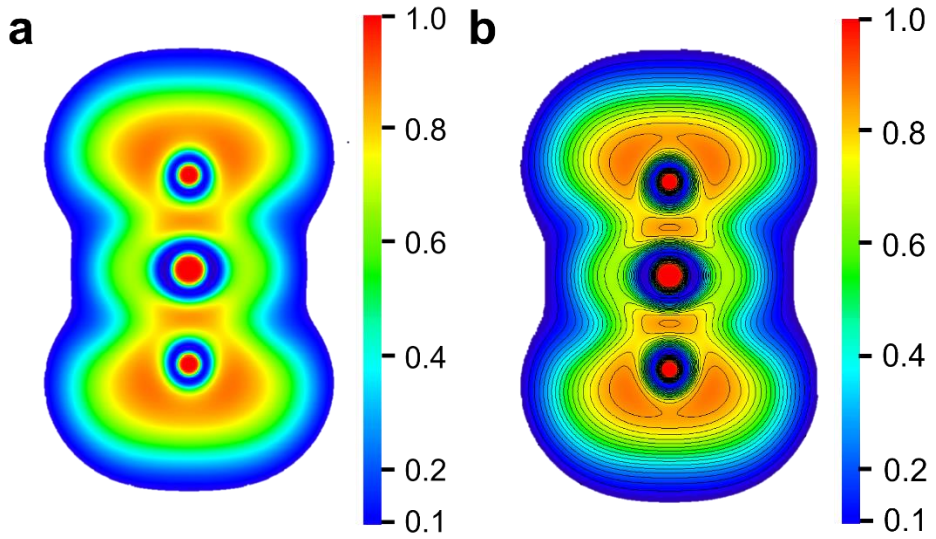

Figure S5. The electron localization function of CO_2 molecule.

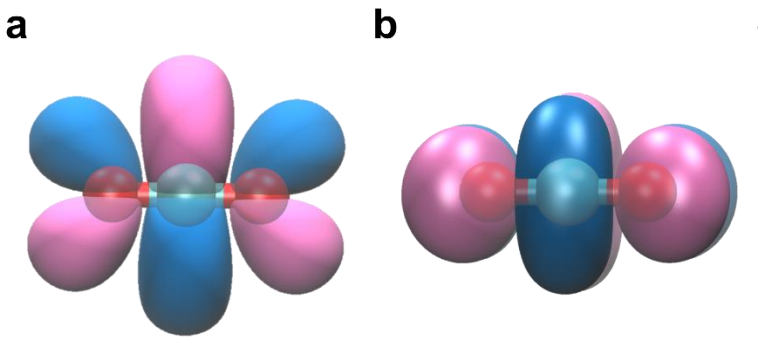

Figure S6. The unoccupied frontier orbital of CO_2 molecule π_1^* (a) and π_2^* (b).

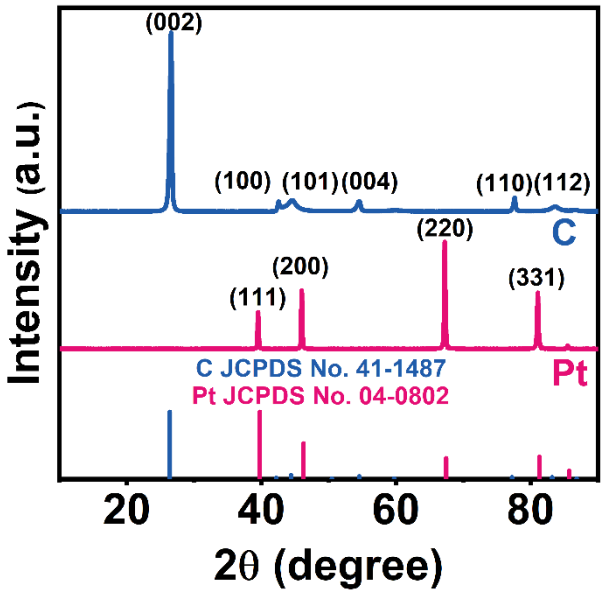

Figure S7. XRD patterns of graphite electrode and platinum electrode.

Table S1. Influence of different carbon-structured cathode materials on carboxylation reaction.

Substrates	Pt ΔE_{ads} (eV)	Graphite ΔE_{ads} (eV)
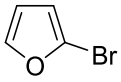	–2.258243	–0.527143
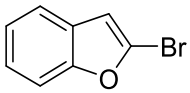	–2.800986	–0.773086

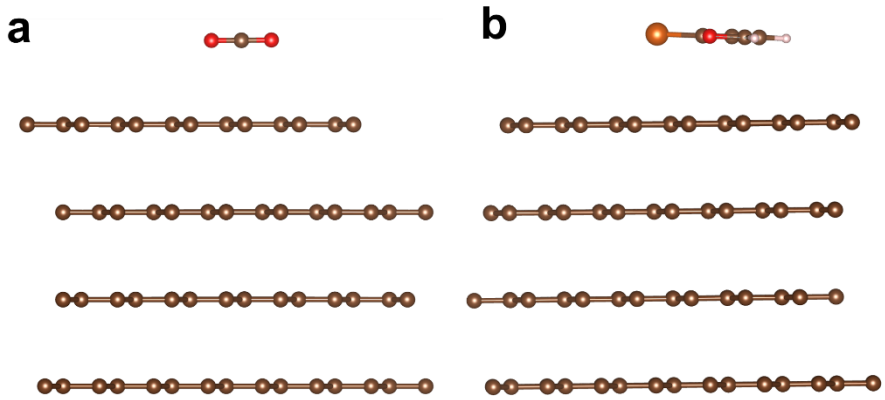

Figure S8. Adsorption diagram of CO_2 (a) and 2-bromofuran (b) on graphite (C(002)). Red, O; brown, C; pink, H; orange, Br.

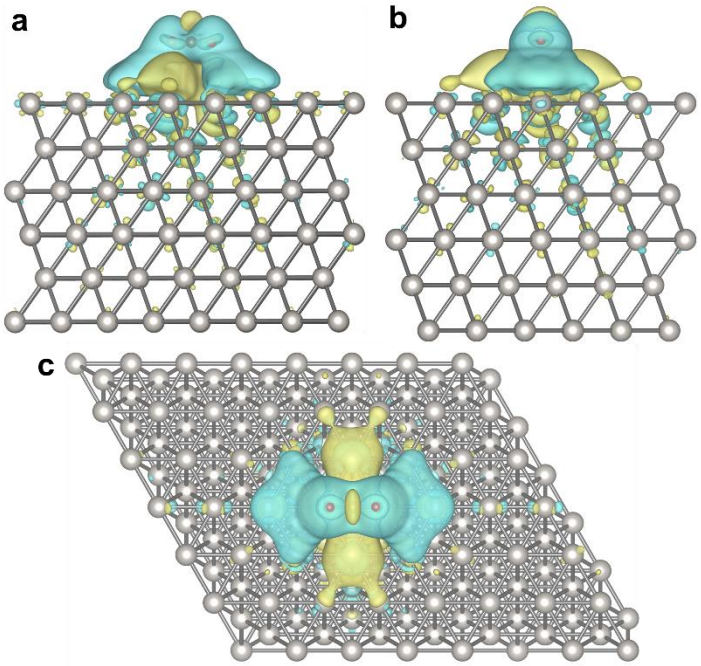

Figure S9. (a-c) Plots of electron density difference for the CO_2 adsorption with Pt(111) at different angles. The yellow and blue contours represent electron density accumulations and depressions, respectively. Red, O; brown, C; grey, Pt.

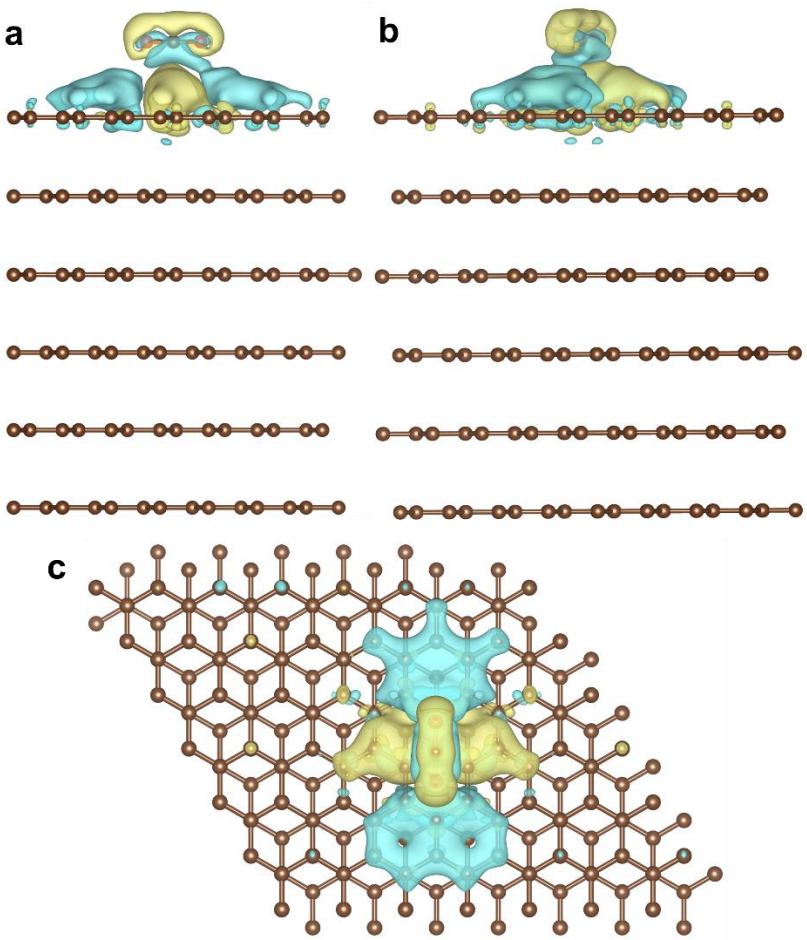

Figure S10. (a-c) Plots of electron density difference for the CO_2 adsorption with C(002) at different angles. The yellow and blue contours represent electron density accumulations and depressions, respectively. Red, O; brown, C.

Table S2. The Bader charge population of CO_2 adsorbed with C(002) and Pt(111)

Materials	Surface atom (Bader charge $\Delta\bar{e}$)		
	C (Transfer charge)	O_1 (Transfer charge)	O_2 (Transfer charge)
Graphite	1.944028(–2.055972)	7.037671 (1. 037671)	7.032115 (1. 032115)
Pt	1.952120 (–2.047879)	7.035962 (1. 035962)	7.040433 (1. 040433)

Table S3. Influence of different carbon-structured cathode materials on carboxylation reaction.[a)]

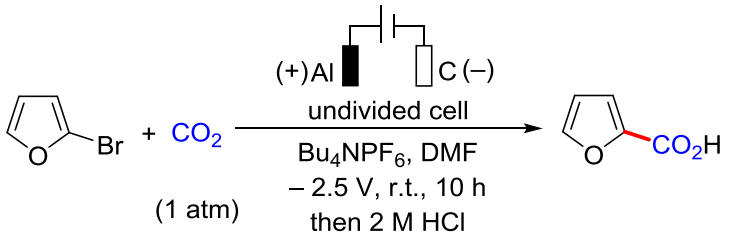

Entry	Cathode	Yield (%)	FE (%)
1	Glassy carbon	n.d.	n.d.
2	Graphite	69	92
3	Graphite felt	84	24

a) Reaction conditions: 2-bromofuran (0.02 mol L^{-1}), Bu_4NPF_6 (0.1 mol L^{-1}), DMF, CO_2 atmosphere (1 atm) under –2.5 V (*vs.* Ag/Ag^+) constant potential in an undivided cell at room temperature for 10 h with aluminum as anode and different C materials as cathode. Determined by HPLC. n.d. = no detection.

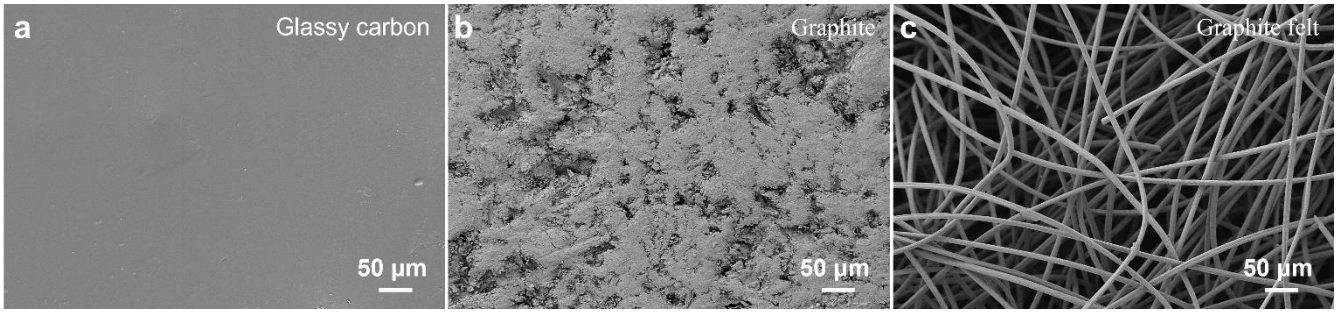

Figure S11. (a-c) SEM images of different carbon-structured cathode materials. (a) Glassy carbon, (b) graphite, (c) graphite felt.

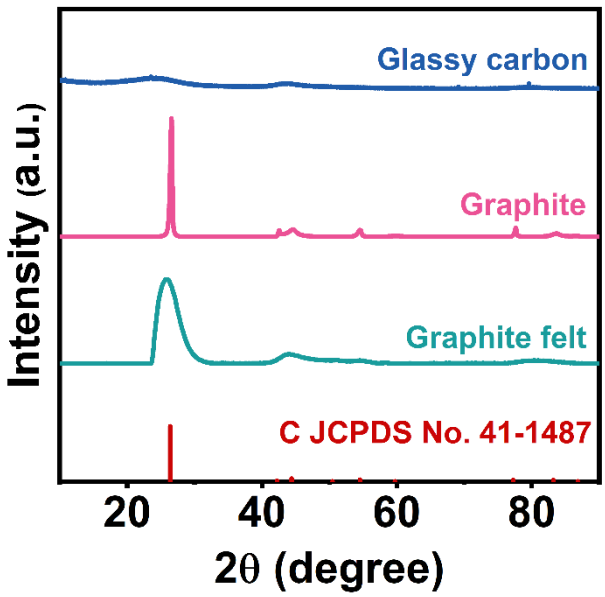

Figure S12. XRD patterns of different carbon-structure materials.

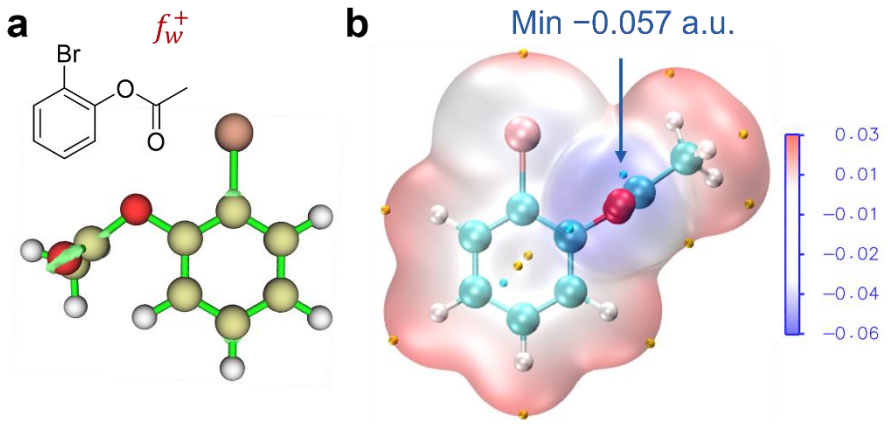

Figure S13. (a) Nucleophilic attacking position from the calculated Fukui function of 2-bromophenyl acetate. (b) Electrostatic potential maps of 2-bromophenyl acetate.

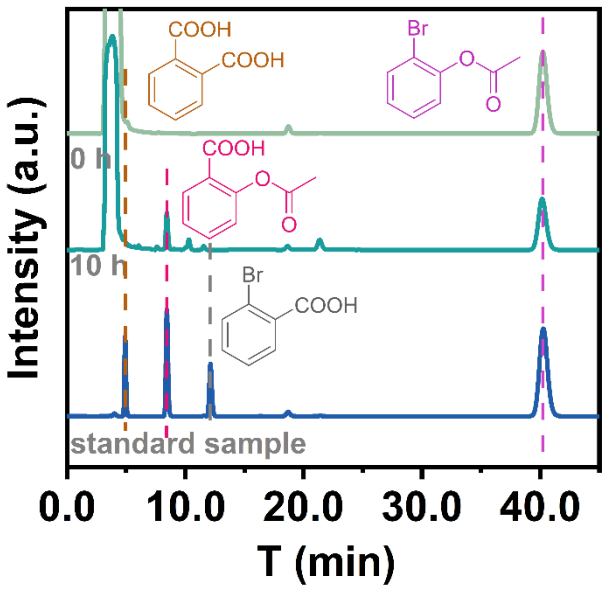

Figure S14. HPLC chromatogram of electrolyte mixture and standard sample before and after 2-bromophenyl acetate reaction.

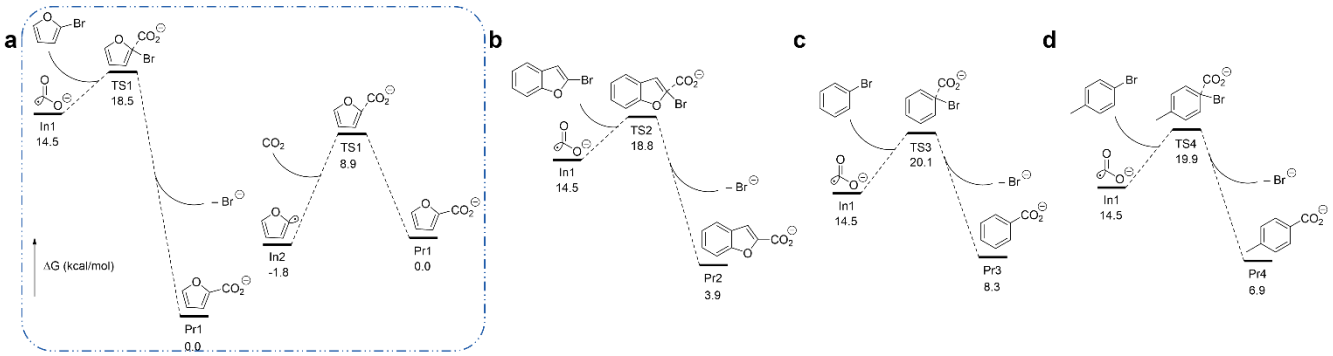

Figure S15. Calculated free energy diagram of reactions of $CO_2^{\bullet-}$ with different substrates. (a) 2-bromofuran carboxylation reaction based on $CO_2^{\bullet-}$ intermediates and $Ar^{\bullet}$ intermediates. (b) 2-bromobenzofuran, (c) bromobenzene, (d) 4-bromotoluene.

Table S4. The effect of base.[a)]

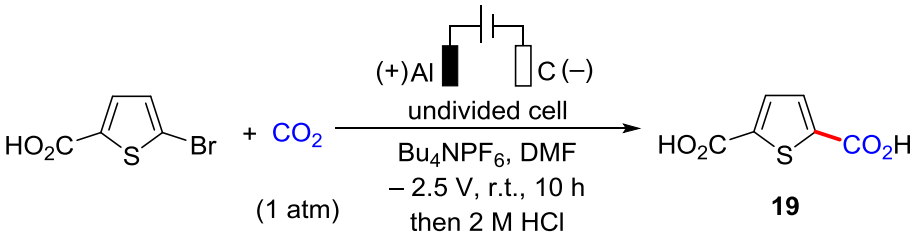

Entry	Base	Yield (%)	FE (%)
1	none	2	4
2	TEA	13	6
3	NaOAc	1	9
4	KO^{t}Bu	2	18
5	DBU	6	6
6	TMA	2	1

a) Reaction conditions: 5-bromothiophene-2-carboxylic (0.02 mol L^{-1}), Bu_4NPF_6 (0.1 mol L^{-1}), base (0.06 mol L^{-1}), DMF, CO_2 atmosphere (1 atm) under –2.5 V (*vs.* Ag/Ag^+) constant potential in an undivided cell at room temperature for 10 h with aluminum as anode and graphite as cathode. DBU = 1,8-diazabicyclo[5.4.0]undec-7-ene, TMA = trimethylamine.

Table S5. The effect of TEA concentration. [a)]

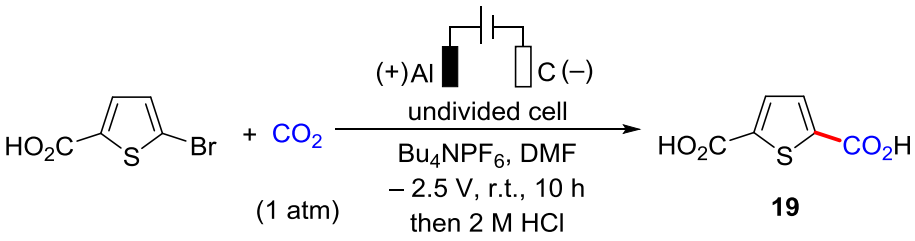

Entry	C (mol L^{-1})	Yield (%)	FE (%)
1	0.02	13	5
2	0.06	13	6
3	0.10	29	15
4	0.15	16	7
5	0.20	40	17
6	0.25	13	2
7	0.50	17	8
8	0.75	20	6
9	1.00	29	20

a) Reaction conditions: 5-bromothiophene-2-carboxylic (0.02 mol L^{-1}), Bu_4NPF_6 (0.1 mol L^{-1}), DMF, CO_2 atmosphere (1 atm) under –2.5 V (*vs.* Ag/Ag^+) constant potential in an undivided cell at room temperature for 10 h with aluminum as anode and graphite as cathode.

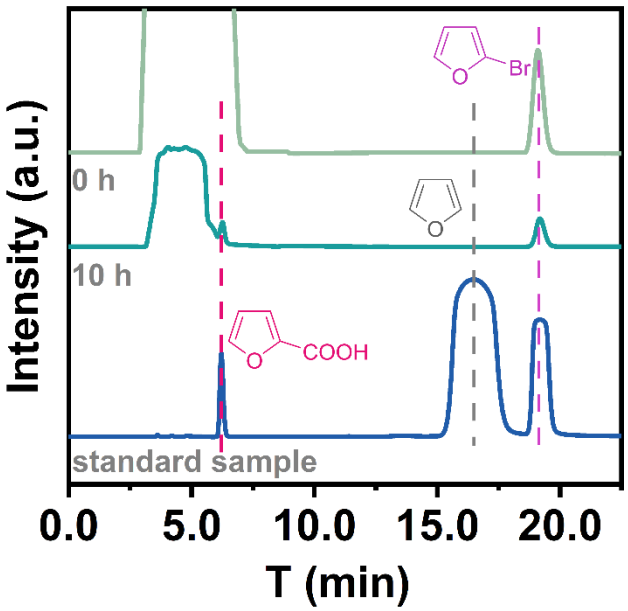

Figure S16. HPLC chromatogram of electrolyte mixture and standard sample before and after 2-bromofuran reaction.

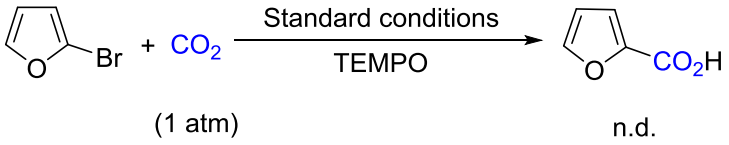

Figure S17. Free radical trapping experiment under optimized conditions. The TEMPO trapping agent was used to trap the radicals. Reaction conditions: 2-bromofuran (0.02 mol L^{-1}), Bu_4NPF_6 (0.1 mol L^{-1}), DMF, CO_2 atmosphere (1 atm) under –2.5 V (*vs.* Ag/Ag^+) constant potential in an undivided cell at room temperature for 10 h with aluminum as anode and graphite as cathode.

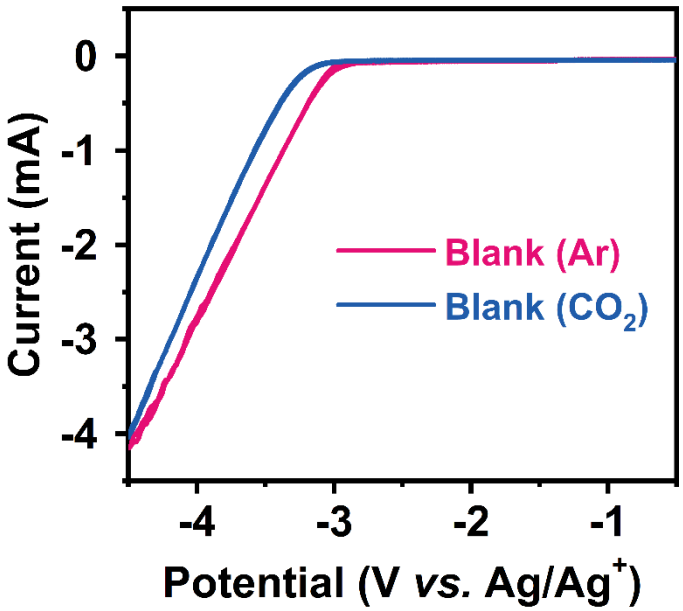

Figure S18.Cyclic voltammograms of blank sample in DMF with Bu_4NPF_6 (0.1 mol L^{-1}) in Ar or CO_2 atmosphere.

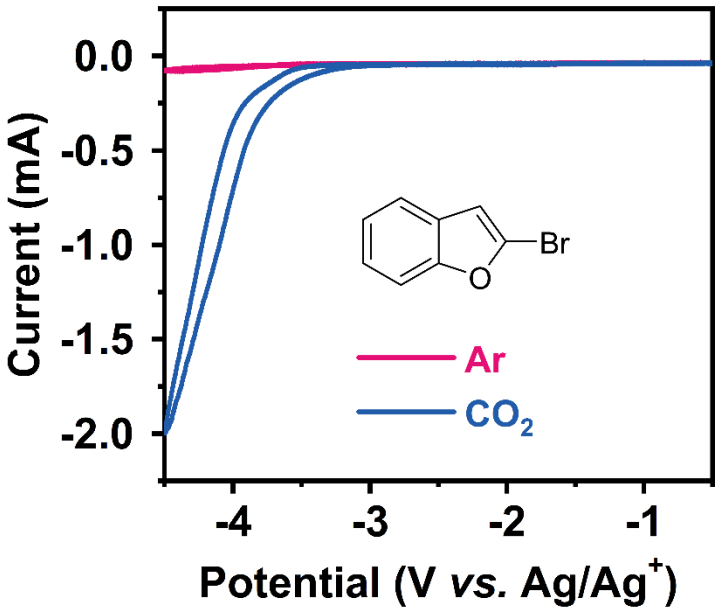

Figure S19. Cyclic voltammograms of 2-bromobenzofuran in DMF with Bu_4NPF_6 (0.1 mol L^{-1}) in Ar or CO_2 atmosphere.

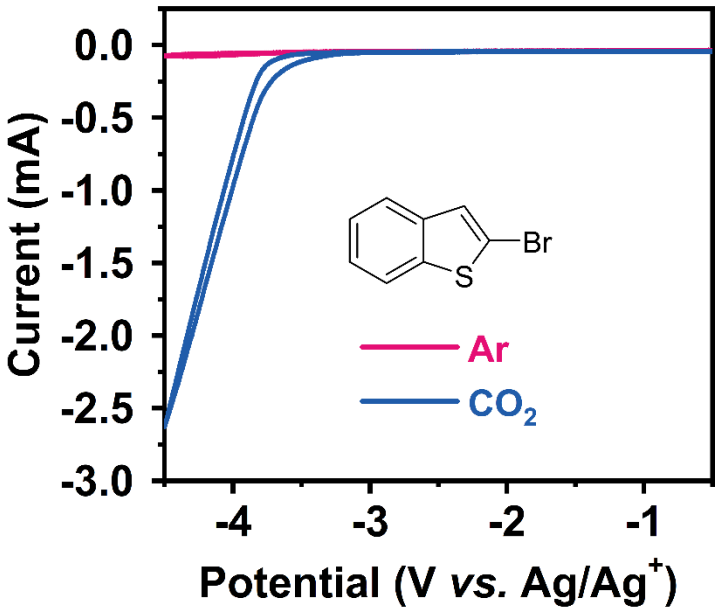

Figure S20. Cyclic voltammograms of 2-bromobenzobthiophene in DMF with Bu_4NPF_6 (0.1 mol L^{-1}) in Ar or CO_2 atmosphere.

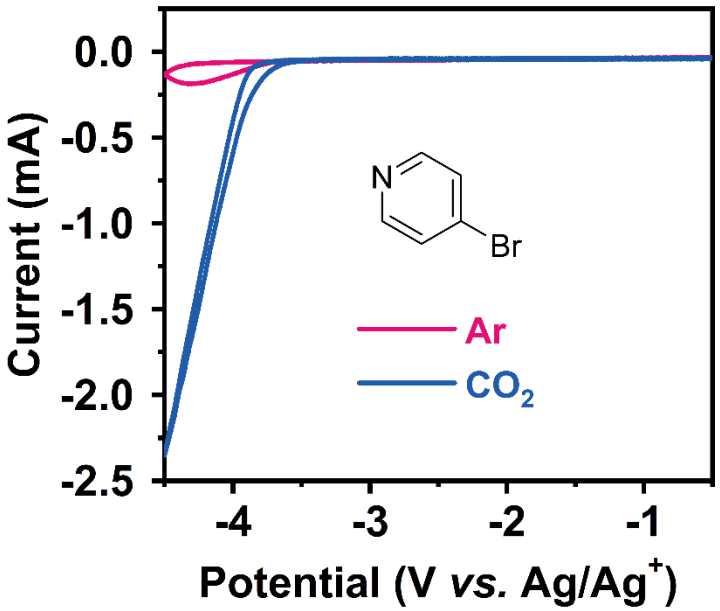

Figure S21. Cyclic voltammograms of 4-bromopyridine in DMF with Bu_4NPF_6 (0.1 mol L^{-1}) in Ar or CO_2 atmosphere.

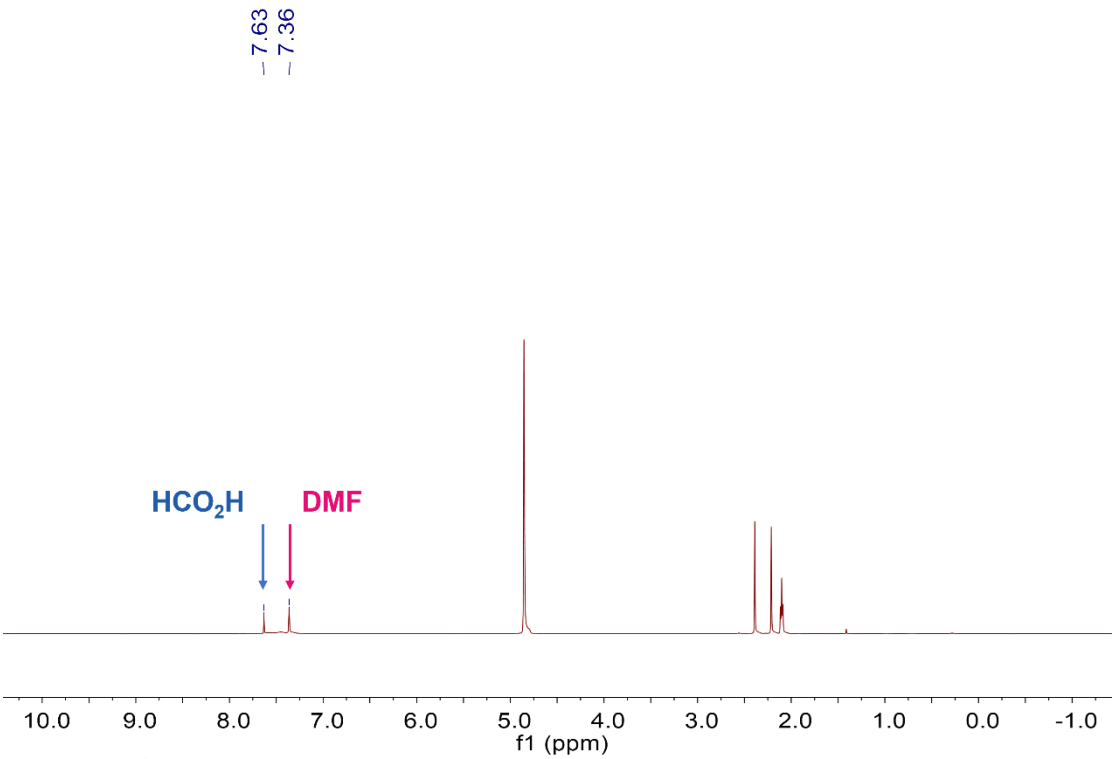

Figure S22. Crude ^{1}H NMR spectrum of the aqueous from research experiment on $CO_2^{\bullet-}$ formation.

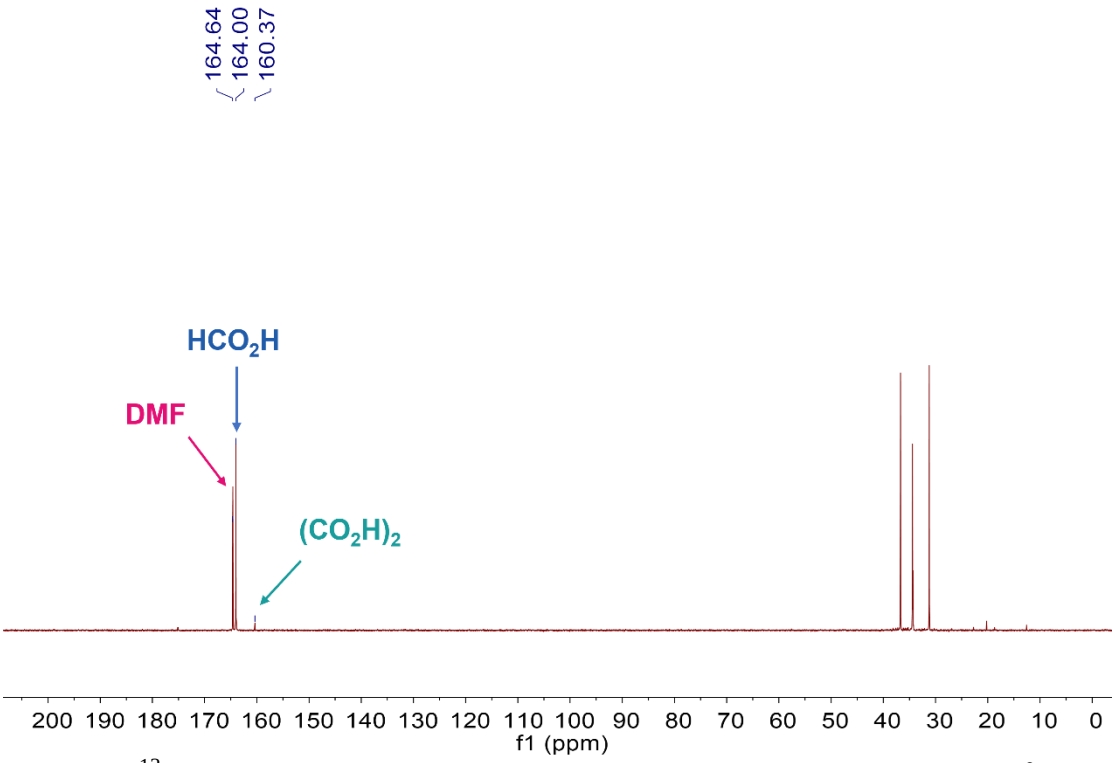

Figure S23. Crude ^{13}C NMR spectrum of the aqueous from research experiment on $CO_2^{\bullet-}$ formation.

High-performance liquid chromatography of standard samples

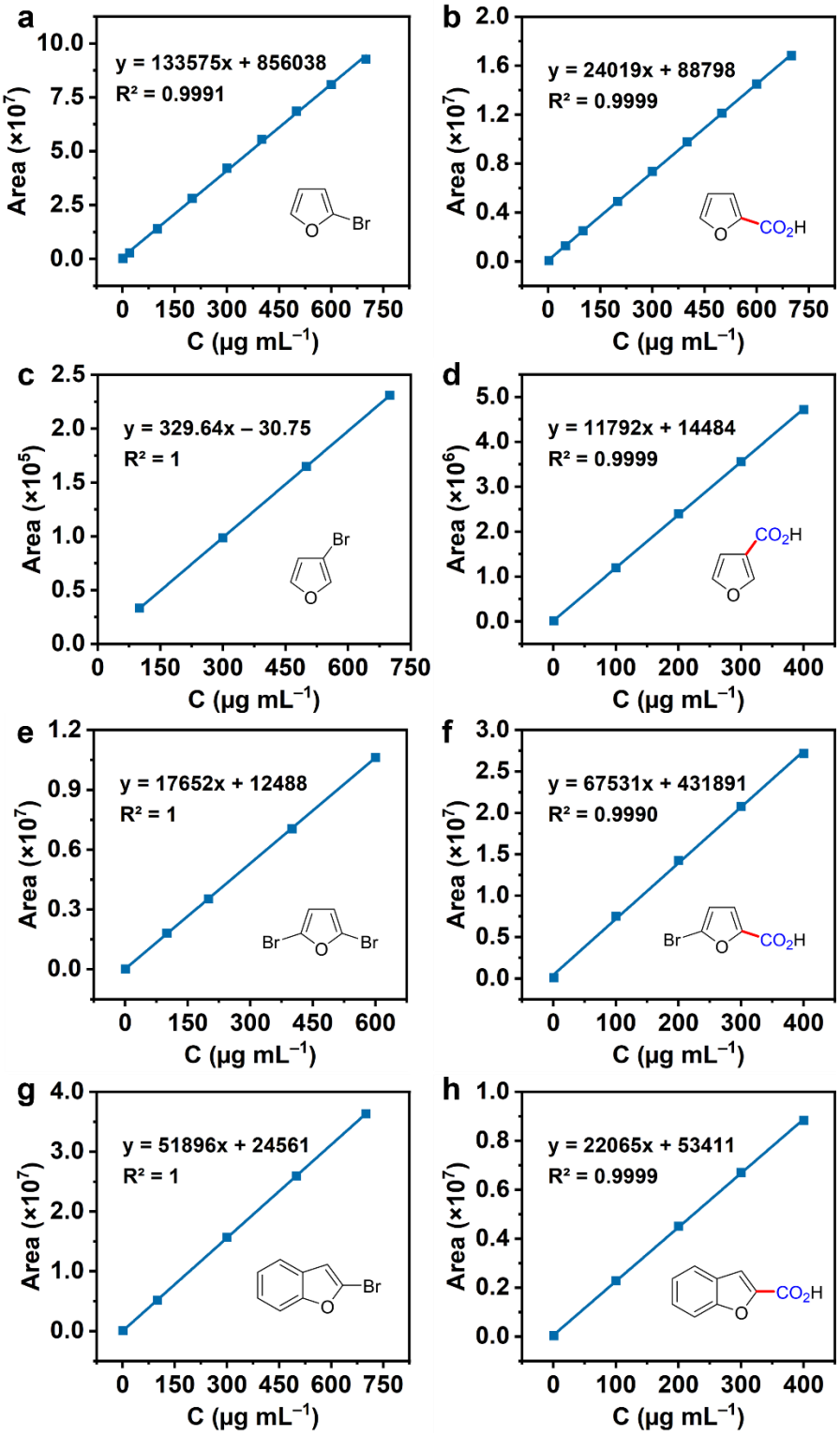

Figure S24. (a-h) Standard curves for various reaction substrates and products.

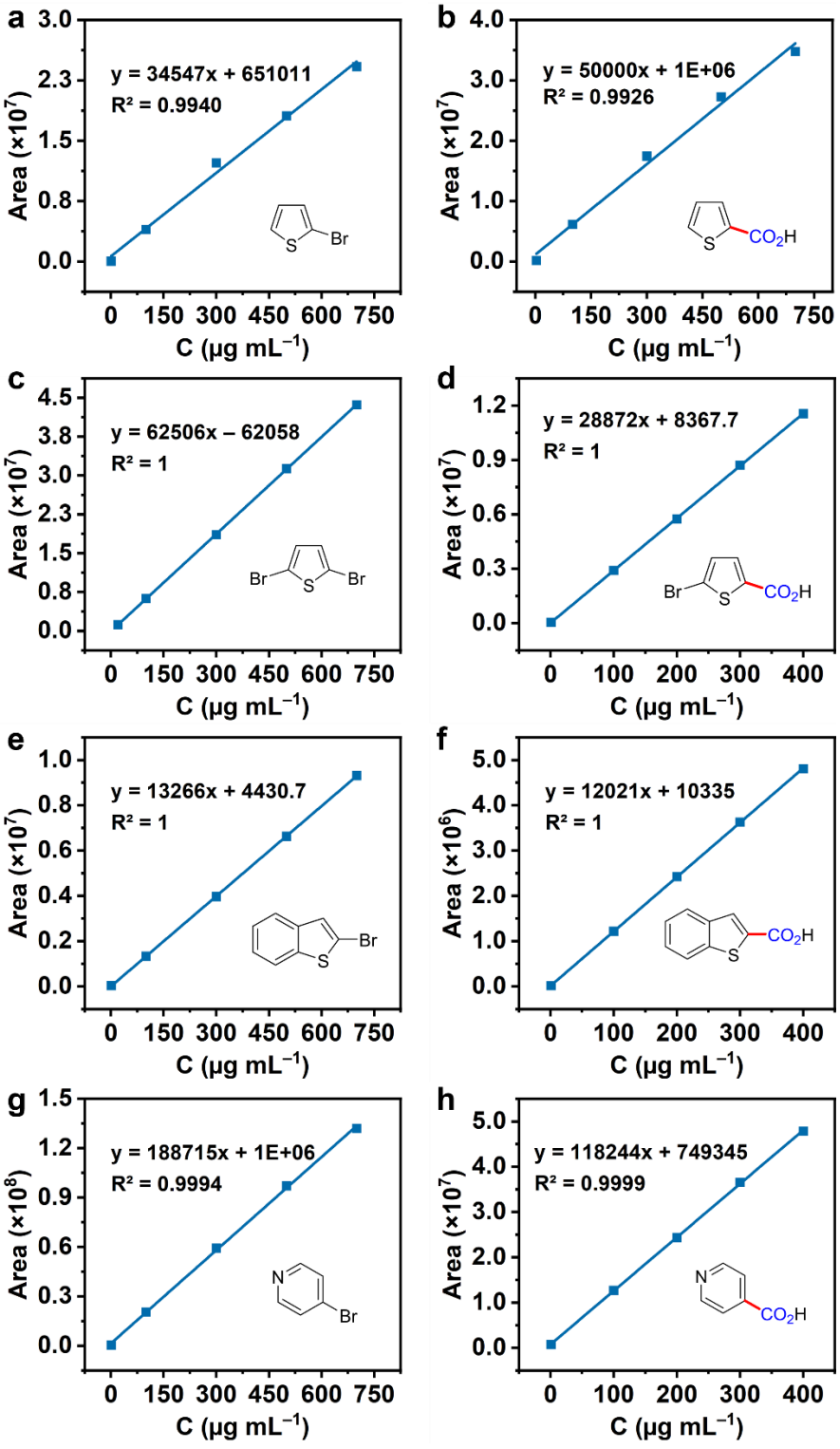

Figure S25. (a-h) Standard curves for various reaction substrates and products.

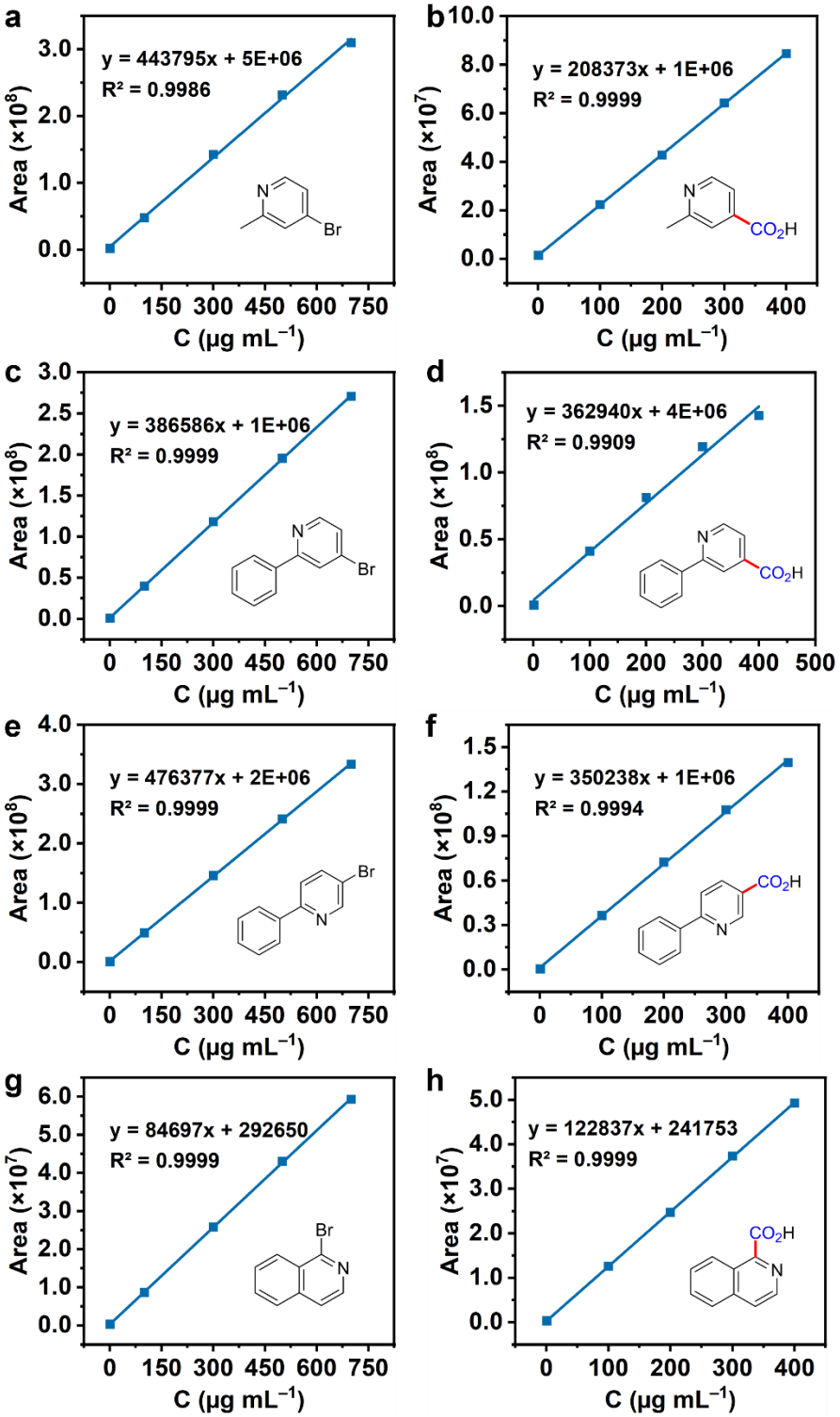

Figure S26. (a-h) Standard curves for various reaction substrates and products.

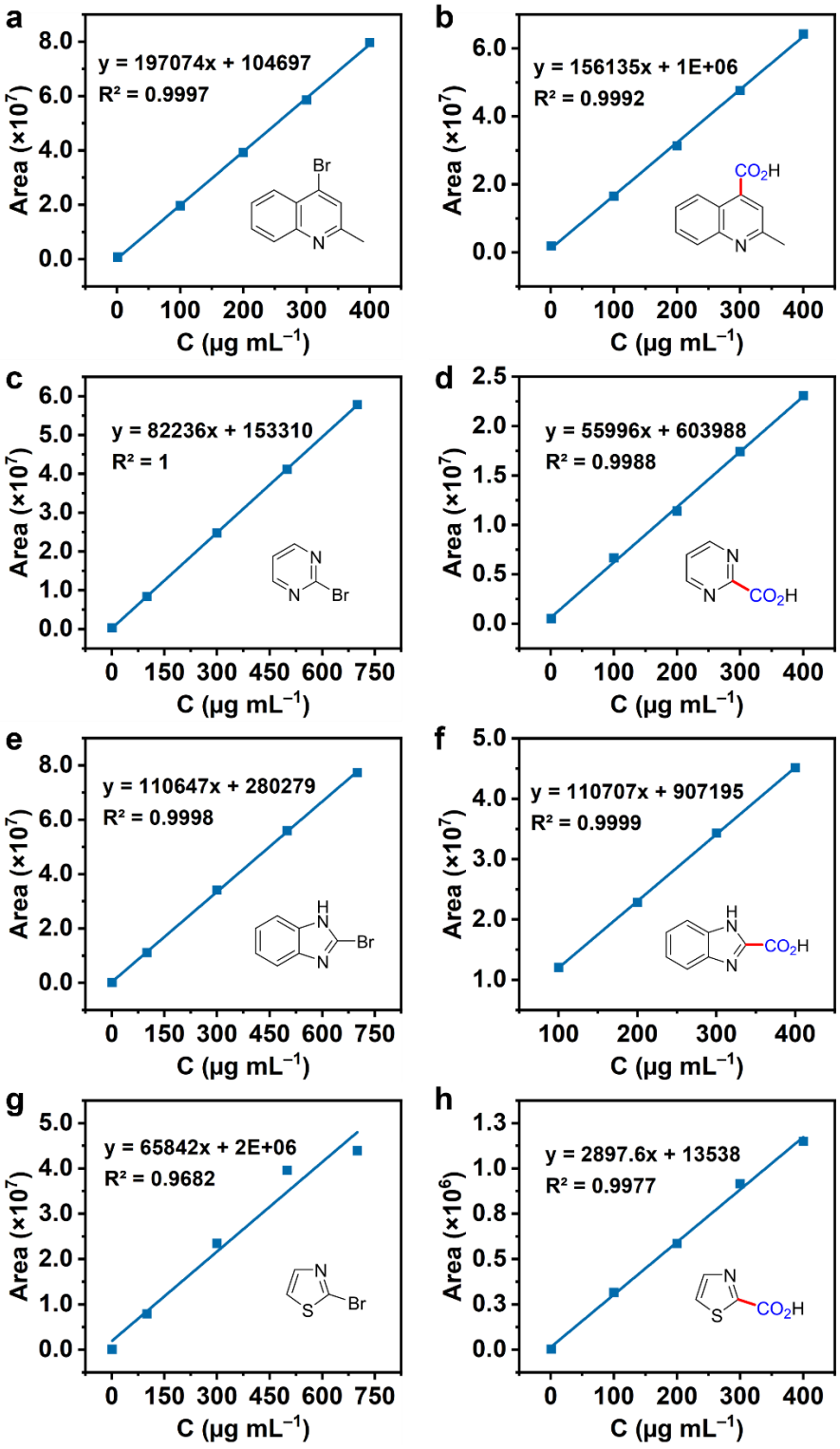

Figure S27. (a-h) Standard curves for various reaction substrates and products.

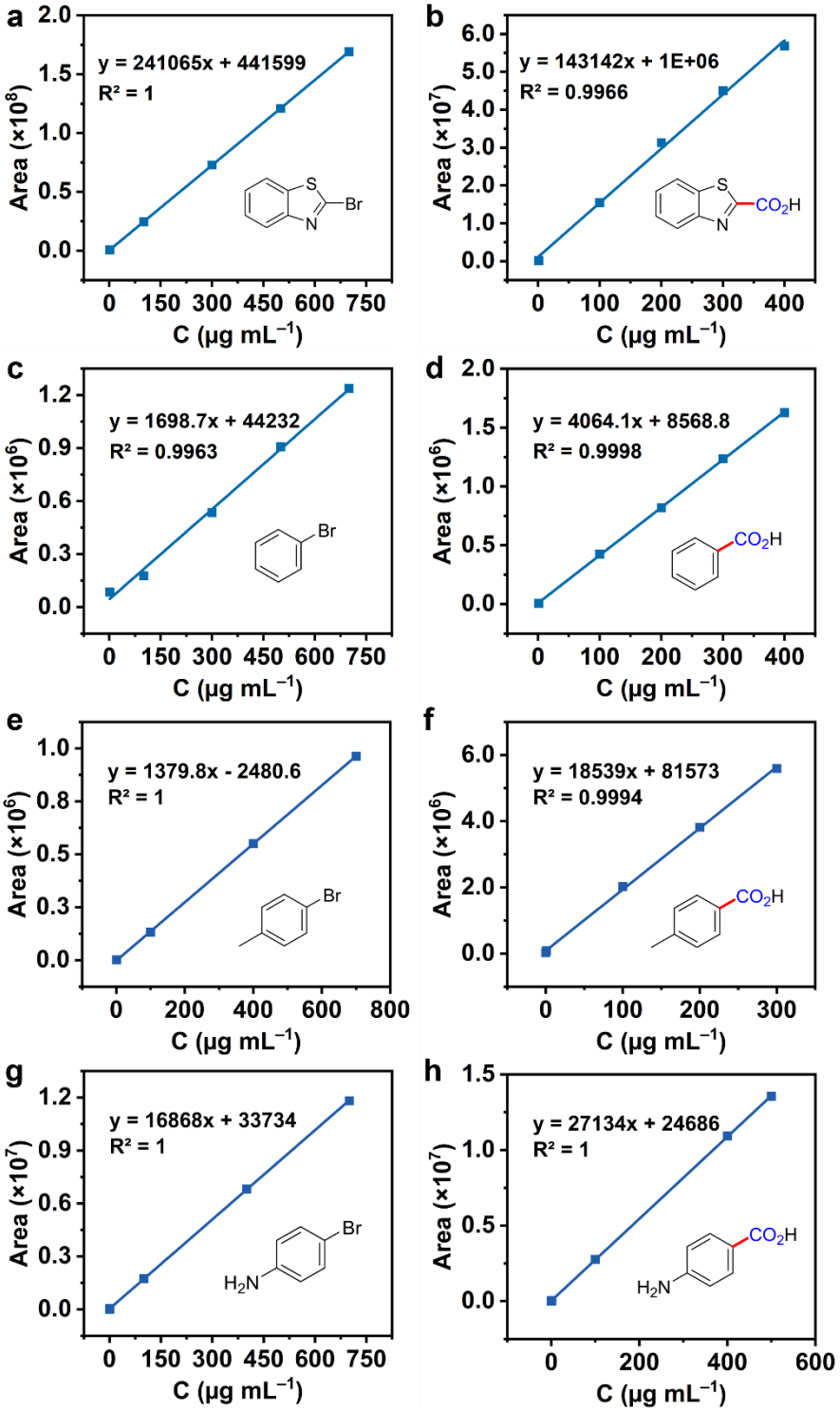

Figure S28. (a-f) Standard curves for various reaction substrates and products.

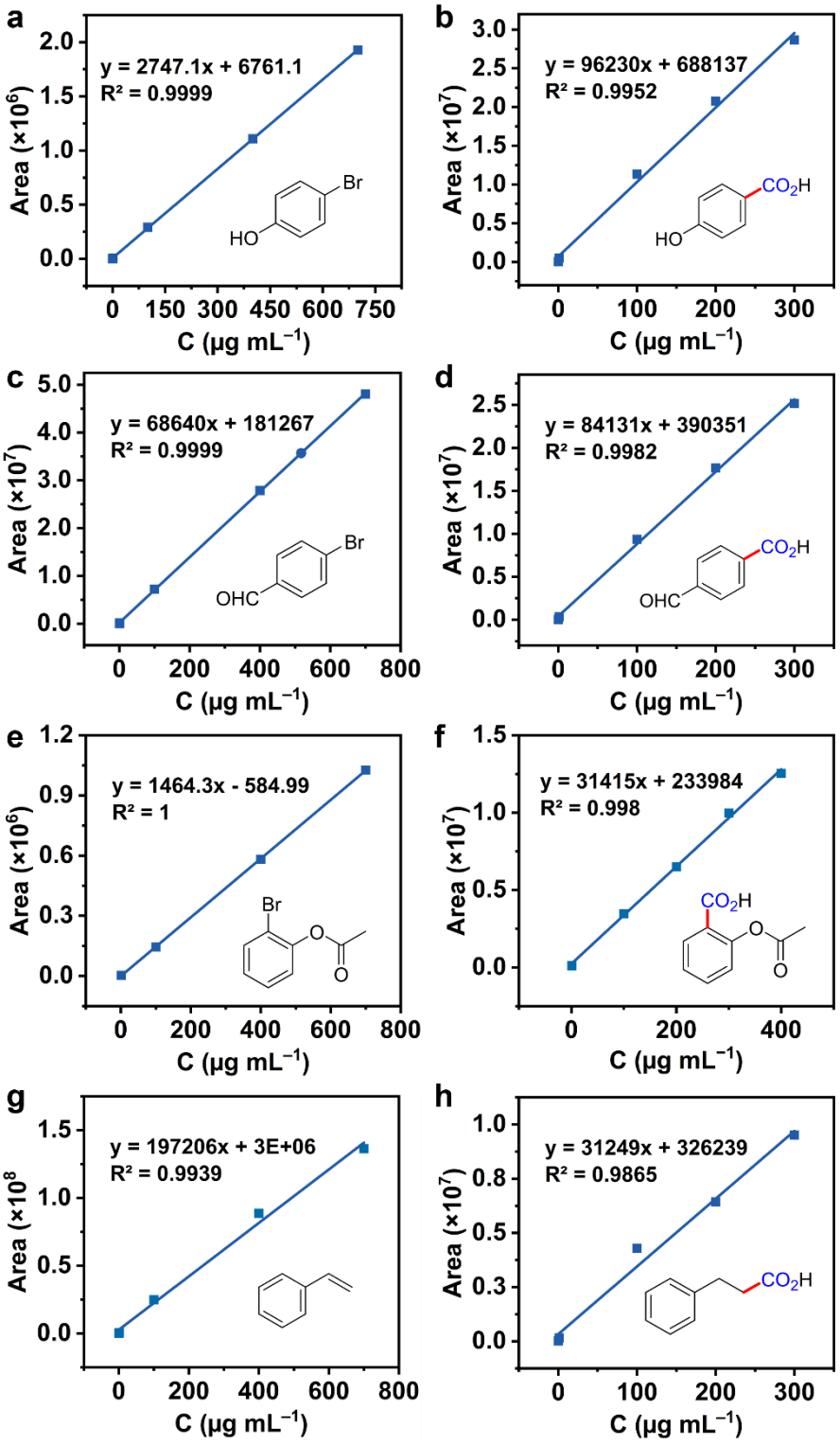

Figure S29. (a-f) Standard curves for various reaction substrates and products.

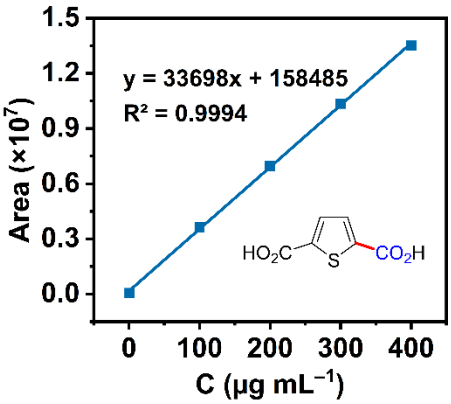

Figure S30. Standard curve for 2,5-thiophenedicarboxylic acid.

NMR results

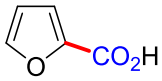

2-Furoic acid (1)
^{1}H NMR (400 MHz, DMSO-*d*$_6$) δ = 13.05 (s, 1H), 8.01 – 7.81 (m, 1H), 7.21 (d, *J* = 3.4 Hz, 1H), 6.66 (dd, *J* = 3.5, 1.8 Hz, 1H).
^{13}C NMR (101 MHz, DMSO-*d*$_6$) δ = 159.80, 147.38, 145.39, 118.12, 112.47.

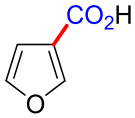

3-Furoic acid (2)
^{1}H NMR (400 MHz, DMSO-*d*$_6$) δ = 12.65 (s, 1H), 8.36 – 8.24 (m, 1H), 7.76 (t, J = 1.7 Hz, 1H), 6.73 (d, J = 1.8 Hz, 1H).
^{13}C NMR (101 MHz, DMSO-*d*$_6$) δ = 164.33, 148.60, 145.08, 120.22, 110.30.

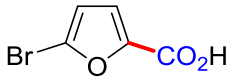

5-Bromo-2-furoic acid (3)
^{1}H NMR (400 MHz, DMSO-*d*$_6$) δ = 13.19 (s, 1H), 7.26 (d, J = 3.5 Hz, 1H), 6.80 (d, J = 3.5 Hz, 1H).
^{13}C NMR (101 MHz, DMSO-*d*$_6$) δ = 158.70, 147.27, 127.17, 120.52, 114.82.

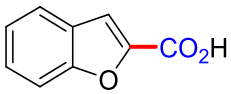

Benzo[b]furan-2-carboxylic acid (4)
^{1}H NMR (400 MHz, DMSO-*d*$_6$) δ = 13.60 (s, 1H), 7.83 (d, J = 7.8 Hz, 1H), 7.80 – 7.64 (m, 2H), 7.53 (ddd, J = 8.4, 7.2, 1.4 Hz, 1H), 7.46 – 7.33 (m, 1H).
^{13}C NMR (101 MHz, DMSO-*d*$_6$) δ = 160.59, 155.46, 146.67, 127.99, 127.32, 124.26, 123.54, 113.95, 112.51.

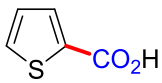

2-Thiophenecarboxylic acid (5)
^{1}H NMR (400 MHz, DMSO-*d*$_6$) δ = 13.02 (s, 1H), 7.89 (d, J = 5.0 Hz, 1H), 7.75 (d, J = 3.8 Hz, 1H), 7.32 – 7.17 (m, 1H).
^{13}C NMR (101 MHz, DMSO-*d*$_6$) δ = 163.38, 135.13, 133.68, 133.66, 128.67.

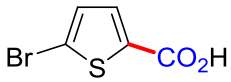

5-Bromo-2-thiophenecarboxylic acid (6)
^{1}H NMR (400 MHz, DMSO-*d*$_6$) δ = 13.04 (s, 1H), 7.55 (dd, J = 4.1, 1.2 Hz, 1H), 7.31 (dd, J = 4.0, 1.2 Hz, 1H).
^{13}C NMR (101 MHz, DMSO-*d*$_6$) δ = 114.82, 120.52, 127.17, 147.27, 158.70.

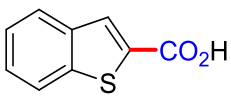

Benzo[b]thiophene-2-carboxylicacid (7)
^{1}H NMR (400 MHz, DMSO-*d*$_6$) δ = 13.51 (s, 1H), 8.72 – 7.98 (m, 3H), 7.78 – 7.44 (m, 2H).

^{13}C NMR (101 MHz, DMSO-d_6) δ = 123.39, 125.48, 126.17, 127.43, 130.69, 135.25, 139.19, 141.81, 164.01.

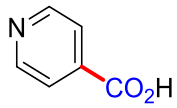

4-Picolinic acid (8)
^{1}H NMR (400 MHz, DMSO-d_6) δ = 13.40 (s, 1H), 9.20 – 8.74 (m, 2H), 8.76 – 7.74 (m, 2H).
^{13}C NMR (101 MHz, DMSO-d_6) δ = 166.65, 151.07, 138.55, 123.21.

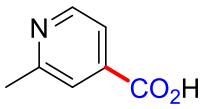

2-Methylpyridine-4-carboxylic acid (9)
^{1}H NMR (400 MHz, DMSO-d_6) δ = 13.42 (s, 1H), 8.63 (d, J = 5.1 Hz, 1H), 7.92 – 7.50 (m, 2H), 2.55 (s, 3H).
^{13}C NMR (101 MHz, DMSO-d_6) δ = 166.83, 159.61, 150.35, 138.93, 122.54, 120.33, 24.43.

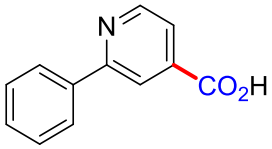

2-Phenylpyridine-4-carboxylic acid (10)
^{1}H NMR (400 MHz, DMSO-d_6) δ = 13.29 (s, 1H), 8.85 (d, J = 4.9 Hz, 1H), 8.29 (s, 1H), 8.22 – 8.09 (m, 2H), 7.78 (dd, J = 4.9, 1.5 Hz, 1H), 7.50 (dt, J = 12.3, 6.8 Hz, 3H).
^{13}C NMR (101 MHz, DMSO-d_6) δ = 166.70, 157.59, 151.06, 139.87, 138.41, 129.93, 129.33, 127.12, 121.90, 119.46.

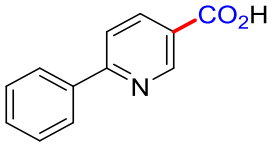

6-Phenylnicotinic acid (11)
^{1}H NMR (400 MHz, DMSO-d_6) δ = 13.39 (s, 1H), 9.20 (d, J = 2.2 Hz, 1H), 8.36 (dd, J = 8.3, 2.3 Hz, 1H), 8.19 (d, J = 6.1 Hz, 2H), 8.11 (d, J = 8.3 Hz, 1H), 7.55 (q, J = 7.3, 6.8 Hz, 3H).
^{13}C NMR (101 MHz, DMSO-d_6) δ = 166.69, 159.82, 150.87, 138.51, 138.08, 130.45, 129.35, 127.52, 125.52, 120.37.

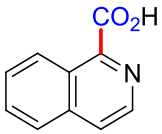

1-Isoquinolinecarboxylic acid (12)
^{1}H NMR (400 MHz, DMSO-d_6) δ = 13.65 (s, 1H), 8.75 – 8.50 (m, 2H), 8.23 – 7.77 (m, 4H).
^{13}C NMR (101 MHz, DMSO-d_6) δ = 167.64, 150.70, 141.42, 136.81, 131.35, 129.23, 127.72, 126.37, 125.62, 124.04.

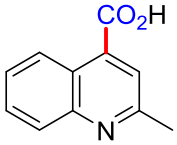

2-Methylquinoline-4-carboxylic acid (13)

^{1}H NMR (400 MHz, DMSO-*d*$_6$) δ = 13.33 (s, 1H), 8.62 (d, J = 8.5 Hz, 1H), 8.00 (d, J = 8.4 Hz, 1H), 7.82 (s, 1H), 7.76 (ddd, J = 8.4, 6.9, 1.5 Hz, 1H), 7.62 (ddd, J = 8.4, 6.9, 1.4 Hz, 1H), 2.70 (s, 3H).
^{13}C NMR (101 MHz, DMSO-*d*$_6$) δ = 168.08, 159.12, 148.56, 136.78, 130.08, 129.28, 127.35, 125.81, 123.24, 123.17, 25.12.

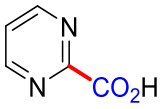

Pyrimidine-2-carboxylic acid (14)
^{1}H NMR (400 MHz, DMSO-*d*$_6$) δ = 12.70 (s, 1H), 8.96 (d, J = 4.8 Hz, 2H), 7.70 (t, J = 4.8 Hz, 1H).
^{13}C NMR (101 MHz, DMSO-*d*$_6$) δ = 165.37, 158.33, 157.99, 123.77.

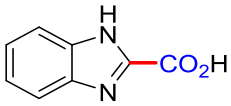

1H-Benzimidazole-2-carboxylic acid (15)
^{1}H NMR (400 MHz, DMSO-*d*$_6$) δ = 10.02 (s, 4H), 7.79 – 7.64 (m, 1H), 7.40 – 7.24 (m, 1H).
^{13}C NMR (101 MHz, DMSO-*d*$_6$) δ = 142.38, 138.47, 122.26, 122.23, 116.42, 115.76.

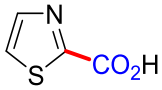

Thiazole-2-carboxylic acid (16)
^{1}H NMR (400 MHz, DMSO-*d*$_6$) δ = 13.67 (s, 1H), 8.12 – 8.08 (m, 2H).
^{13}C NMR (101 MHz, DMSO-*d*$_6$) δ = 154.50, 143.78, 124.67, 120.43.

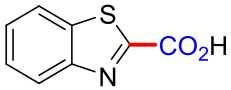

Benzothiazole-2-carboxylic acid (17)
^{1}H NMR (400 MHz, DMSO-*d*$_6$) δ = 9.44 (s, 1H), 8.24 (dt, J = 7.5, 2.4 Hz, 2H), 7.65 (pd, J = 7.2, 1.6 Hz, 2H).
^{13}C NMR (101 MHz, DMSO-*d*$_6$) δ = 156.52, 153.43, 134.00, 126.63, 125.93, 123.46, 122.94.

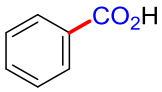

Benzoic acid (18)
^{1}H NMR (400 MHz, DMSO-*d*$_6$) δ = 12.98 (s, 1H), 7.99 (dd, J = 8.0, 1.6 Hz, 2H), 7.68 – 7.59 (m, 1H), 7.52 (t, J = 7.6 Hz, 2H).
^{13}C NMR (101 MHz, DMSO-*d*$_6$) δ = 167.80, 133.29, 131.23, 129.72, 129.00.

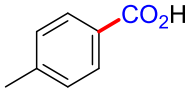

4-Methylbenzoic acid (19)
^{1}H NMR (400 MHz, DMSO-*d*$_6$) δ = 12.77 (s, 1H), 7.84 (dt, J = 8.1, 1.8 Hz, 2H), 7.29 (d, J = 7.7 Hz, 2H), 2.36 (d, J = 2.9 Hz, 3H).
^{13}C NMR (101 MHz, DMSO-*d*$_6$) δ = 167.77, 143.47, 129.79, 129.56, 128.50, 21.59, 21.56.

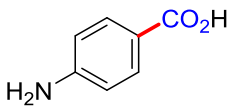

4-Aminobenzoic acid (20)

^{1}H NMR (400 MHz, DMSO-*d*$_6$) δ = 11.93 (s, 1H), 8.29 – 7.55 (m, 2H), 7.10 – 6.52 (m, 2H), 5.85 (s, 2H).
^{13}C NMR (101 MHz, DMSO-*d*$_6$) δ = 167.95, 153.59, 131.67, 117.39, 113.04.

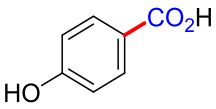

4-Hydroxybenzoic acid (21)
^{1}H NMR (400 MHz, DMSO-*d*$_6$) δ = 12.39 (s, 1H), 10.21 (s, 1H), 8.17 – 7.66 (m, 2H), 7.19 – 6.66 (m, 2H).
^{13}C NMR (101 MHz, DMSO-*d*$_6$) δ = 167.62, 162.06, 131.98, 121.84, 115.58.

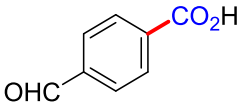

4-Formylbenzoic acid (22)
^{1}H NMR (400 MHz, DMSO-*d*$_6$) δ = 13.33 (s, 1H), 10.11 (d, J = 2.4 Hz, 1H), 8.35 – 7.96 (m, 4H).
^{13}C NMR (101 MHz, DMSO-*d*$_6$) δ = 193.45, 167.04, 139.35, 136.19, 130.38, 130.00.

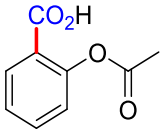

2-Acetylsalicylic acid (23)
^{1}H NMR (400 MHz, DMSO-*d*$_6$) δ = 13.06 (s, 1H), 7.93 (dd, J = 7.8, 1.8 Hz, 1H), 7.66 – 7.60 (m, 1H), 7.38 (td, J = 7.6, 1.2 Hz, 1H), 7.20 (dd, J = 8.0, 1.1 Hz, 1H), 2.25 (s, 3H).
^{13}C NMR (101 MHz, DMSO-*d*$_6$) δ = 169.64, 166.08, 150.65, 134.24, 131.83, 126.53, 124.54, 124.24, 21.31.

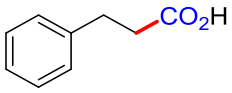

3-Phenylpropanoic acid (24)
^{1}H NMR (400 MHz, DMSO-*d*$_6$) δ = 12.11 (s, 1H), 8.08 – 6.47 (m, 5H), 2.82 (s, 1H), 2.54 (d, J = 7.7 Hz, 1H).
^{13}C NMR (101 MHz, DMSO-*d*$_6$) δ = 174.20, 141.34, 128.75, 128.68, 126.42, 35.69, 30.81.

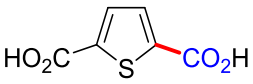

2,5-Thiophenedicarboxylic acid (25)
^{1}H NMR (400 MHz, DMSO-*d*$_6$) δ = 13.51 (s, 2H), 7.79 – 7.68 (m, 2H).
^{13}C NMR (101 MHz, DMSO-*d*$_6$) δ = 162.86, 140.24, 133.64.

Copies of ^{1}H and ^{13}C NMR spectra for compounds

^{1}H NMR and ^{13}C NMR of **1**

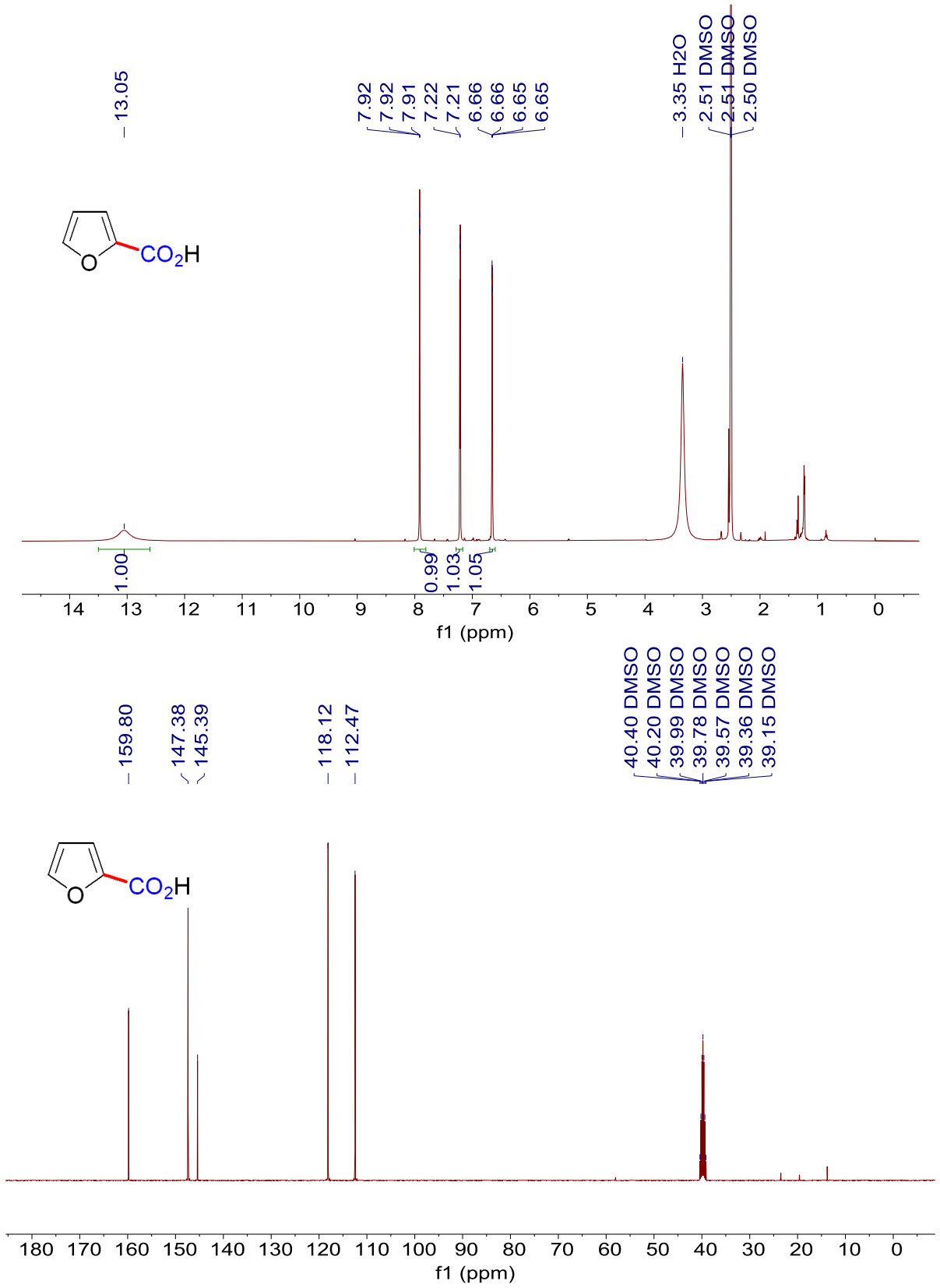

^{1}H NMR and ^{13}C NMR of **2**

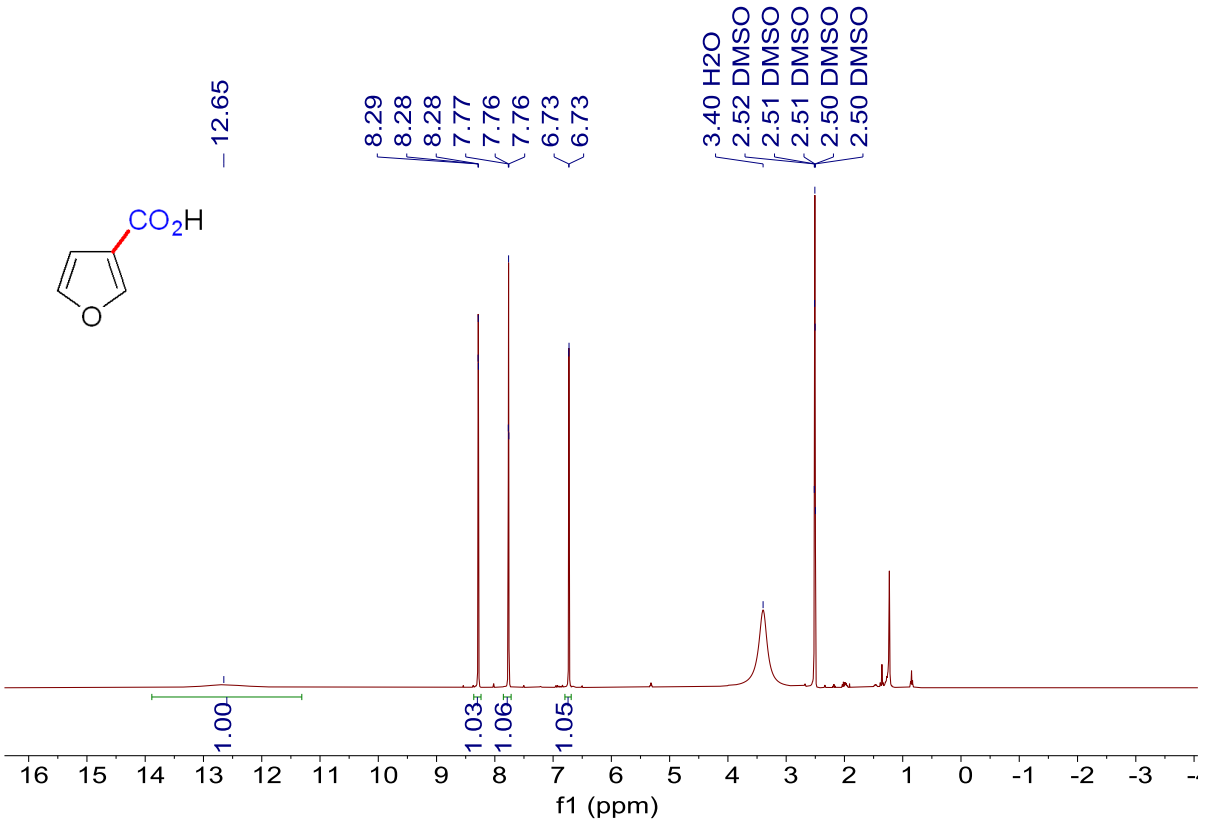

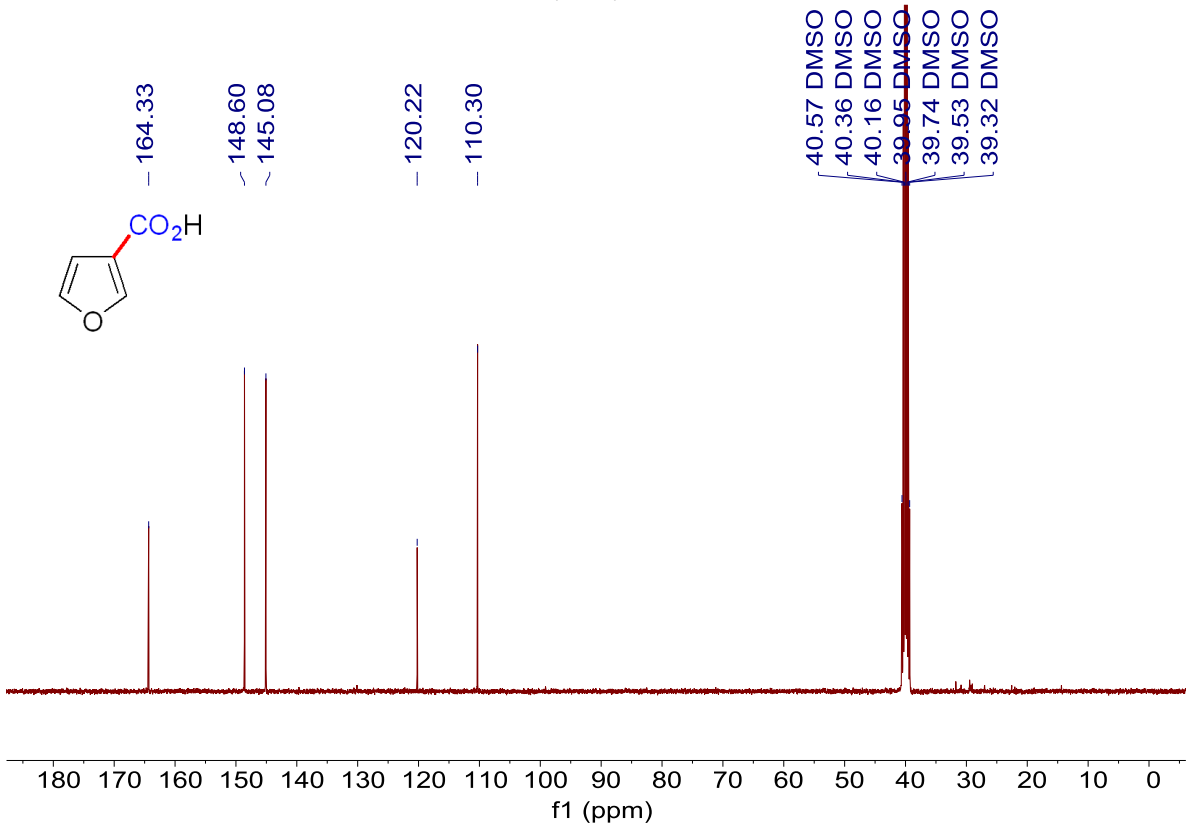

^{1}H NMR and ^{13}C NMR of **3**

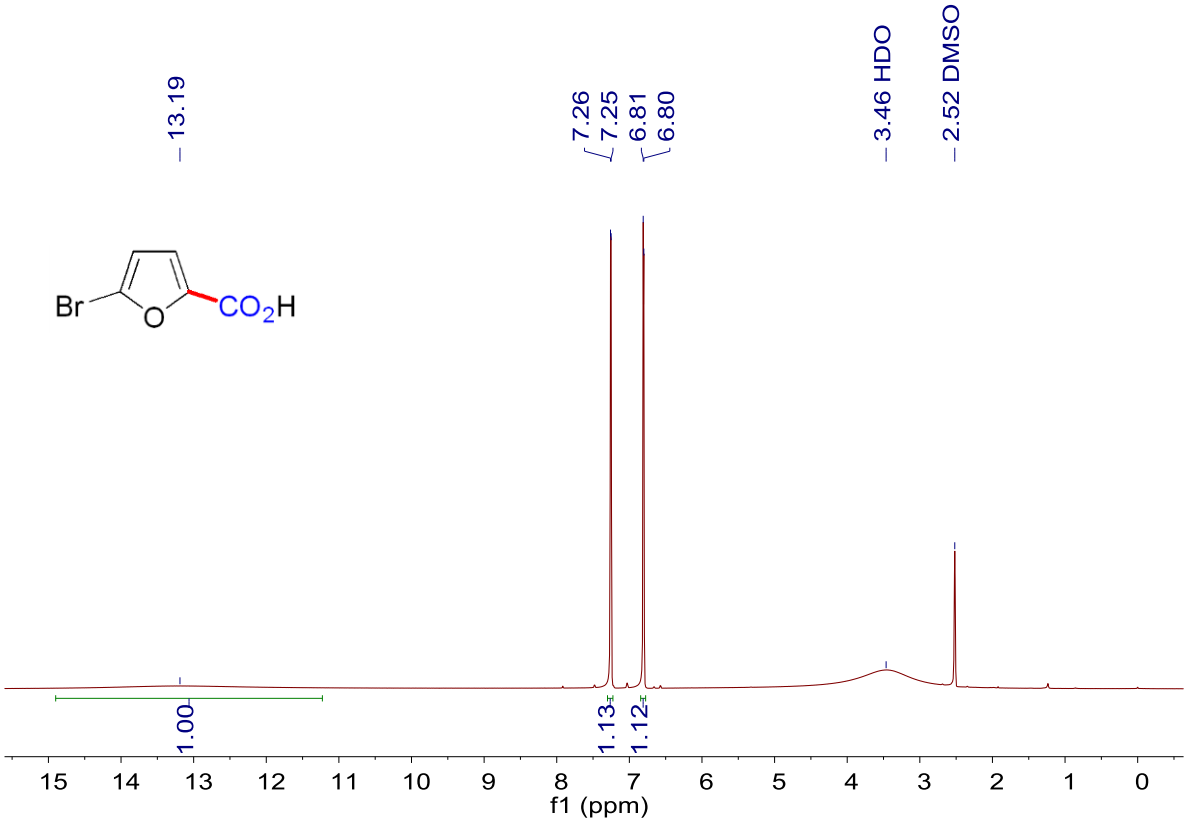

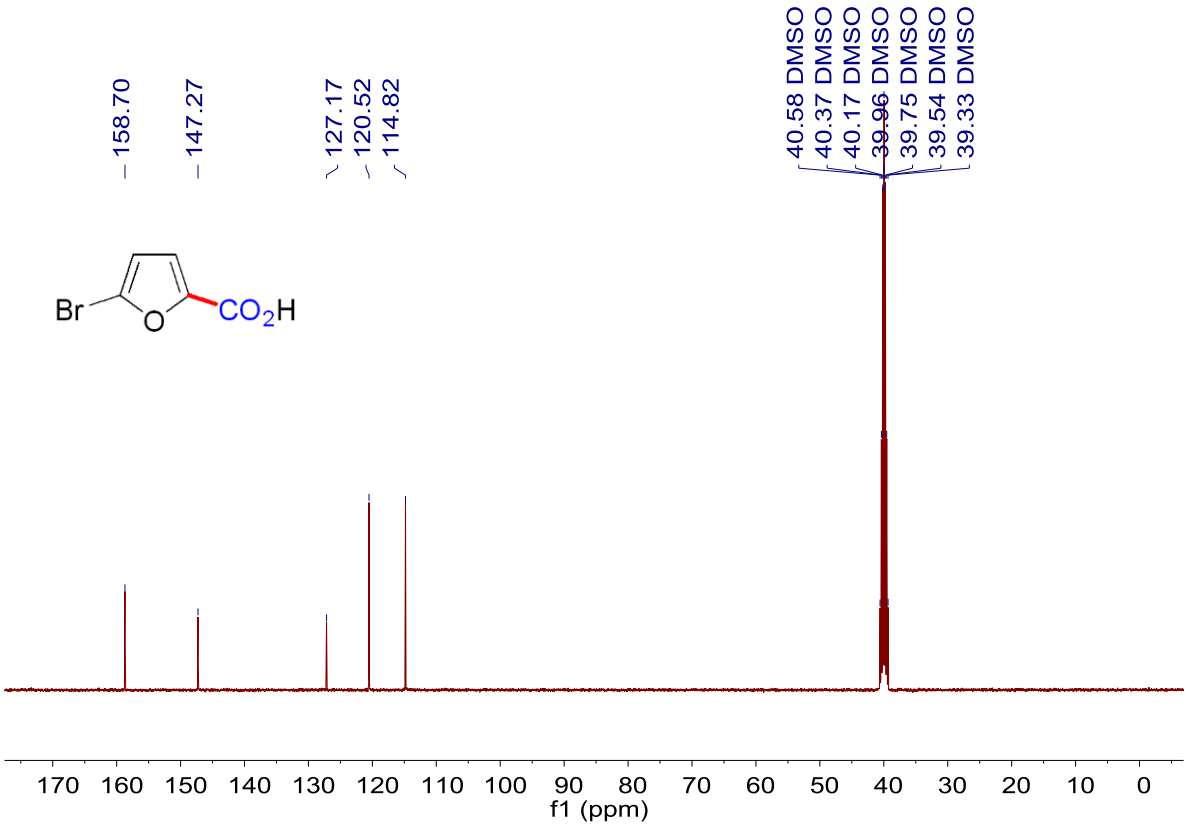

^{1}H NMR and ^{13}C NMR of **4**

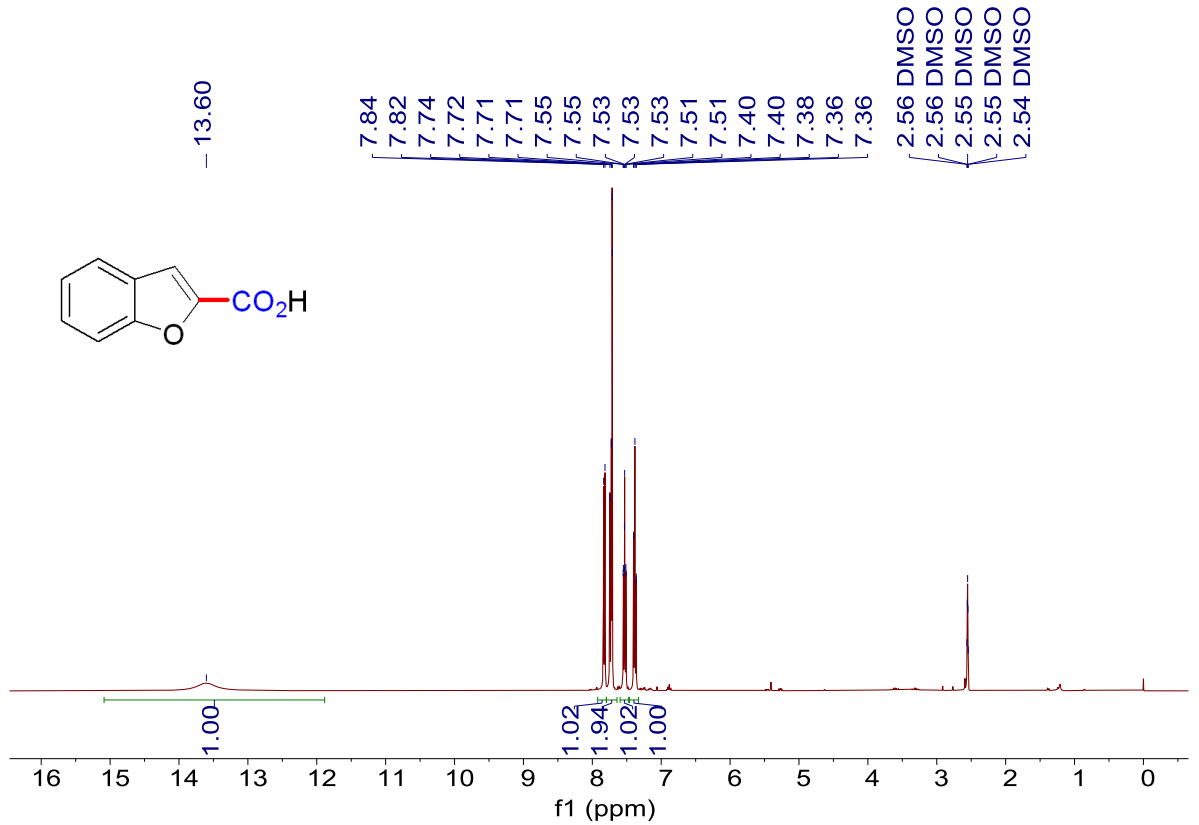

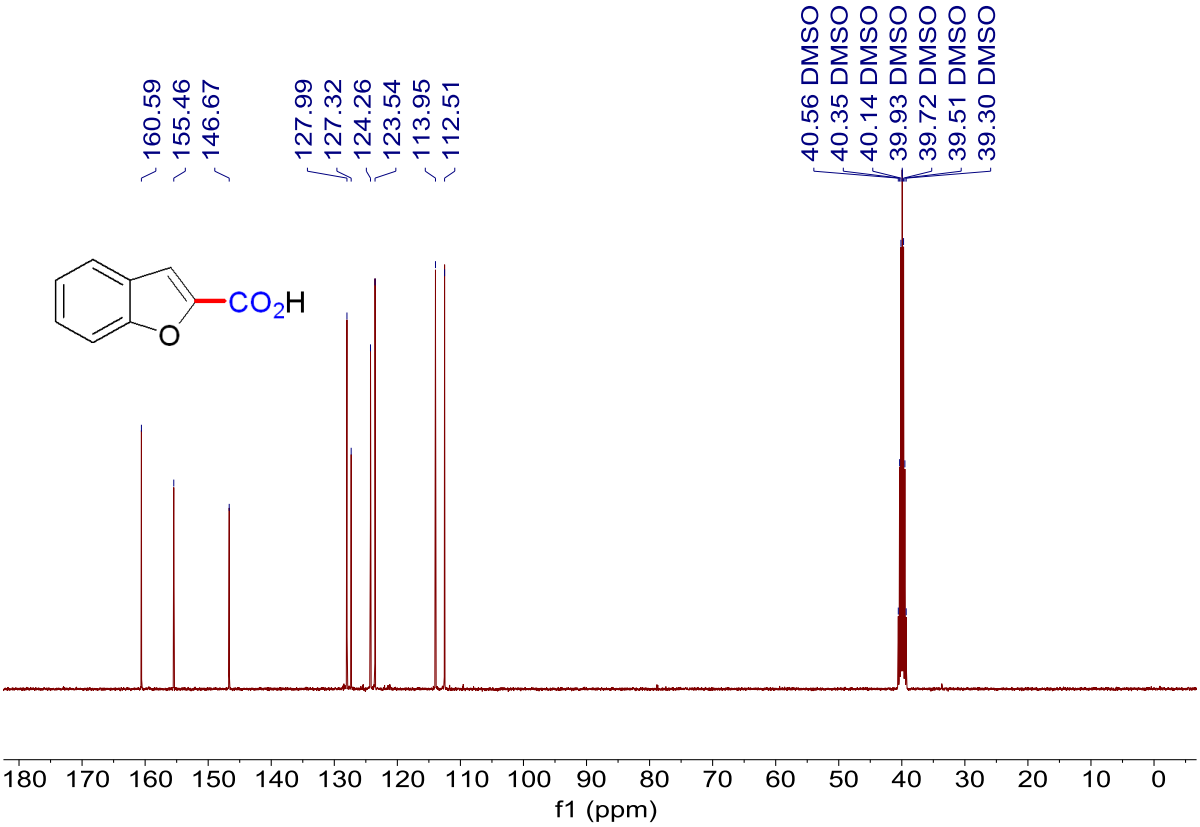

^{1}H NMR and ^{13}C NMR of **5**

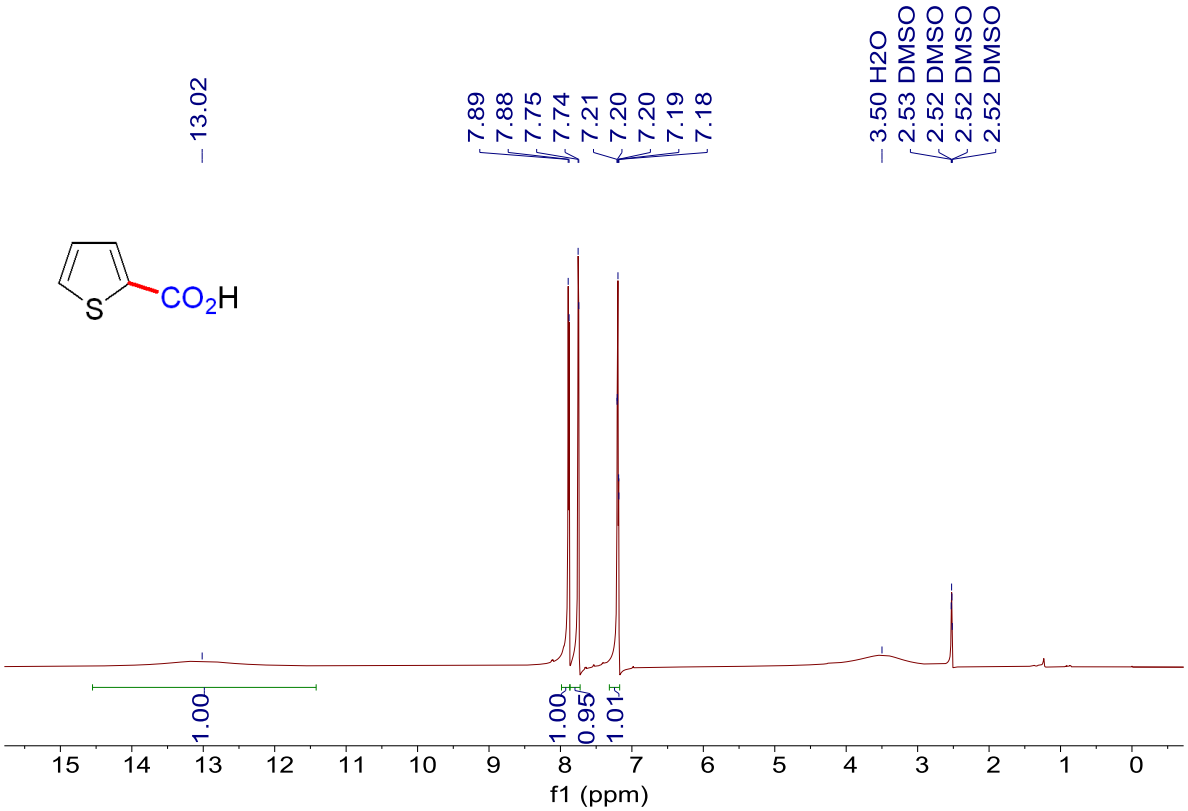

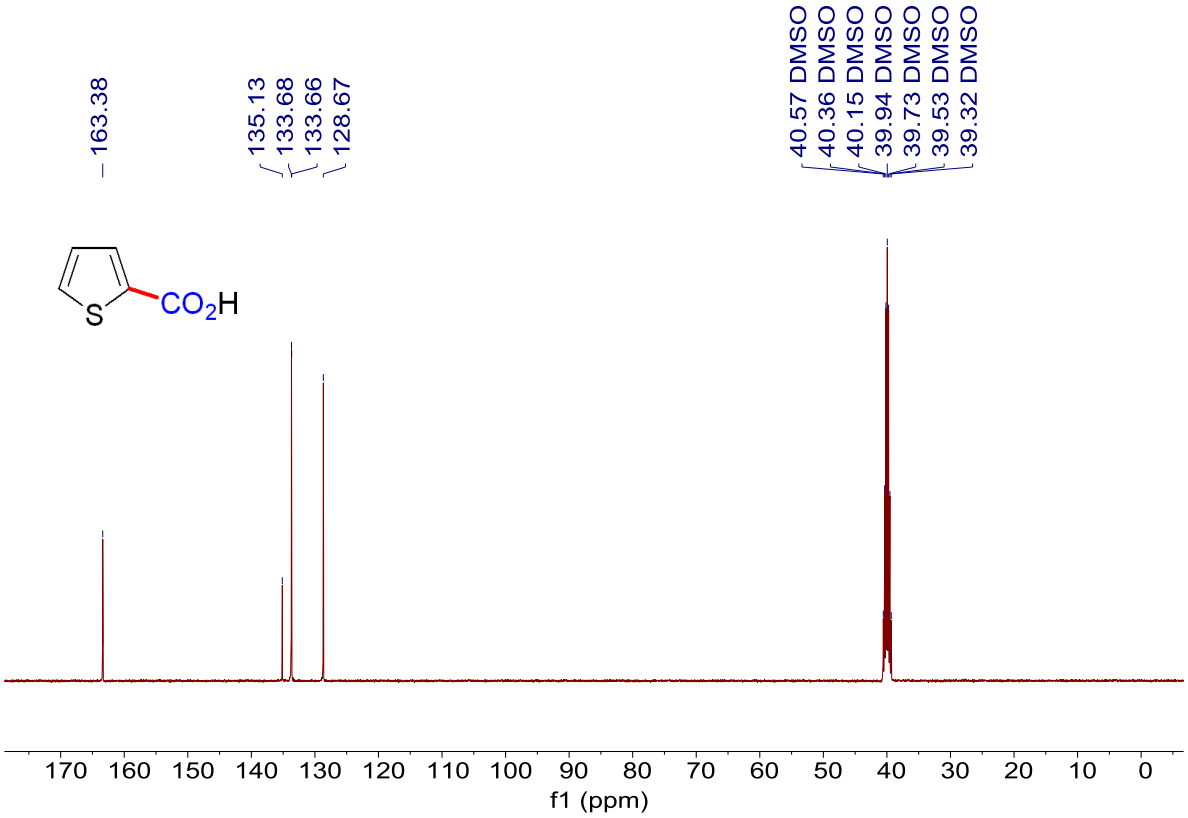

^{1}H NMR and ^{13}C NMR of **6**

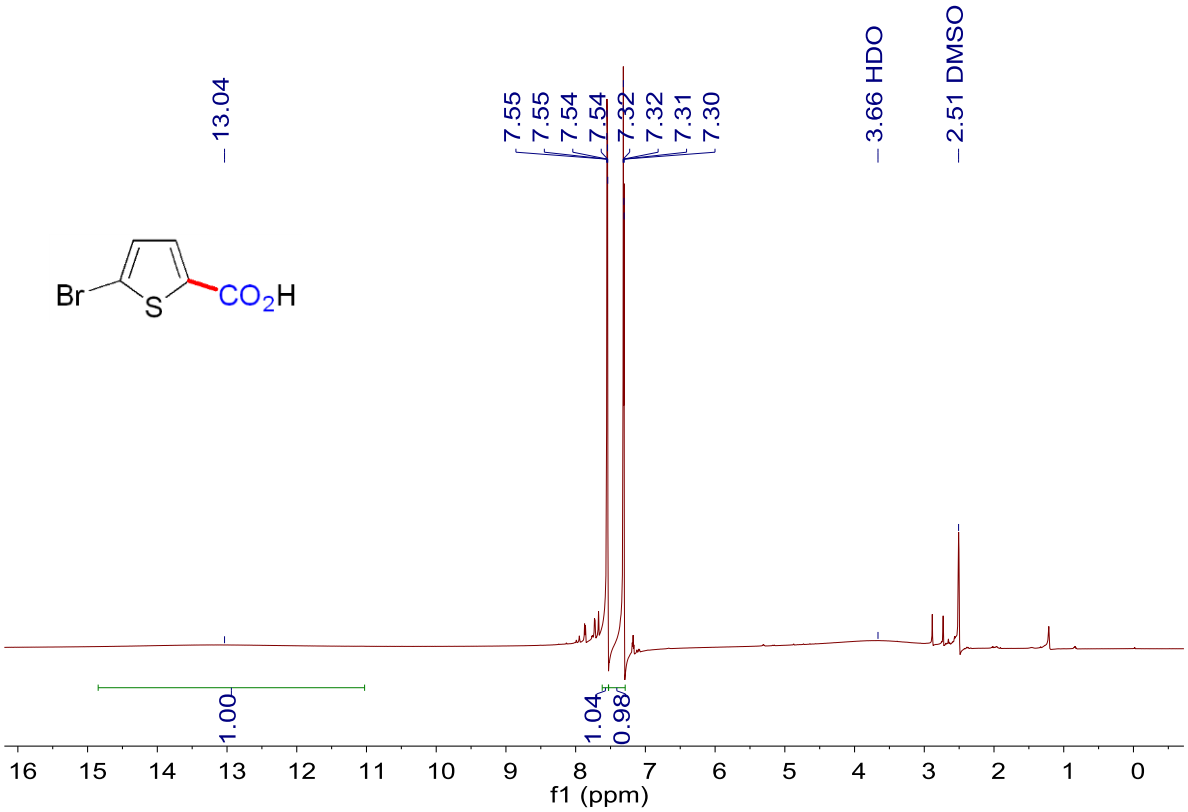

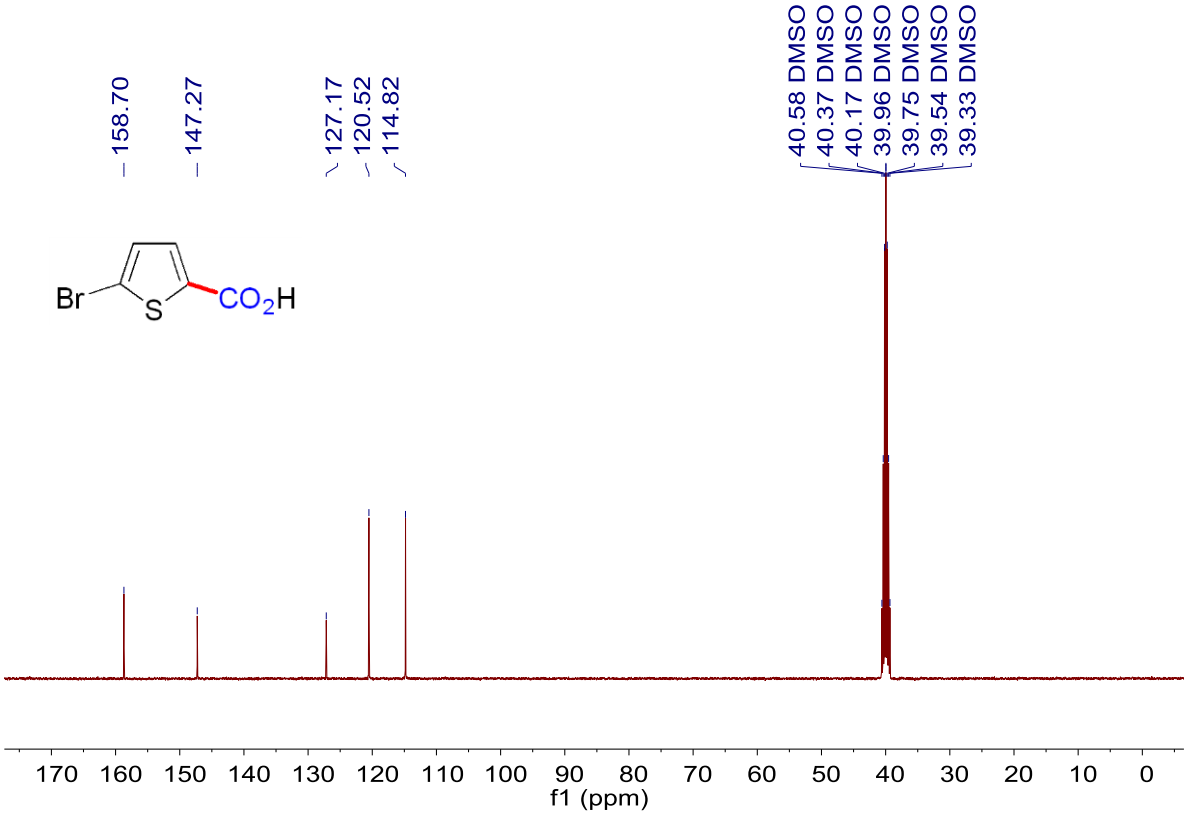

^{1}H NMR and ^{13}C NMR of **7**

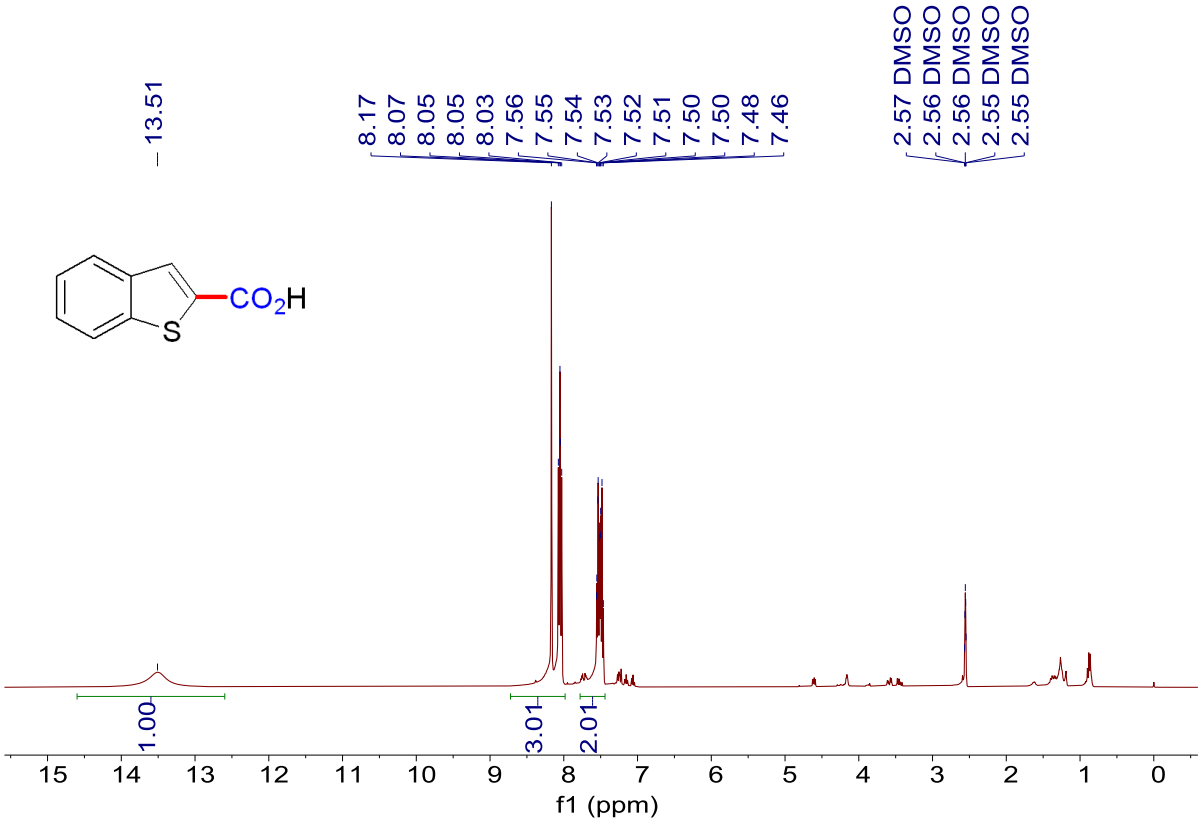

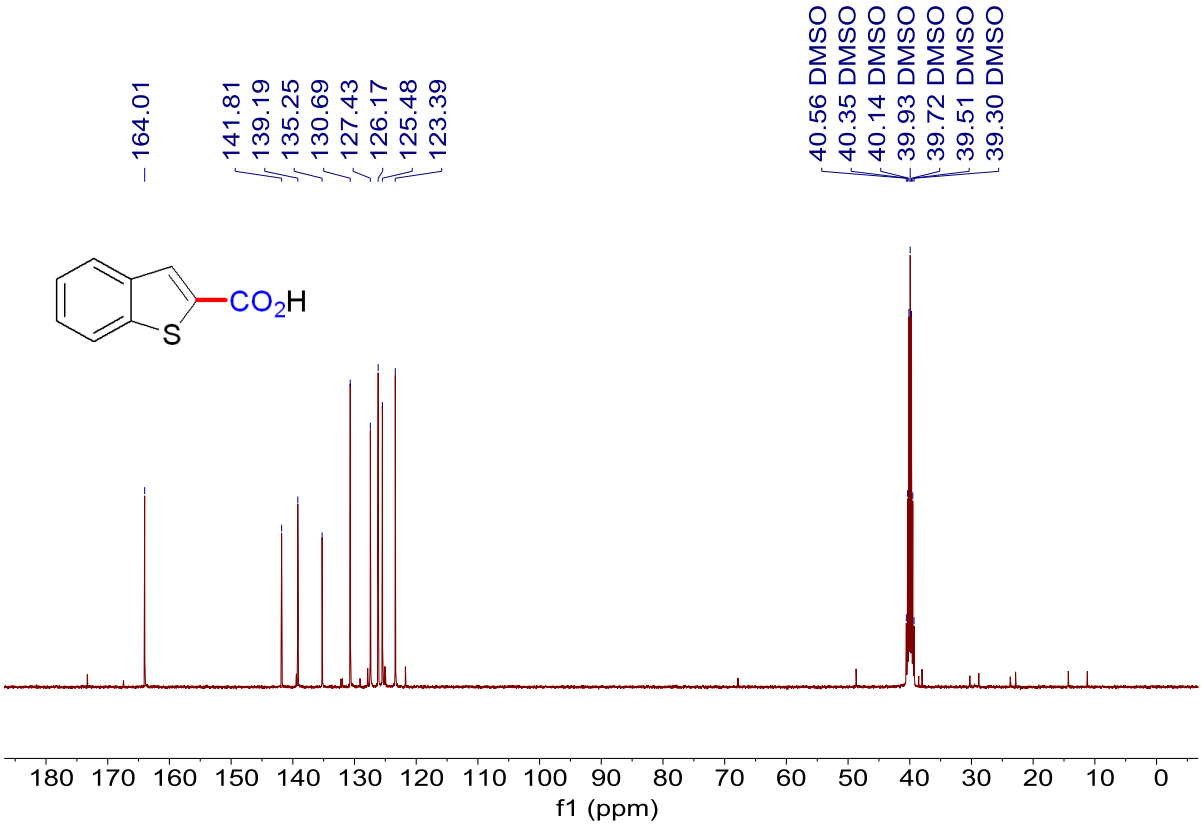

^{1}H NMR and ^{13}C NMR of **8**

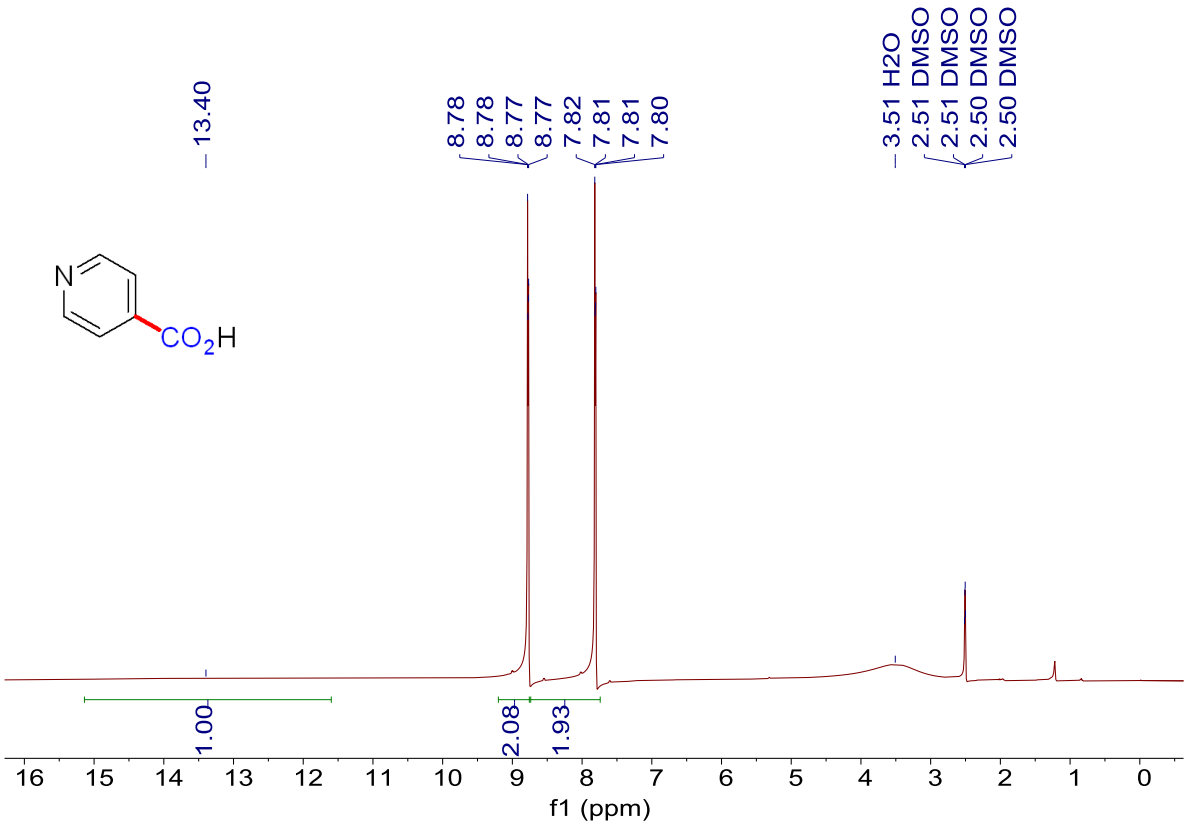

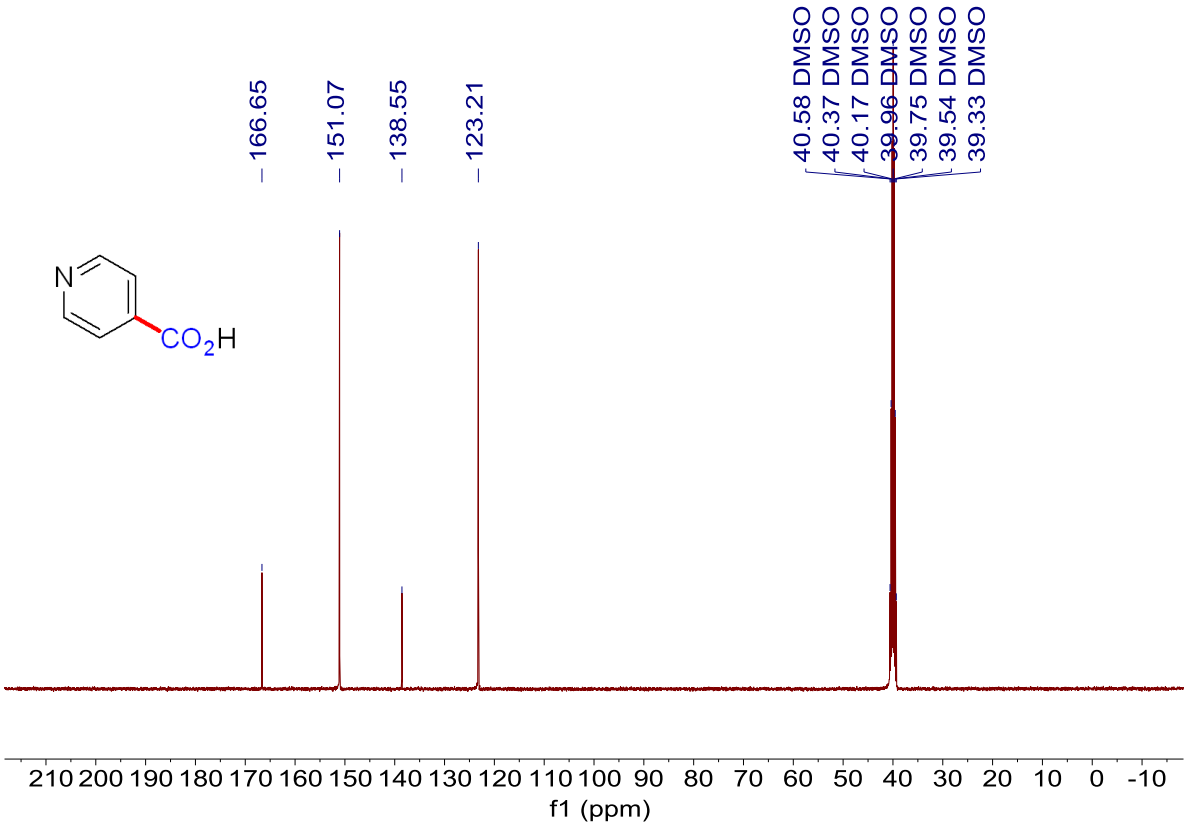

^{1}H NMR and ^{13}C NMR of **9**

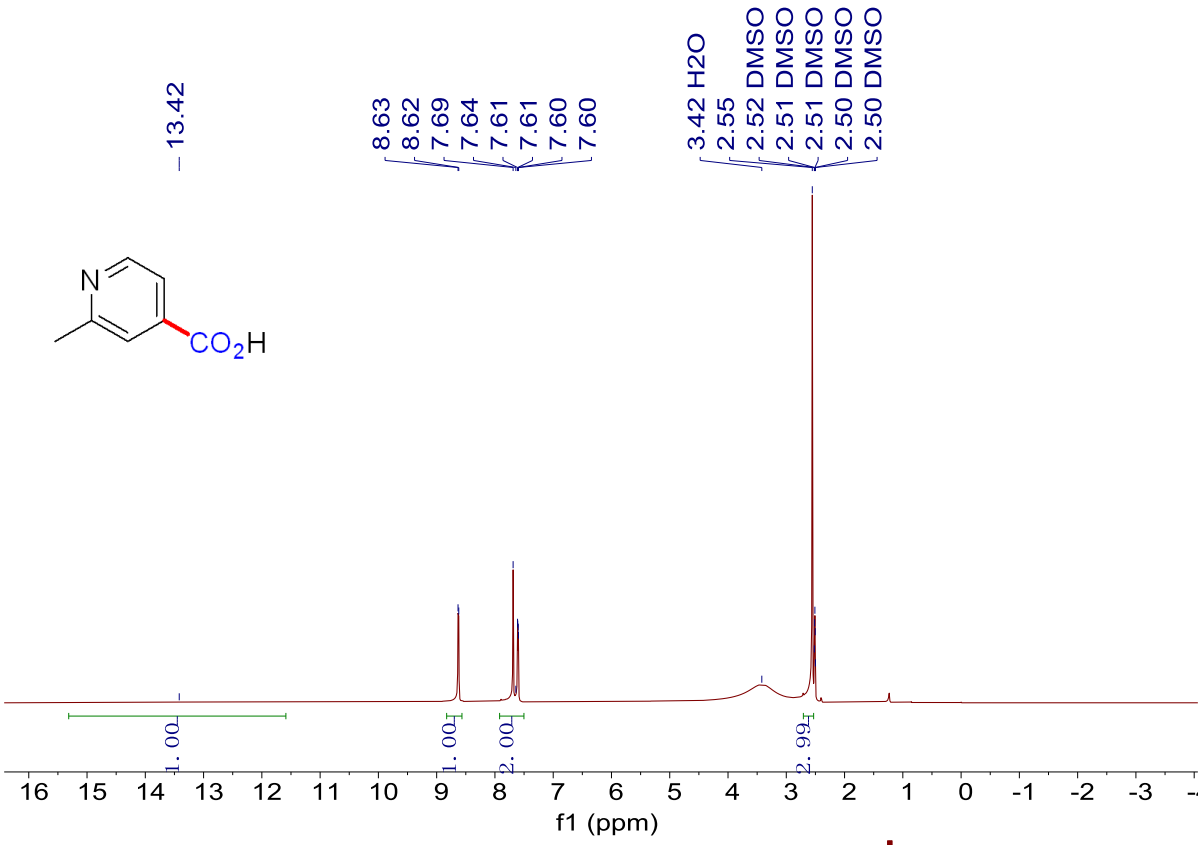

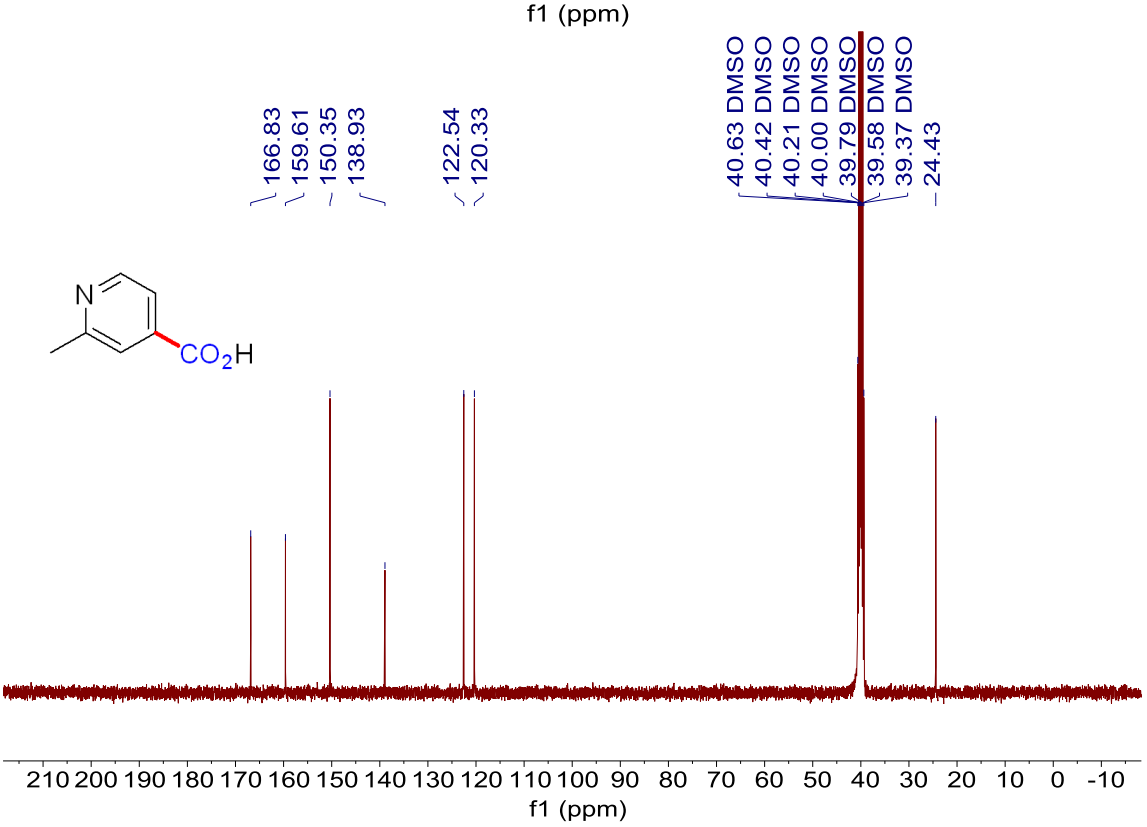

^{1}H NMR and ^{13}C NMR of **10**

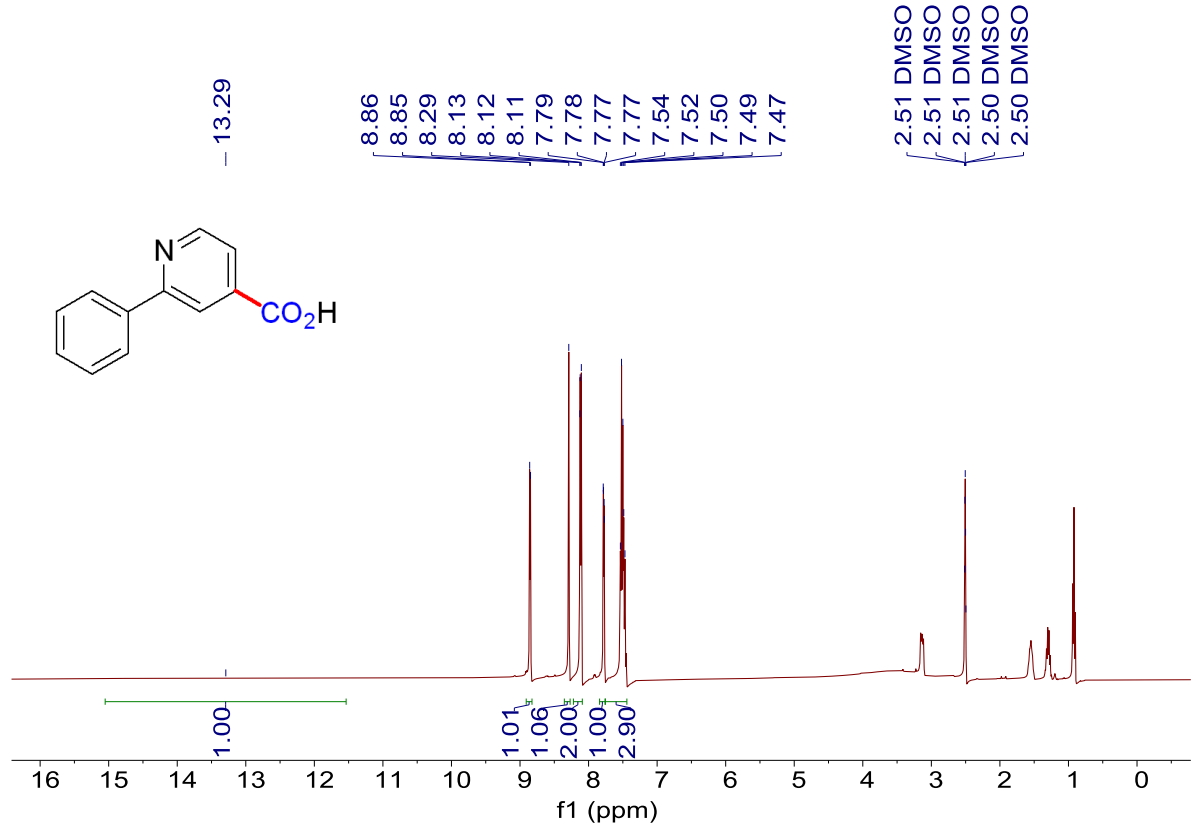

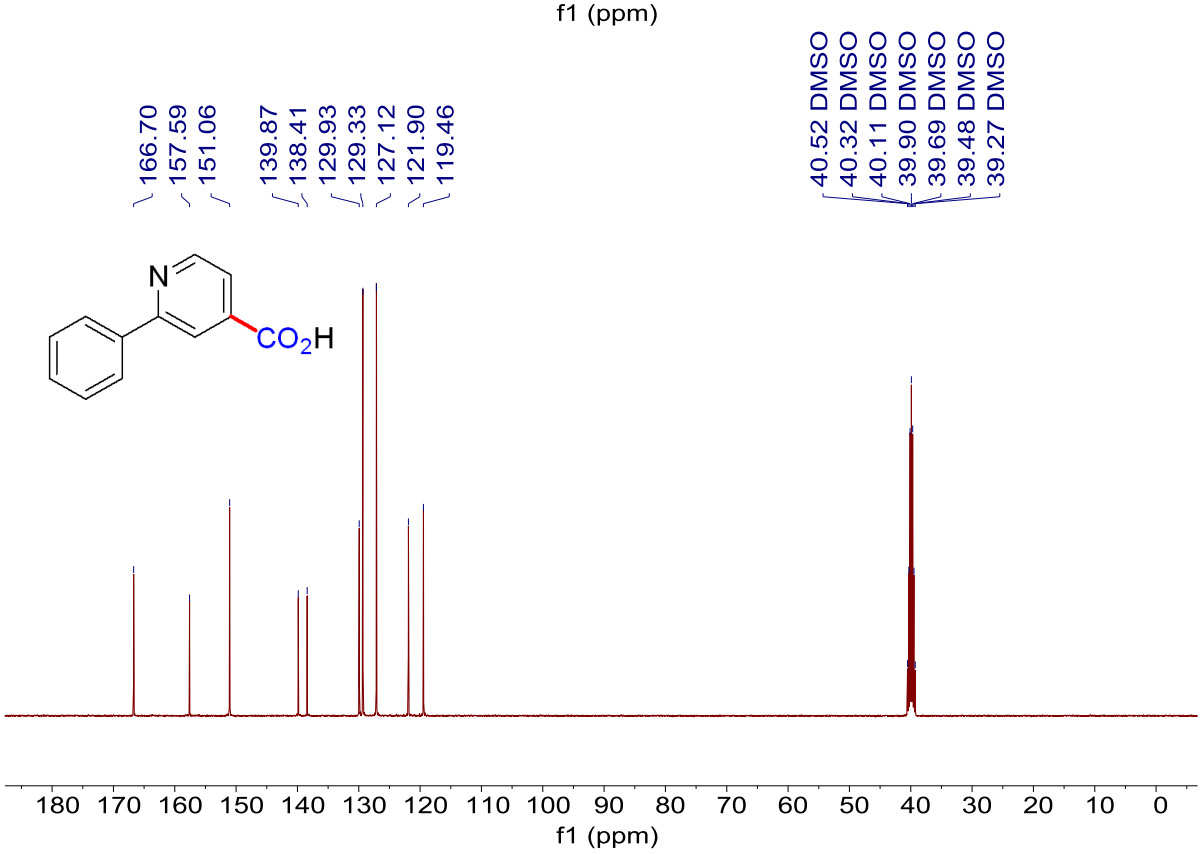

^{1}H NMR and ^{13}C NMR of **11**

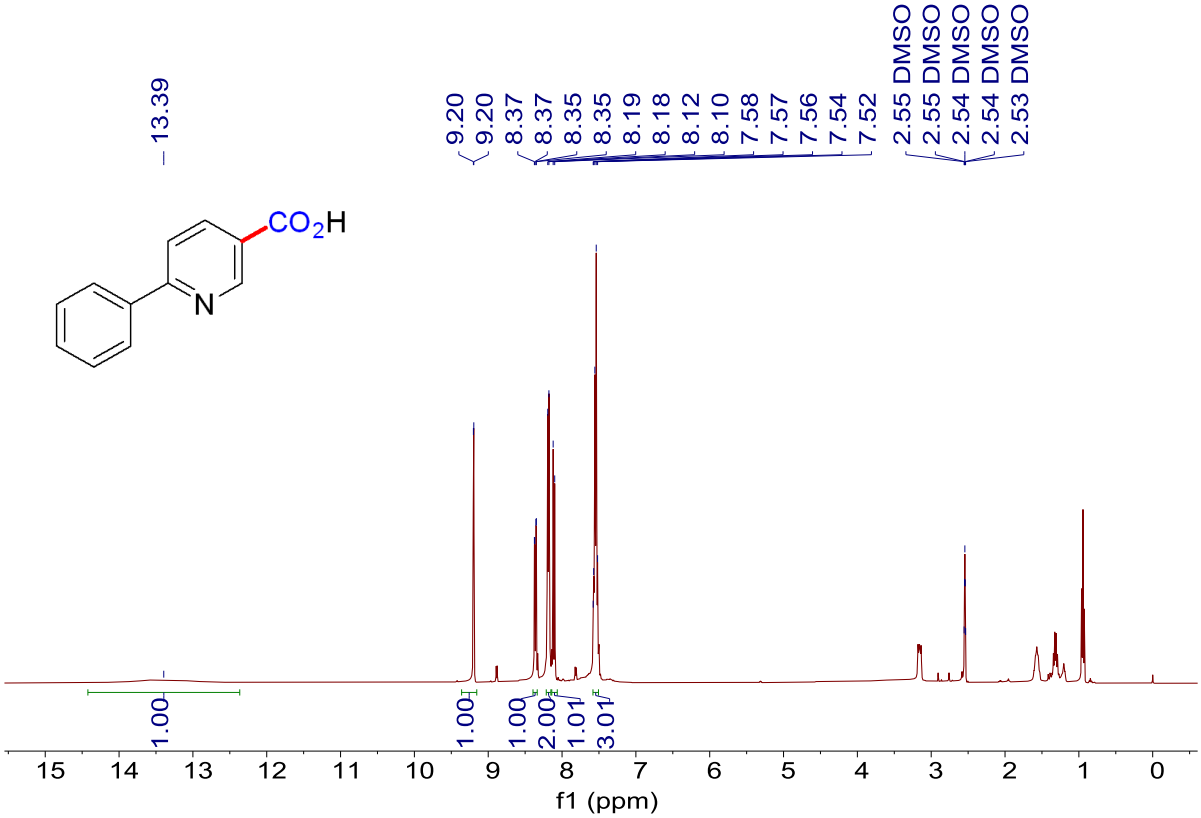

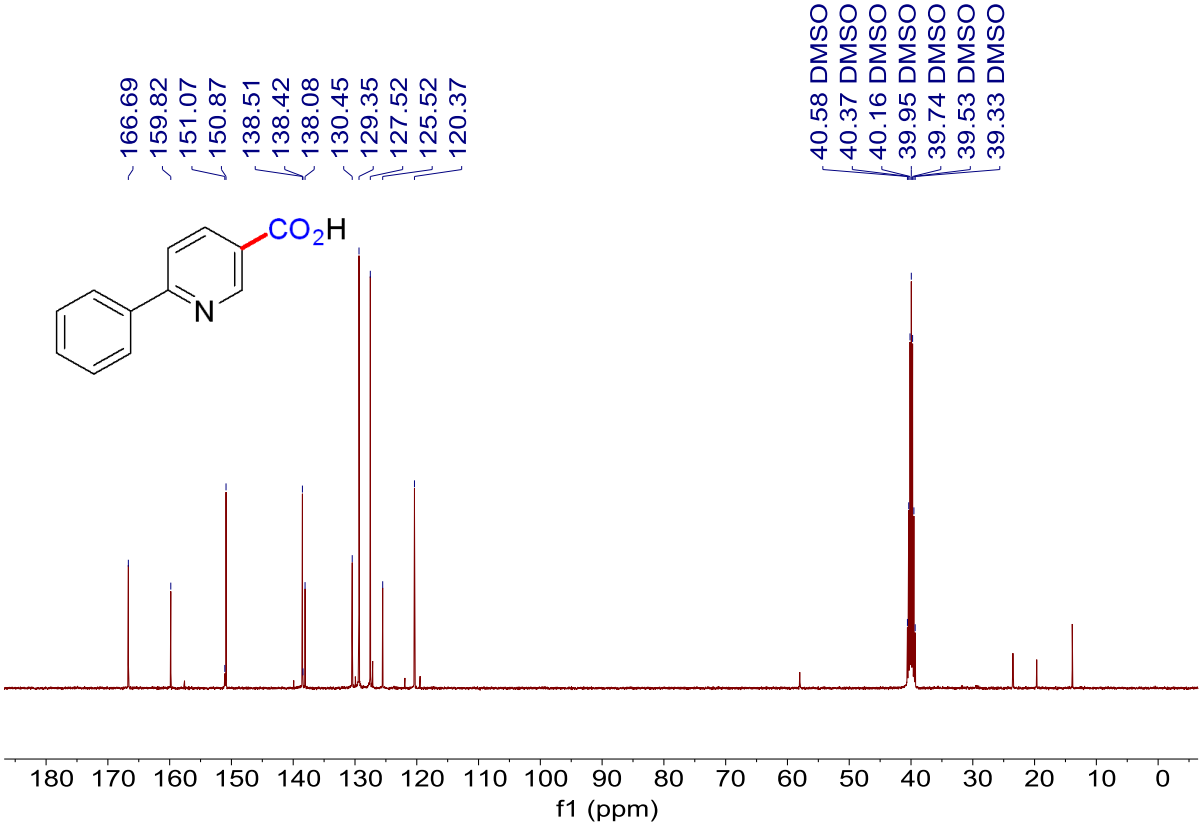

^{1}H NMR and ^{13}C NMR of **12**

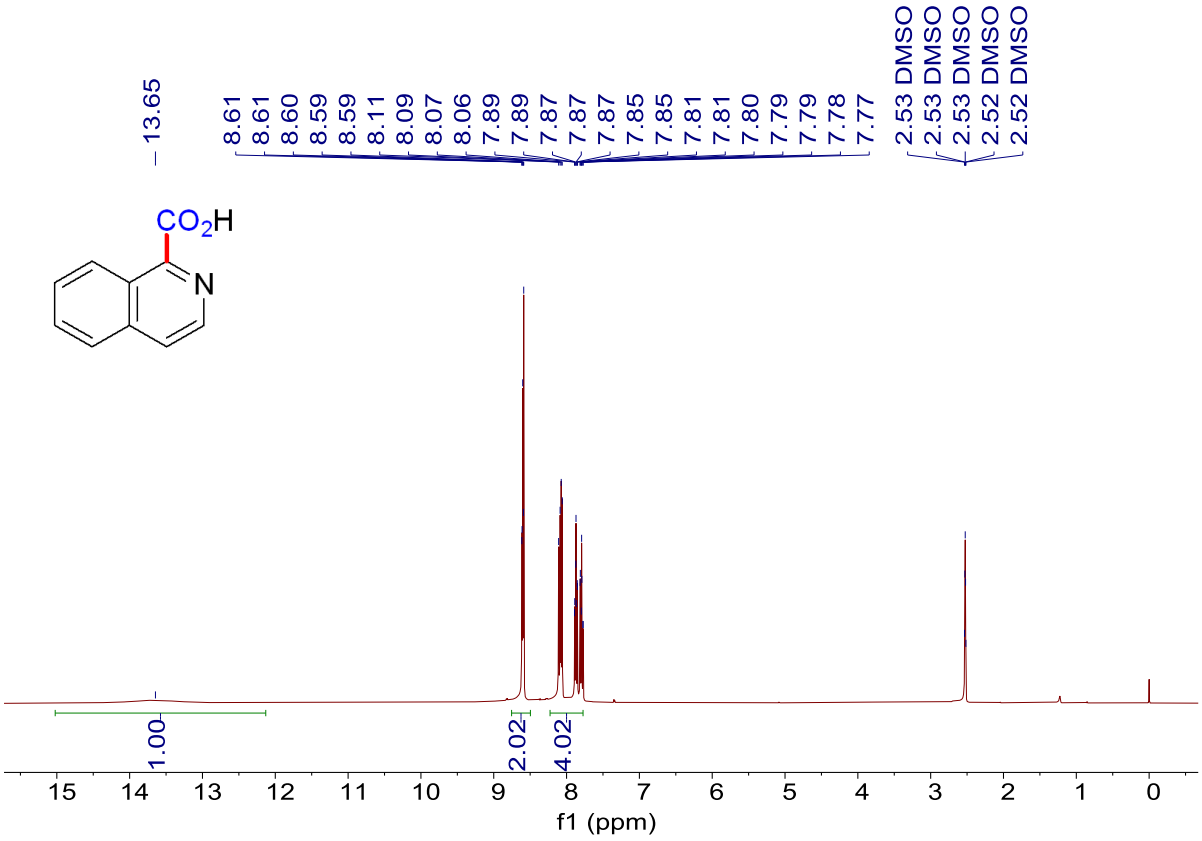

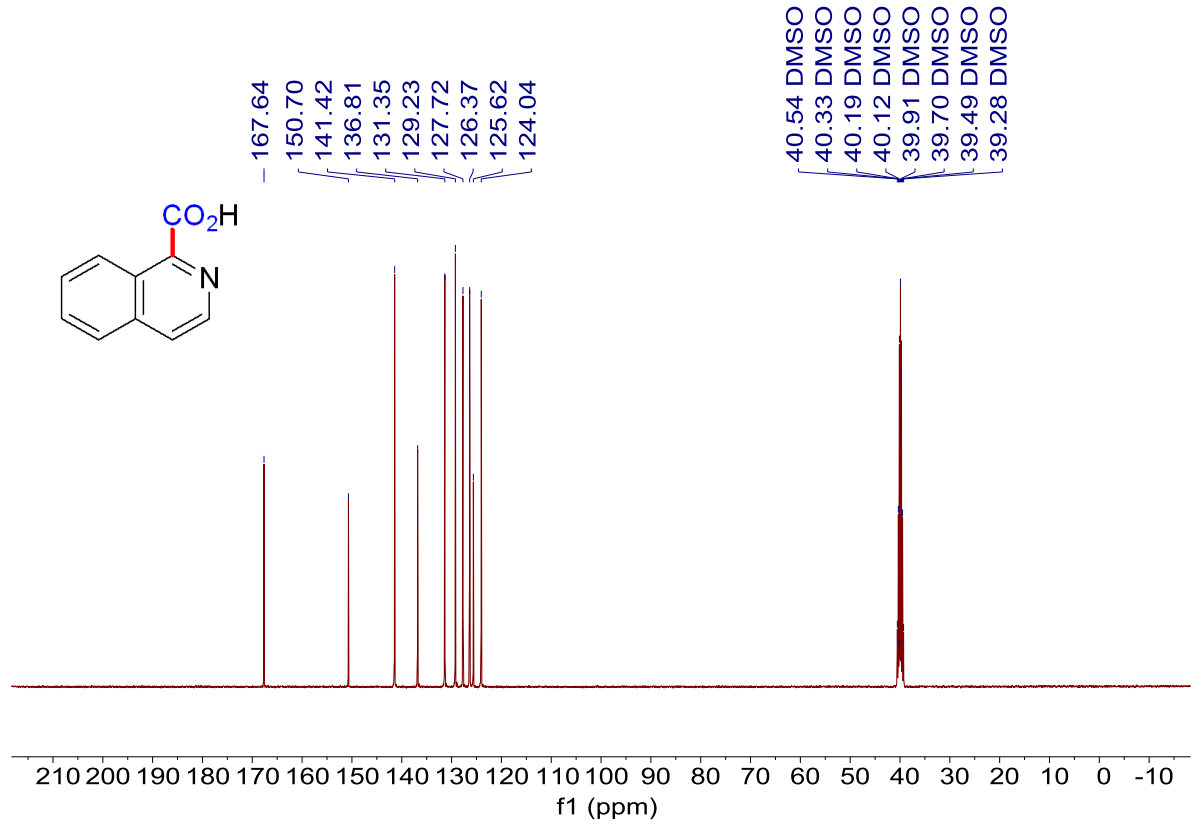

^{1}H NMR and ^{13}C NMR of **13**

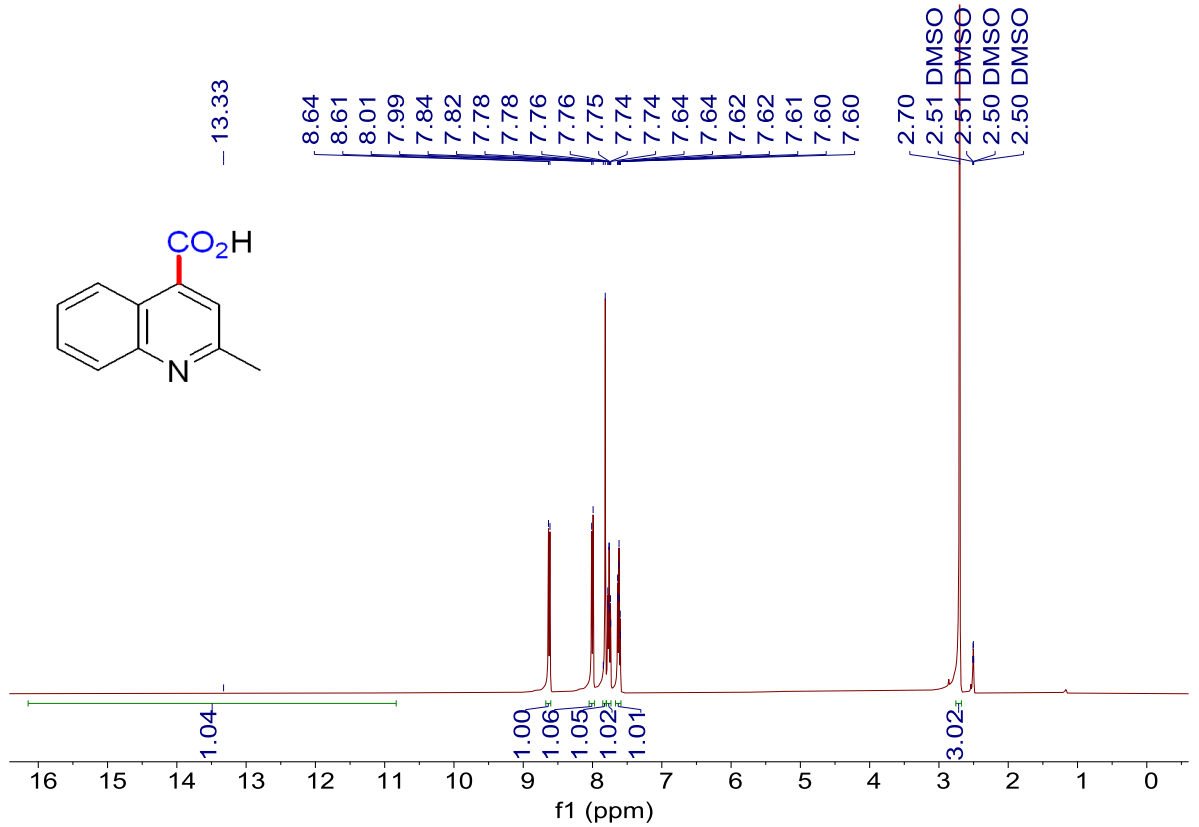

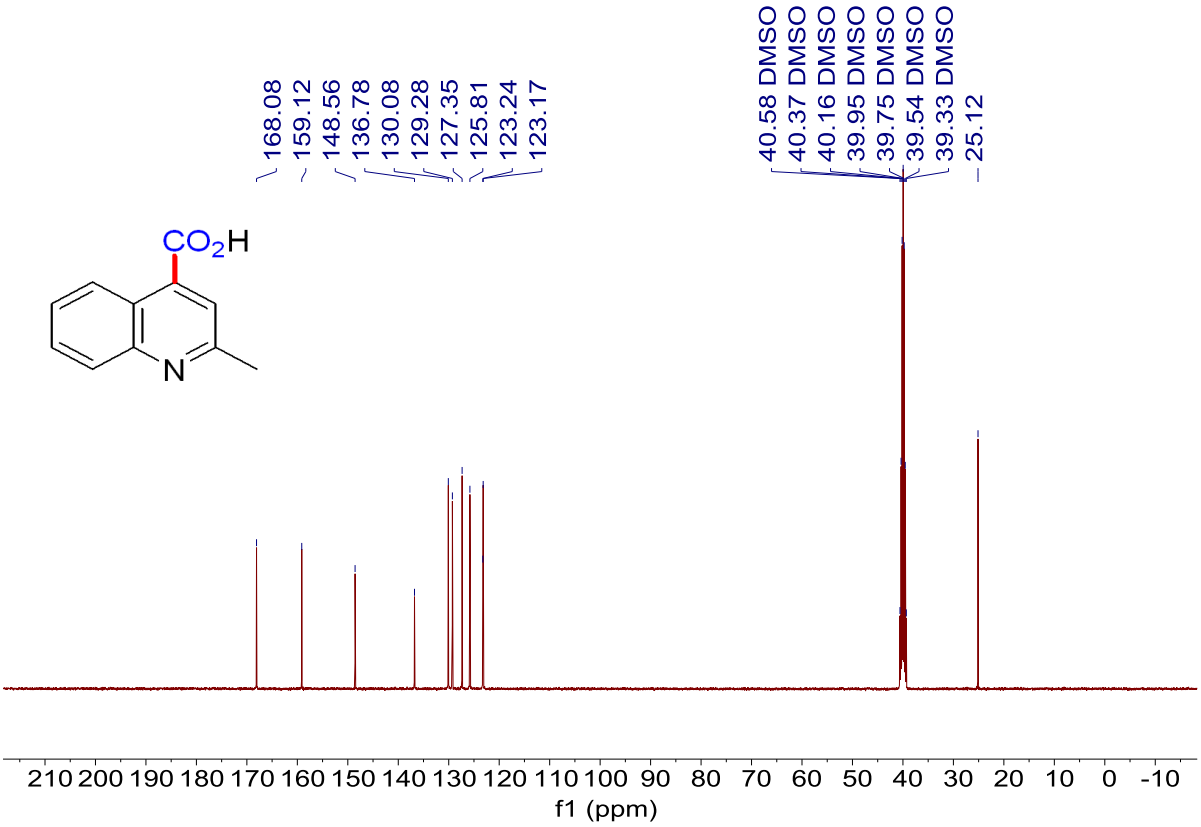

^{1}H NMR and ^{13}C NMR of **14**

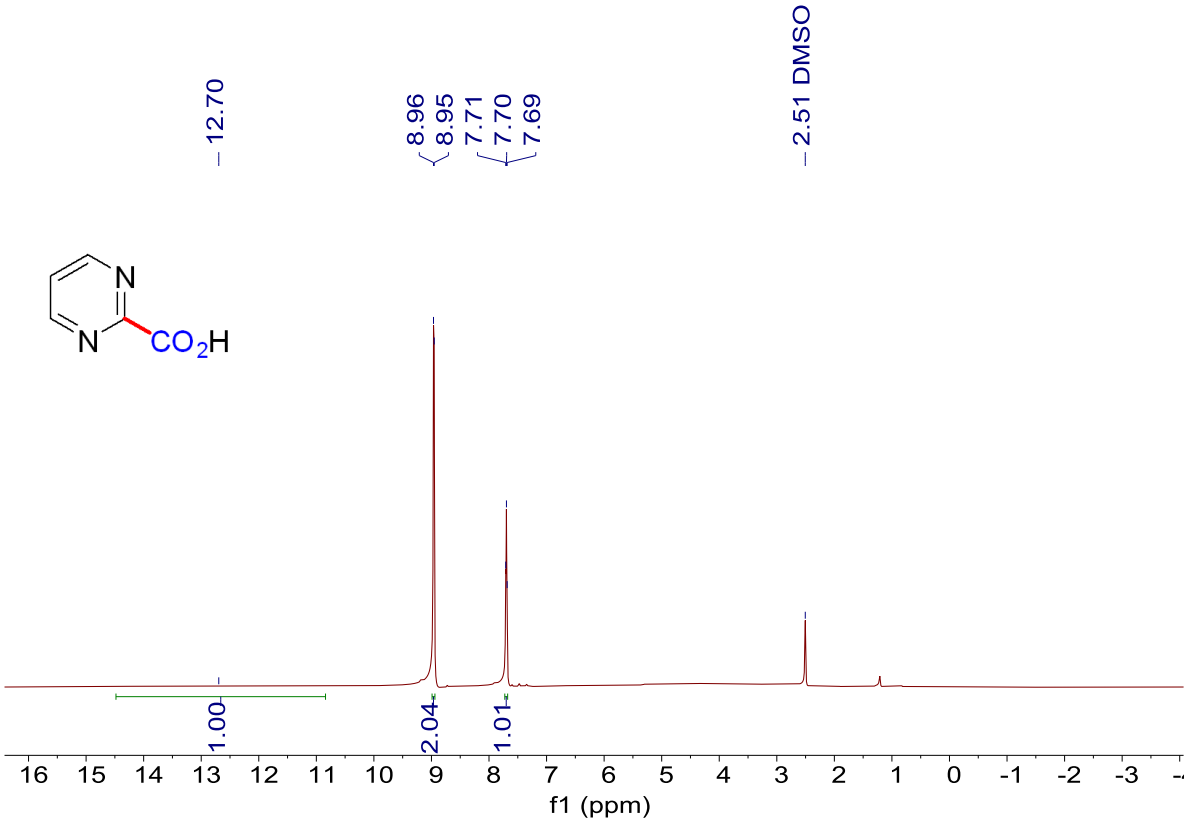

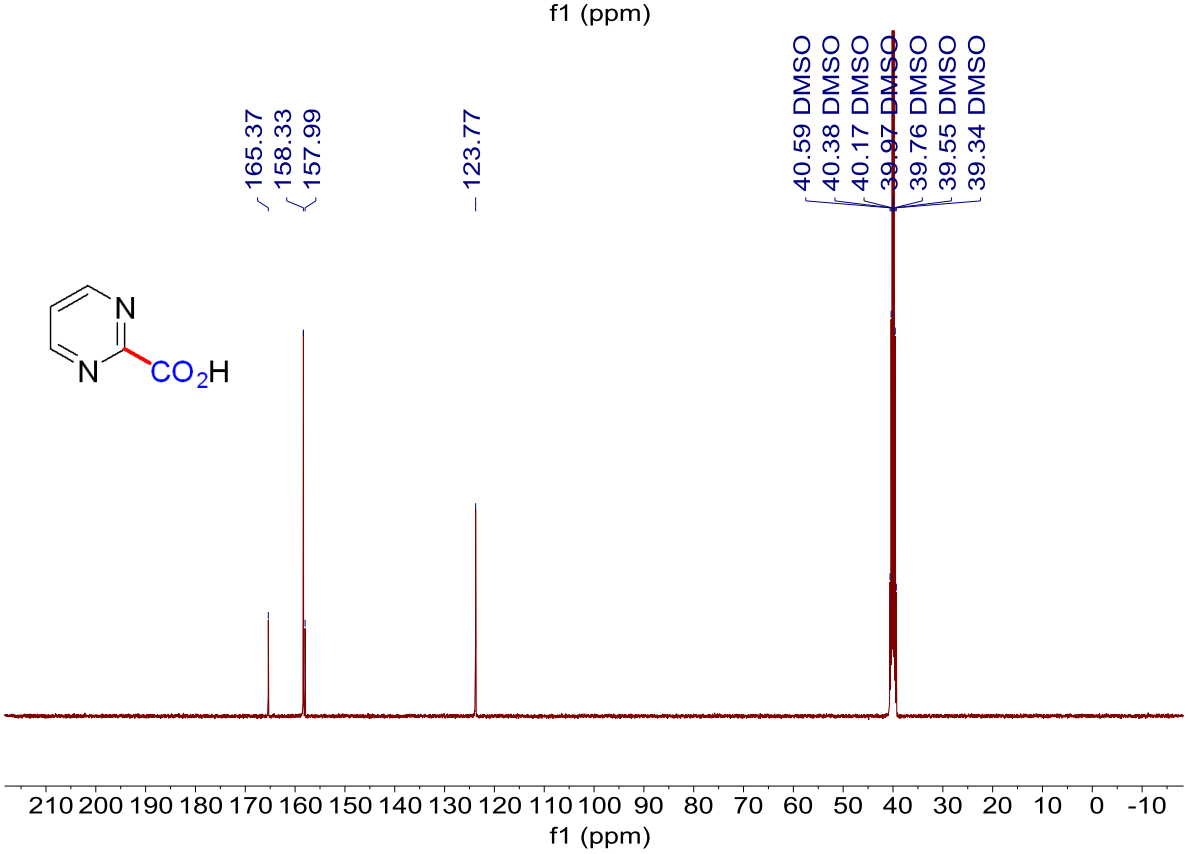

^{1}H NMR and ^{13}C NMR of **15**

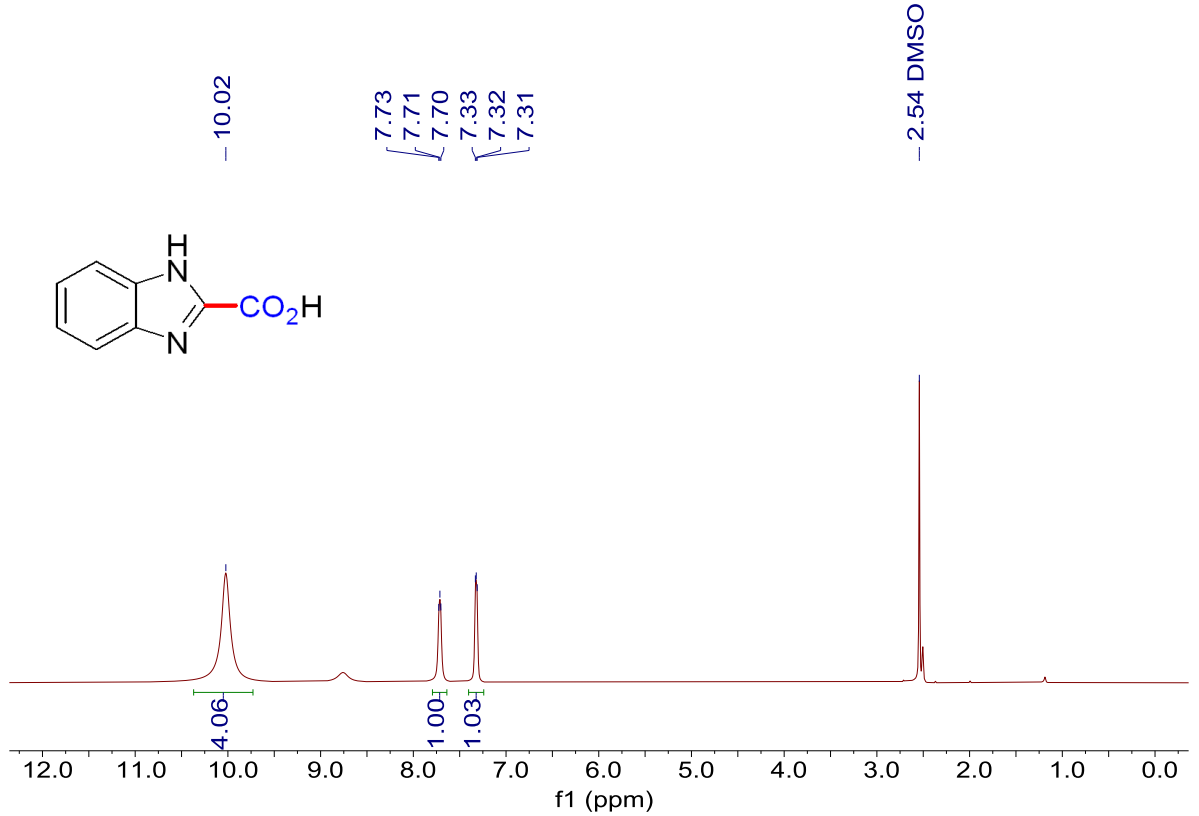

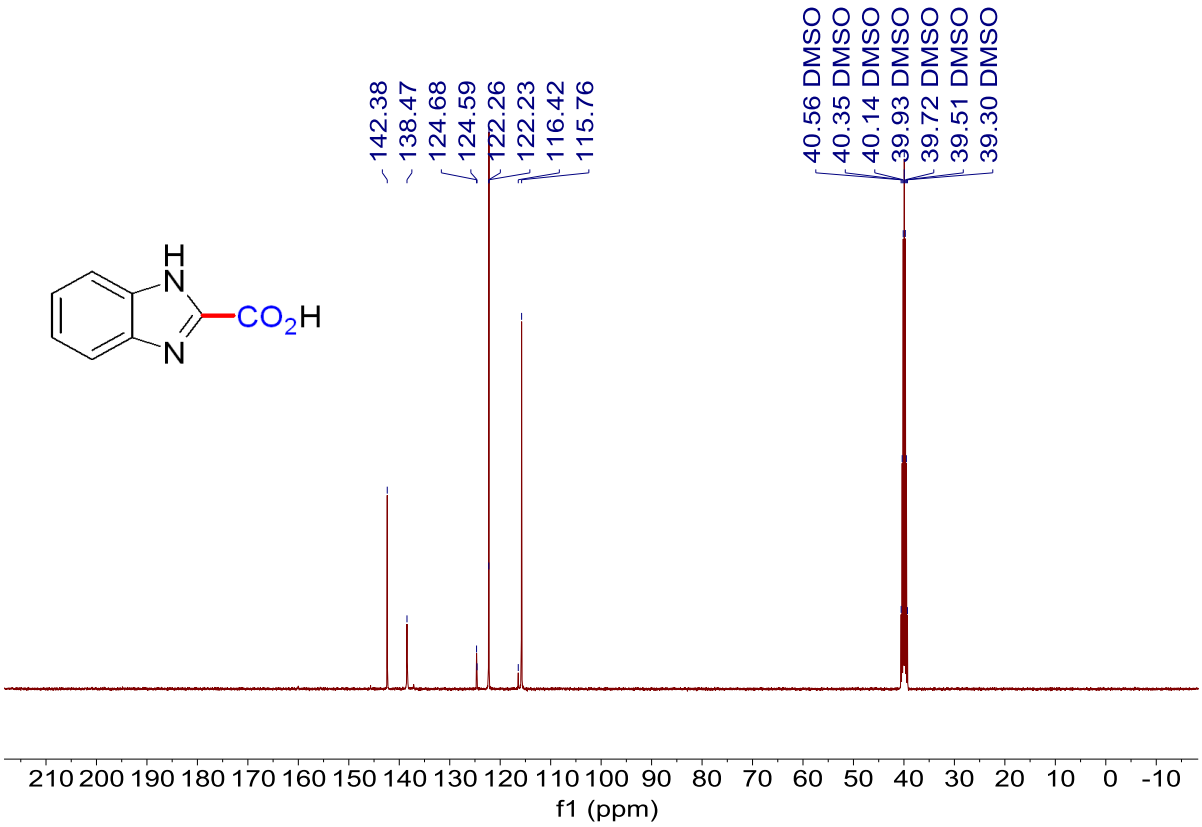

^{1}H NMR and ^{13}C NMR of **16**

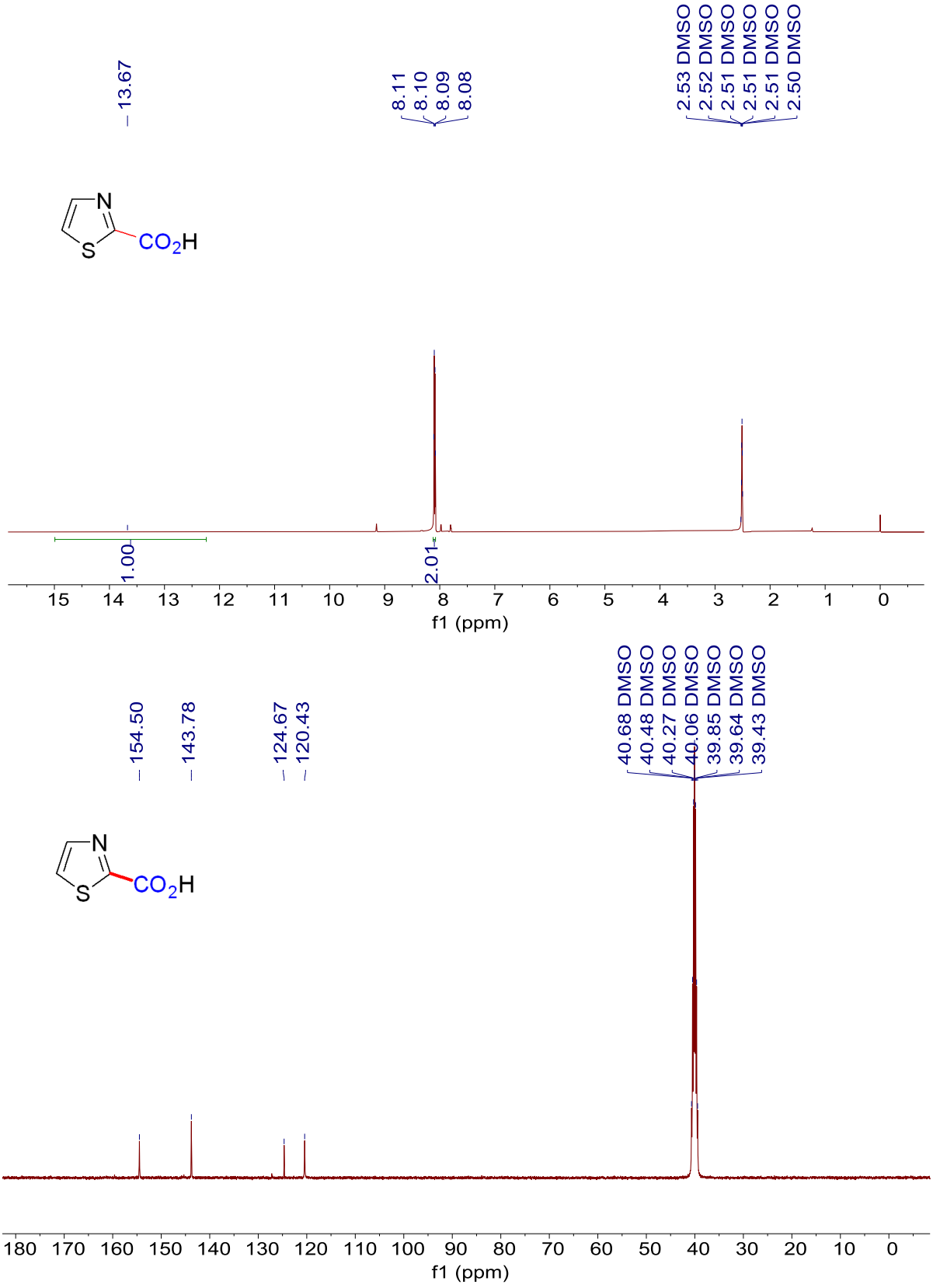

^{1}H NMR and ^{13}C NMR of **17**

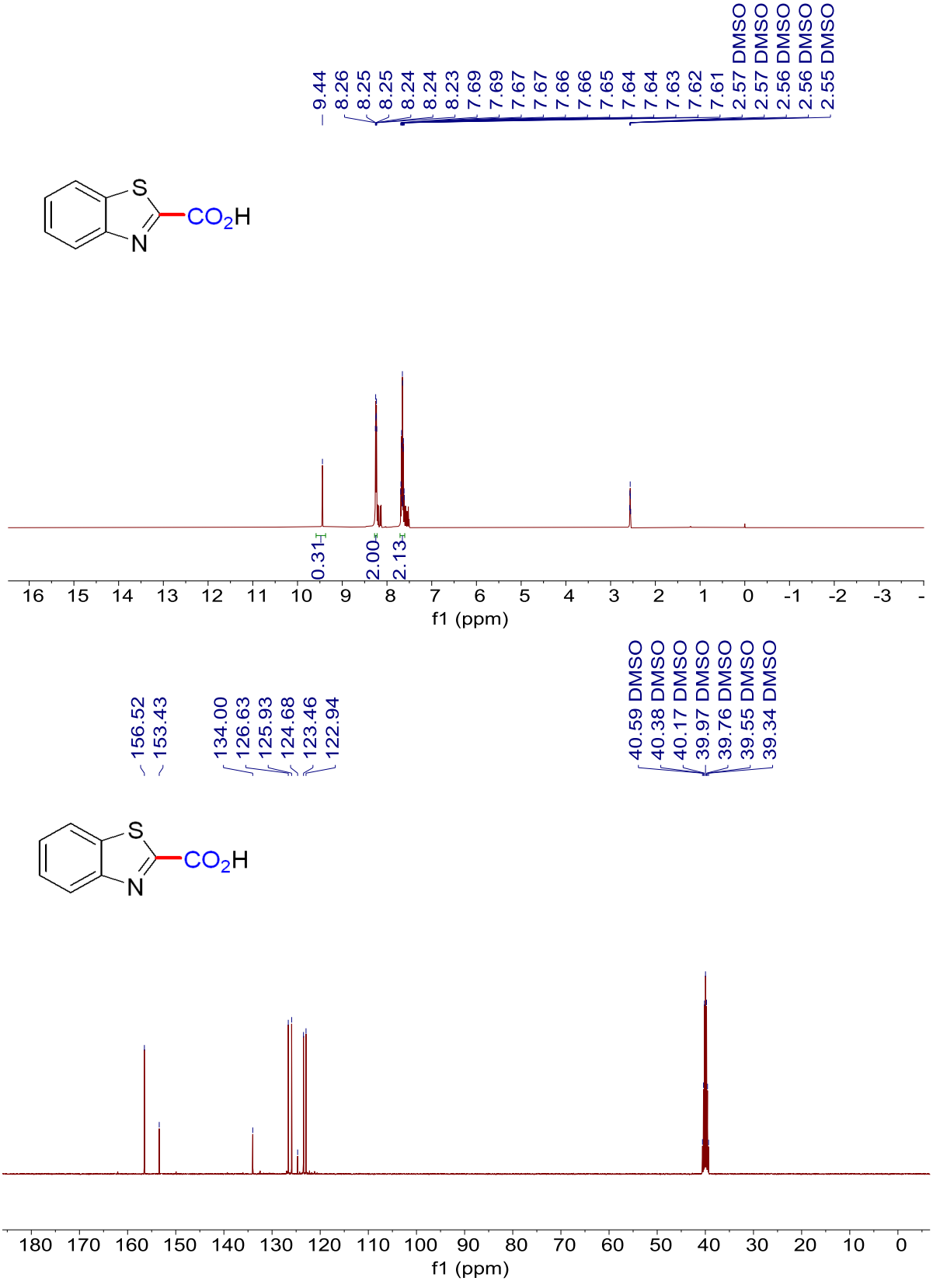

^{1}H NMR and ^{13}C NMR of **18**

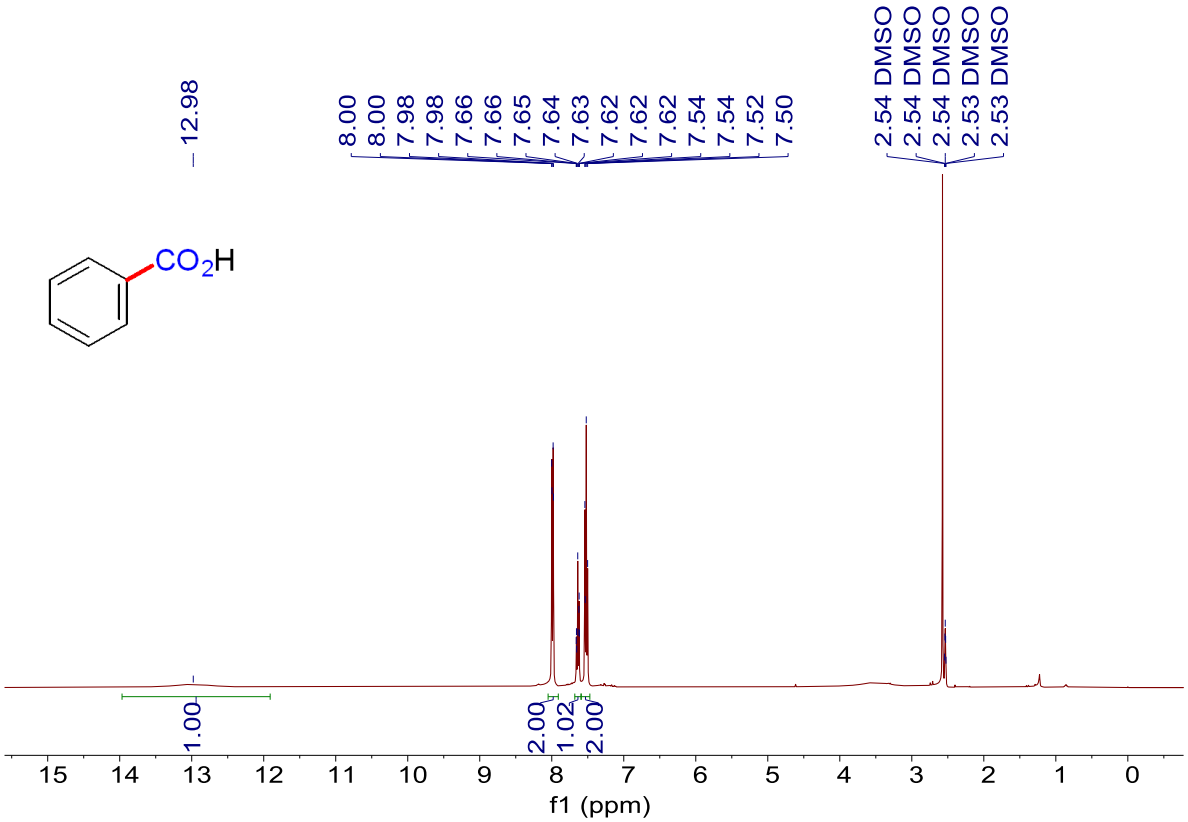

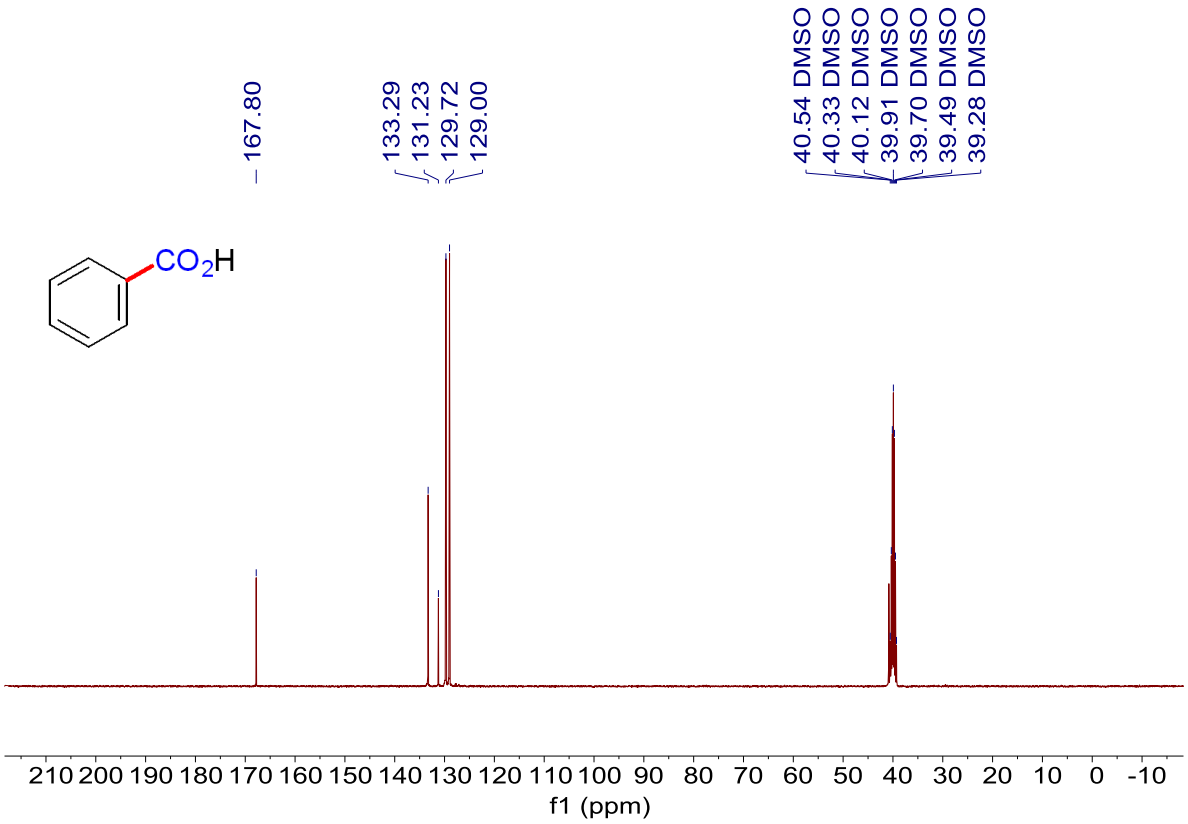

^{1}H NMR and ^{13}C NMR of **19**

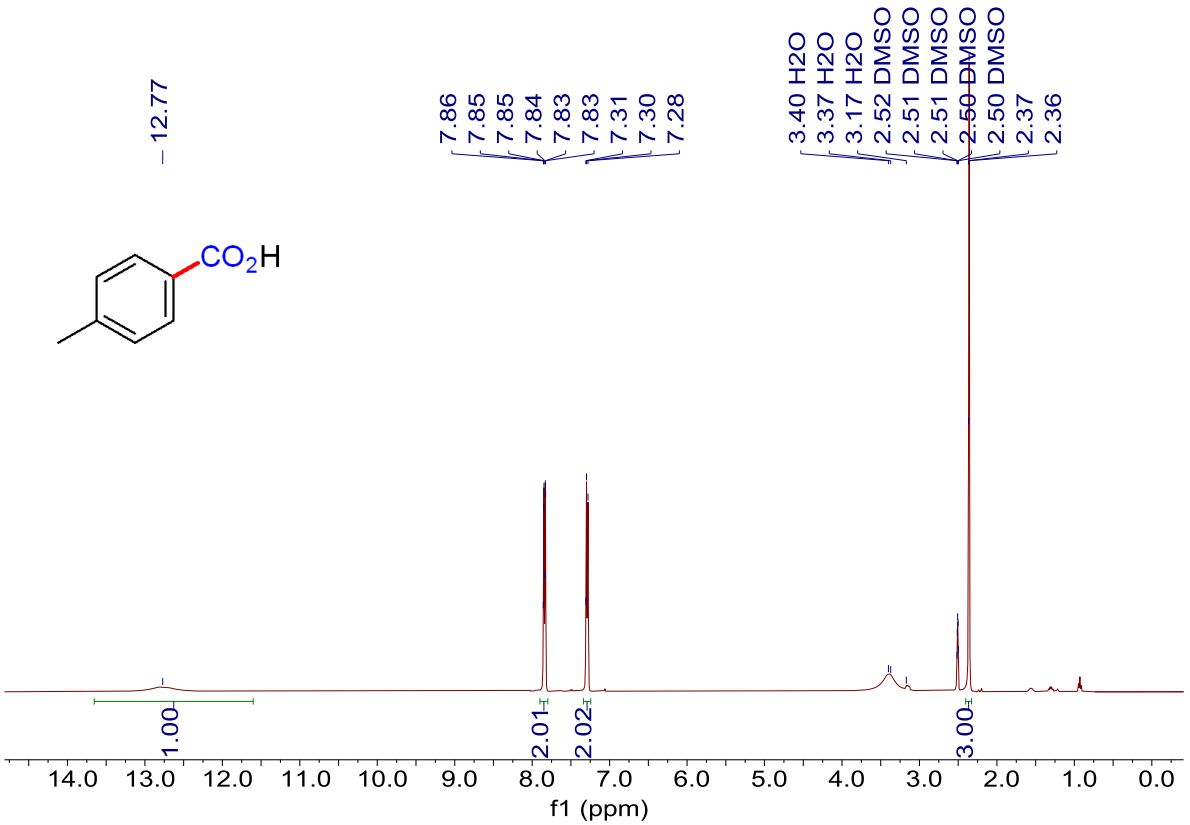

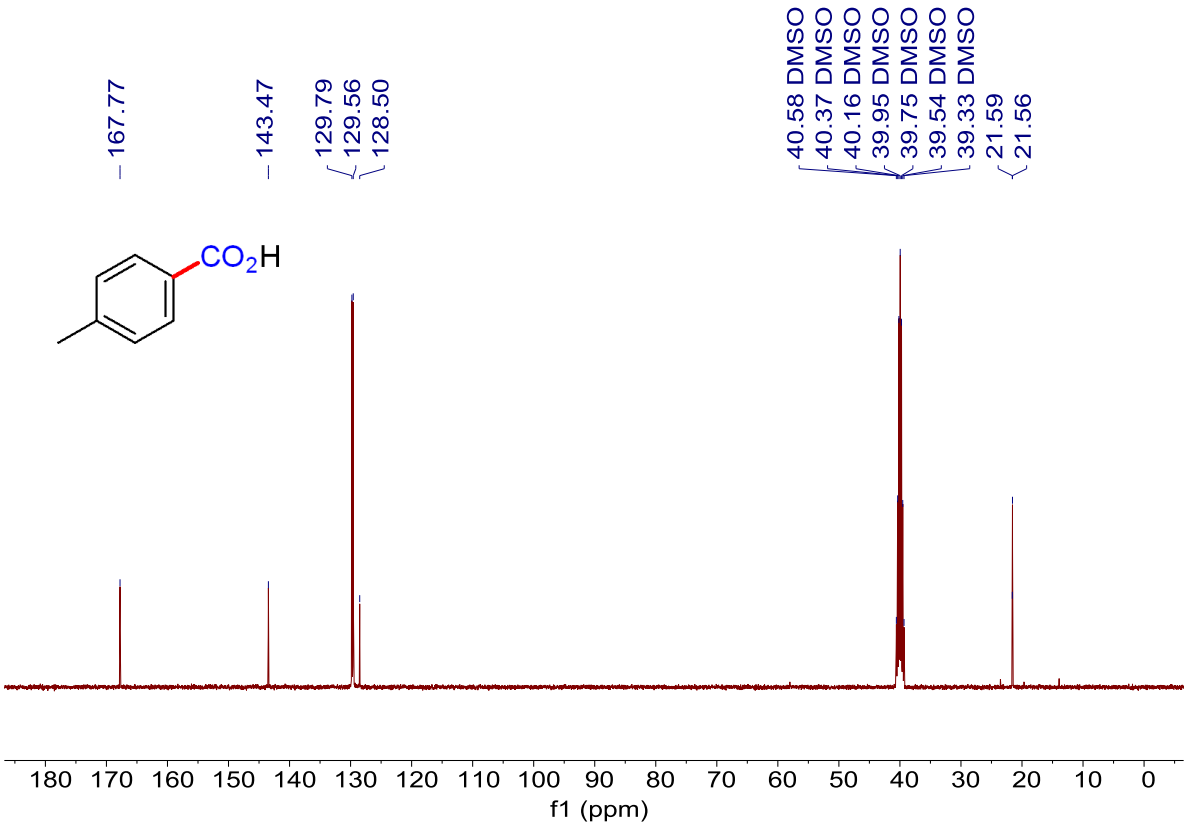

^{1}H NMR and ^{13}C NMR of **20**

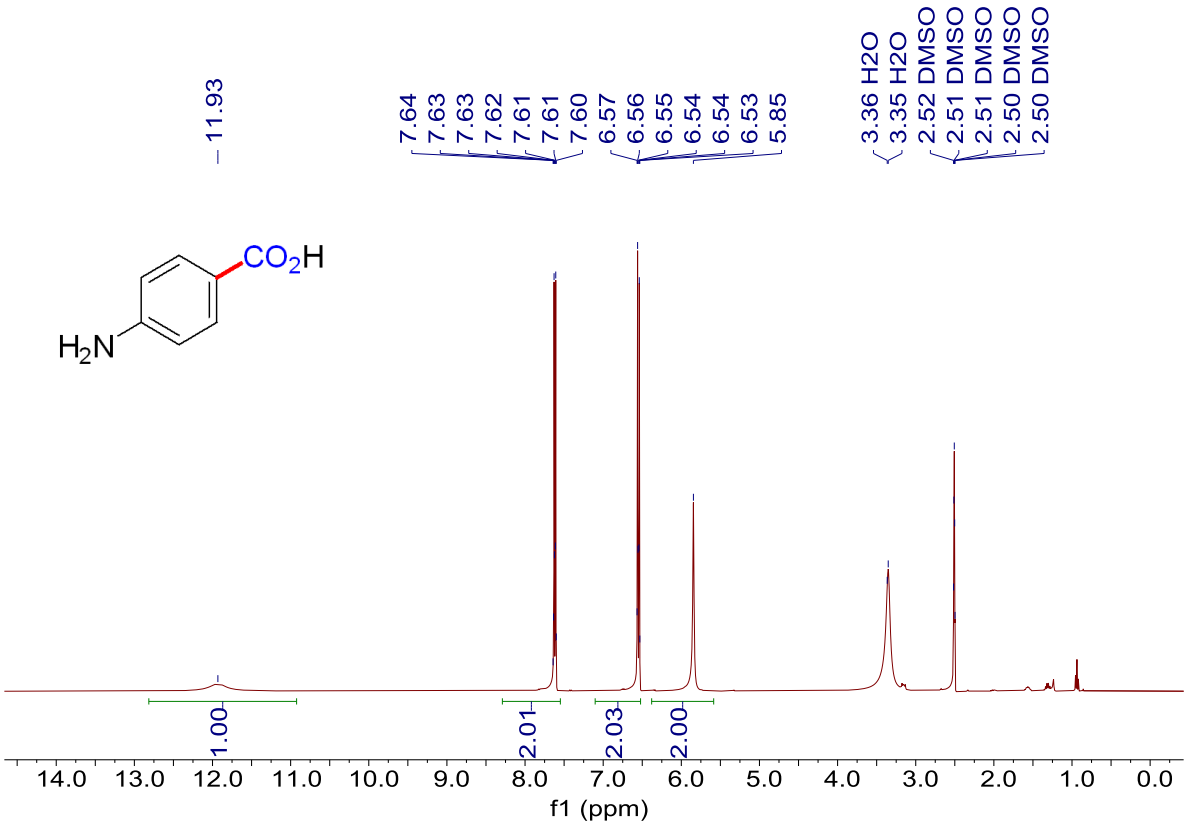

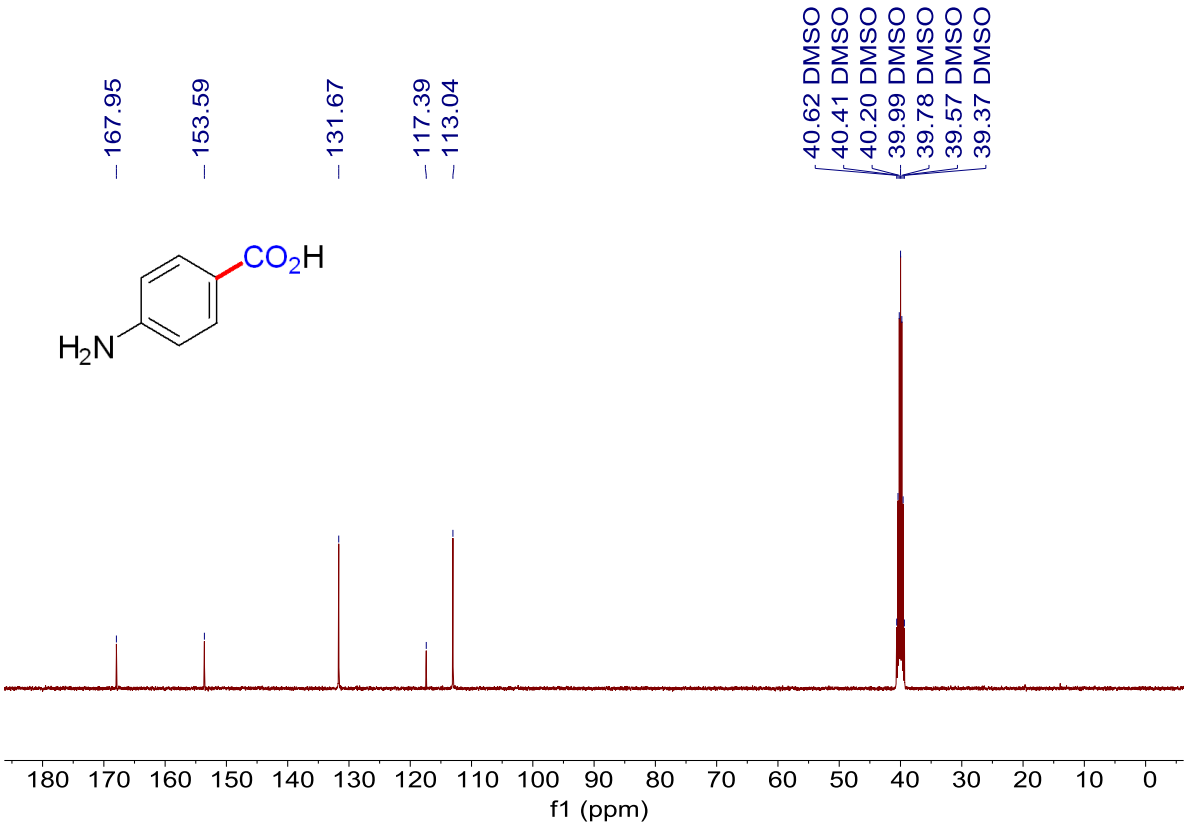

^{1}H NMR and ^{13}C NMR of **21**

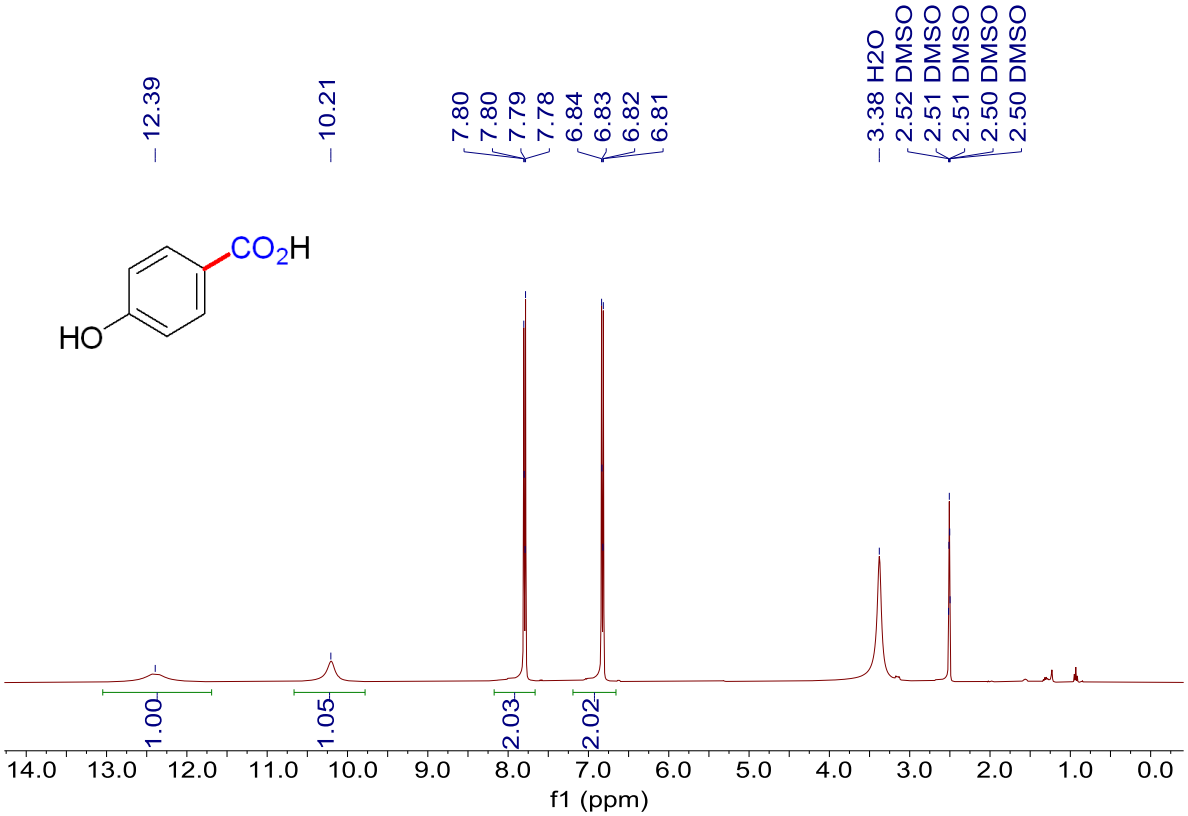

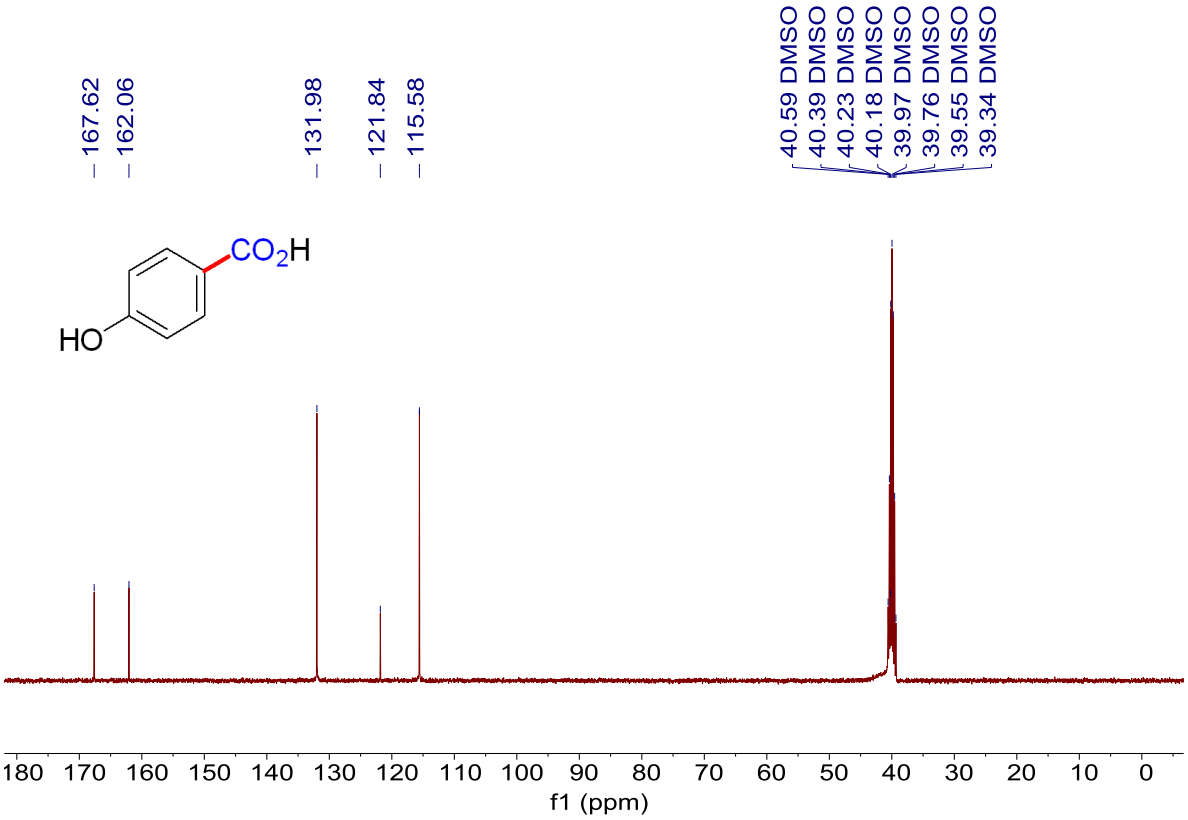

^{1}H NMR and ^{13}C NMR of **22**

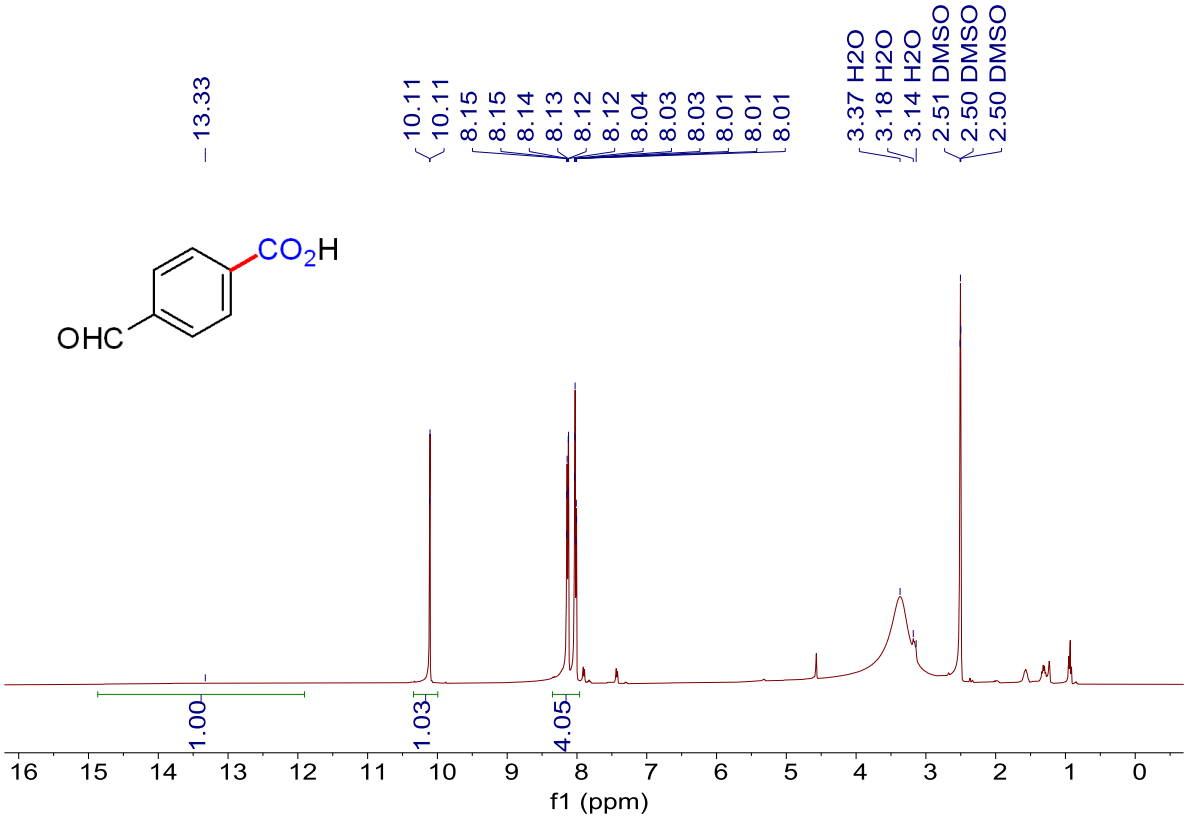

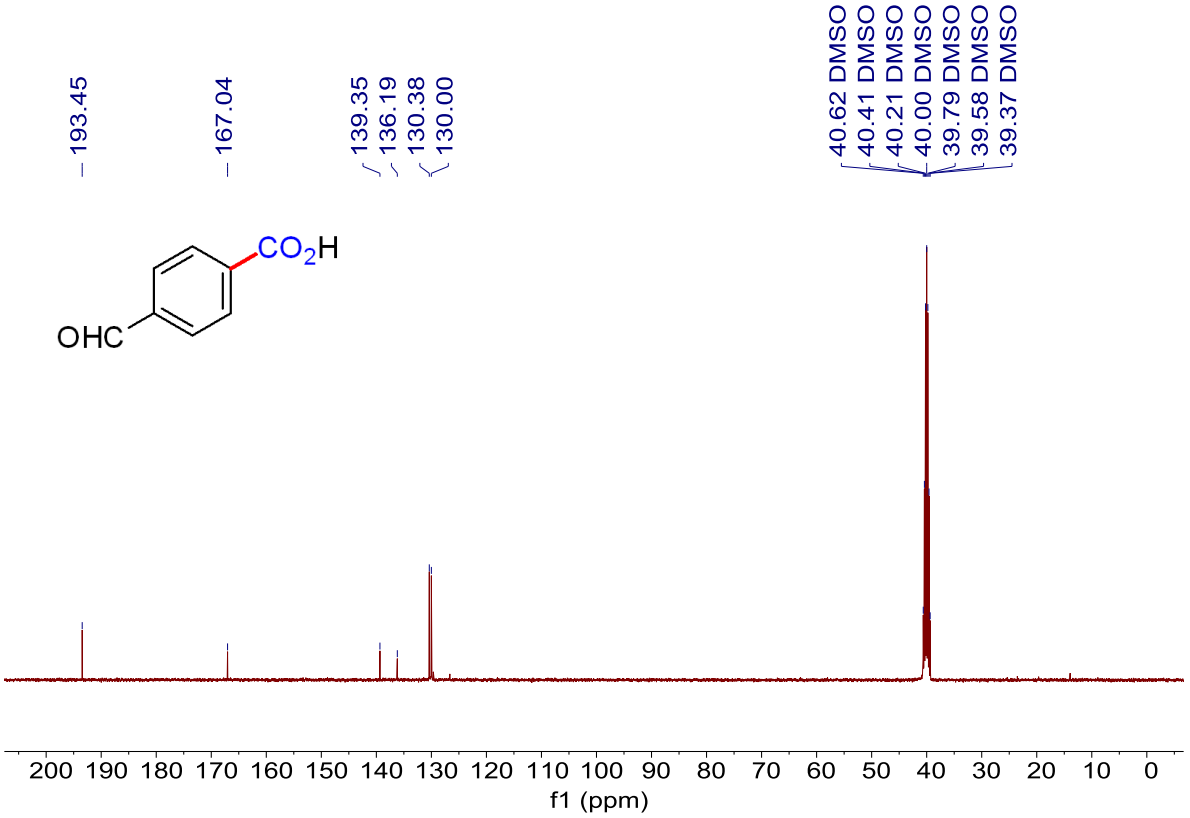

^{1}H NMR and ^{13}C NMR of **23**

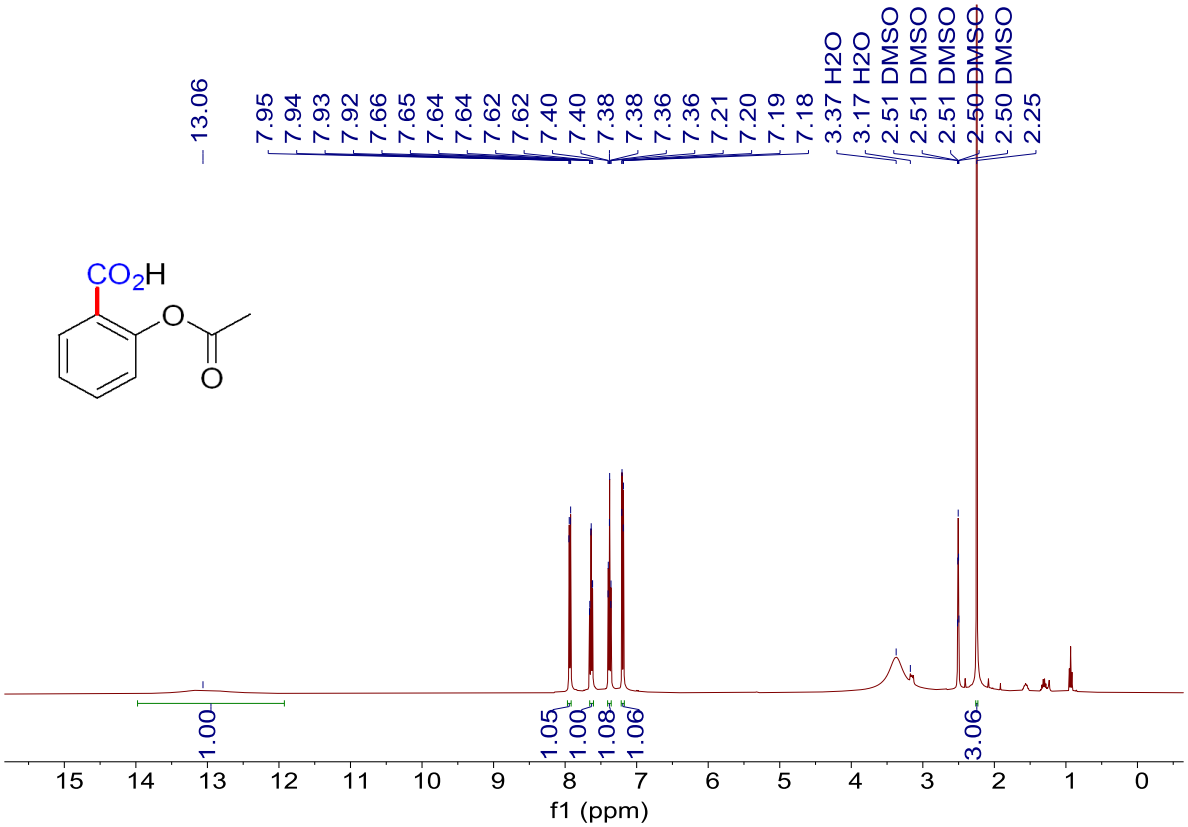

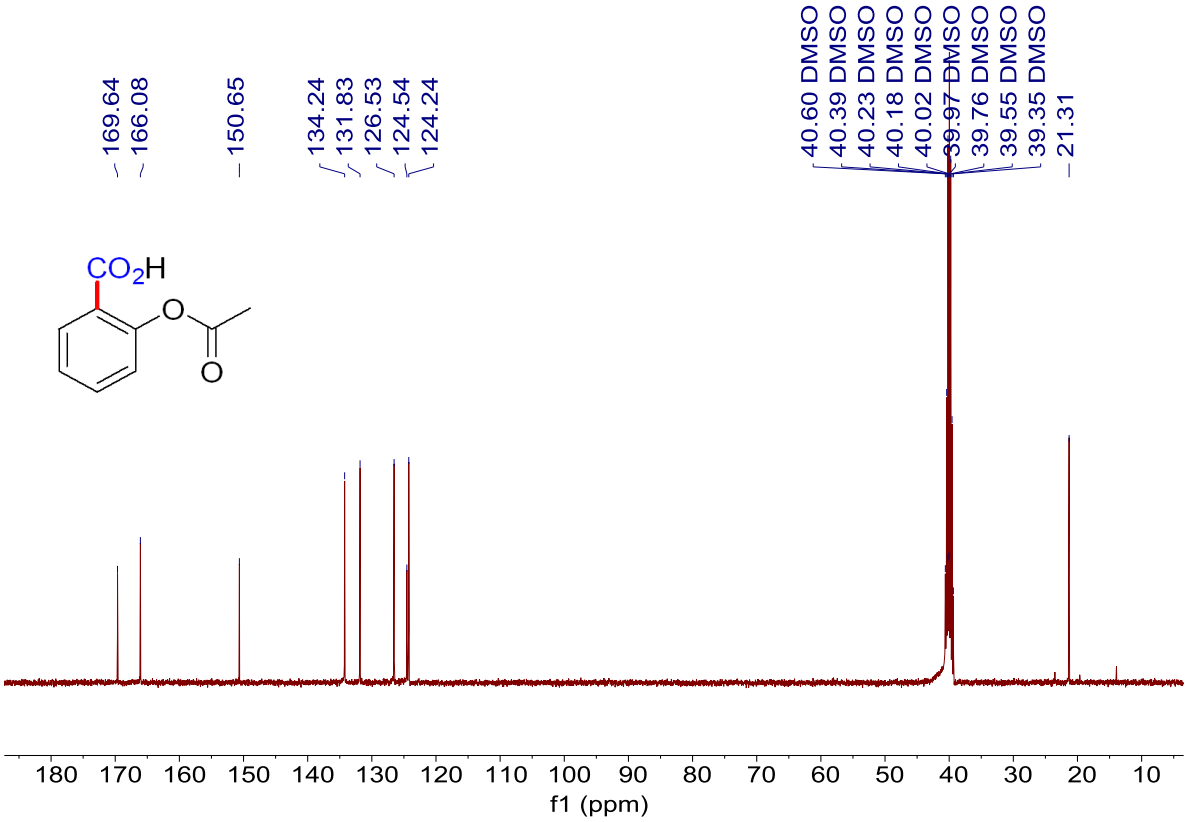

^{1}H NMR and ^{13}C NMR of **24**

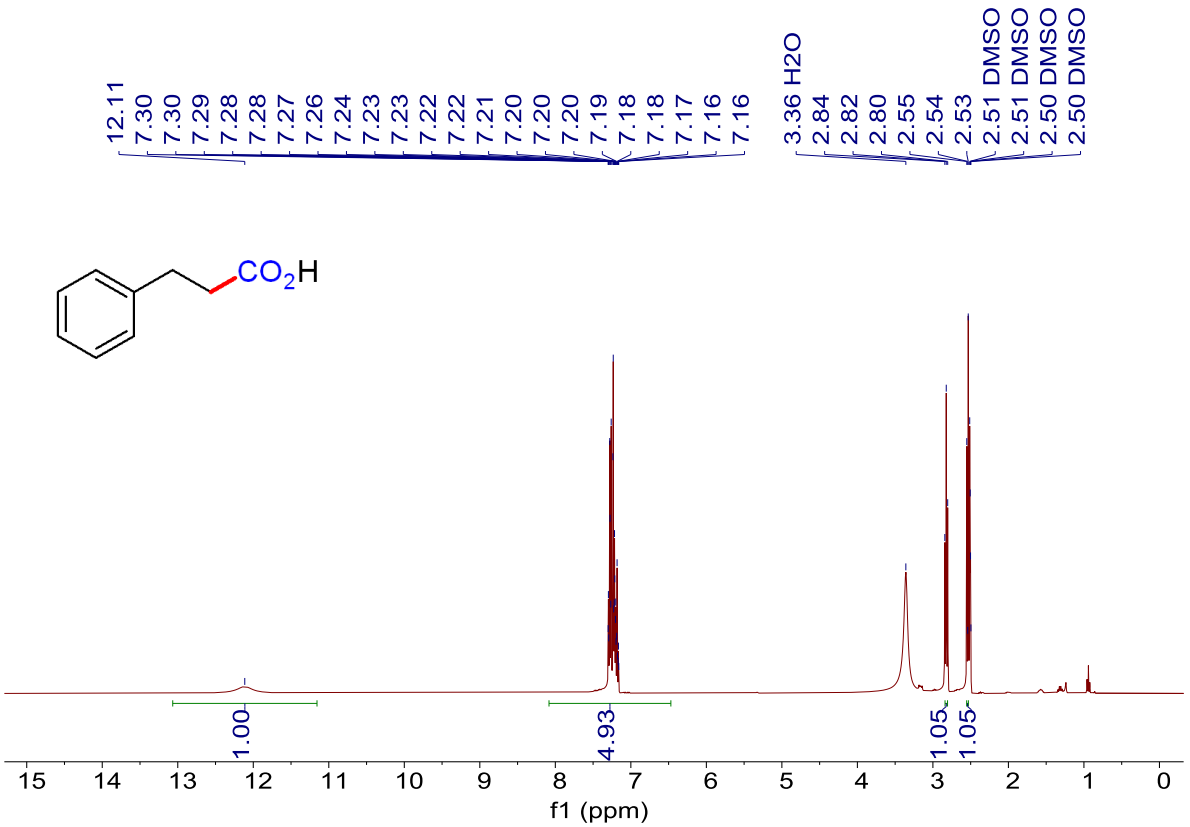

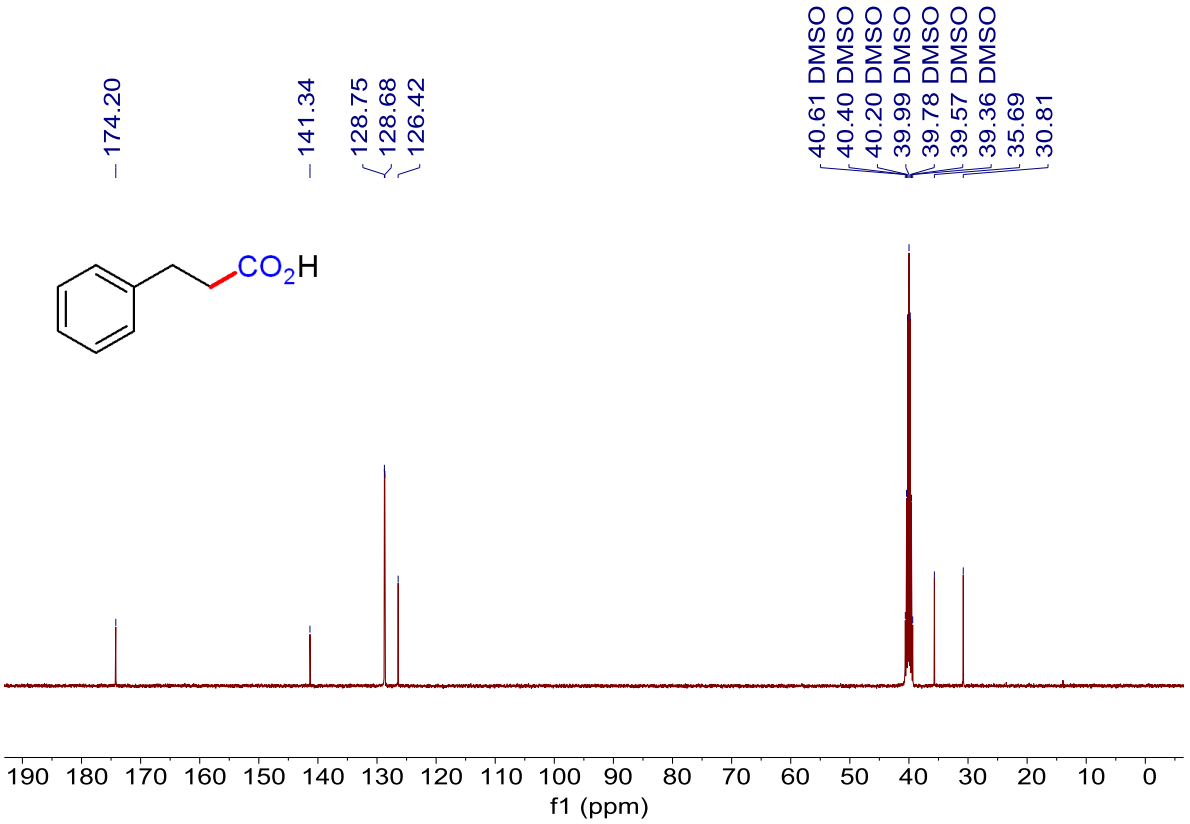

^{1}H NMR and ^{13}C NMR of **25**

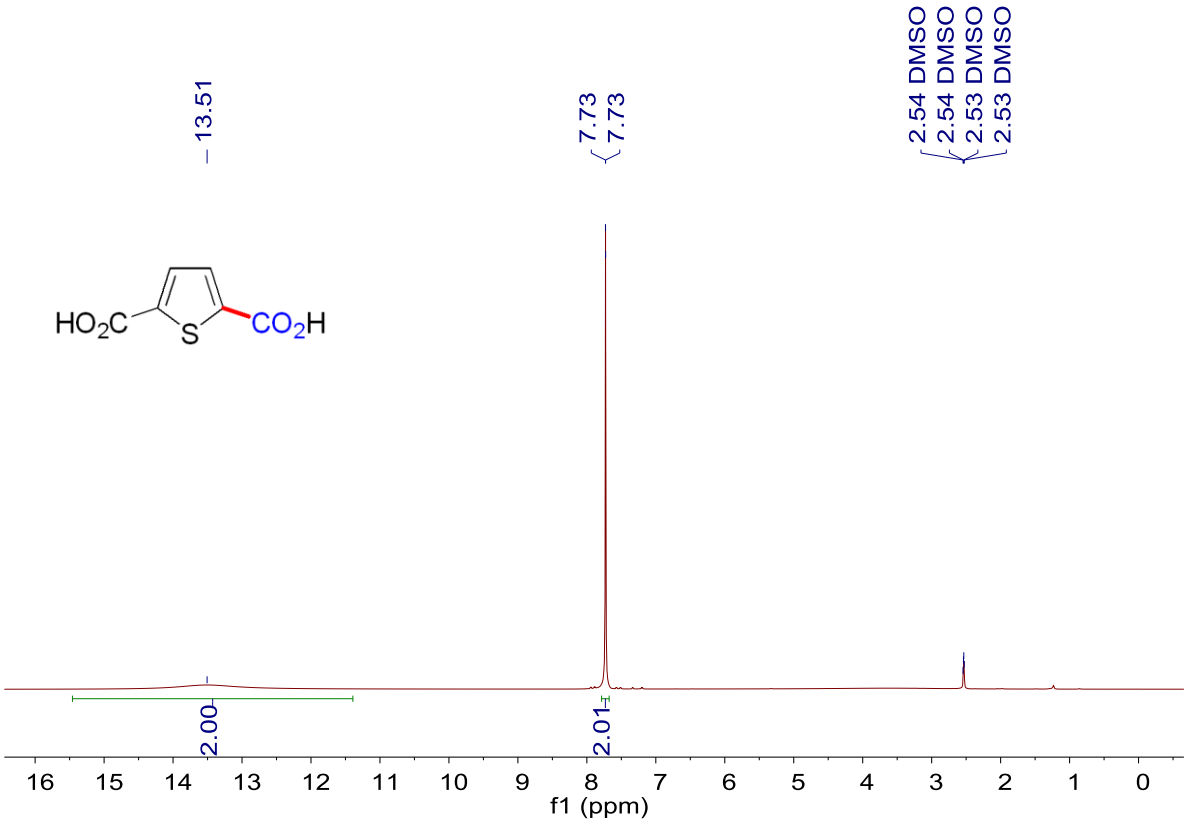

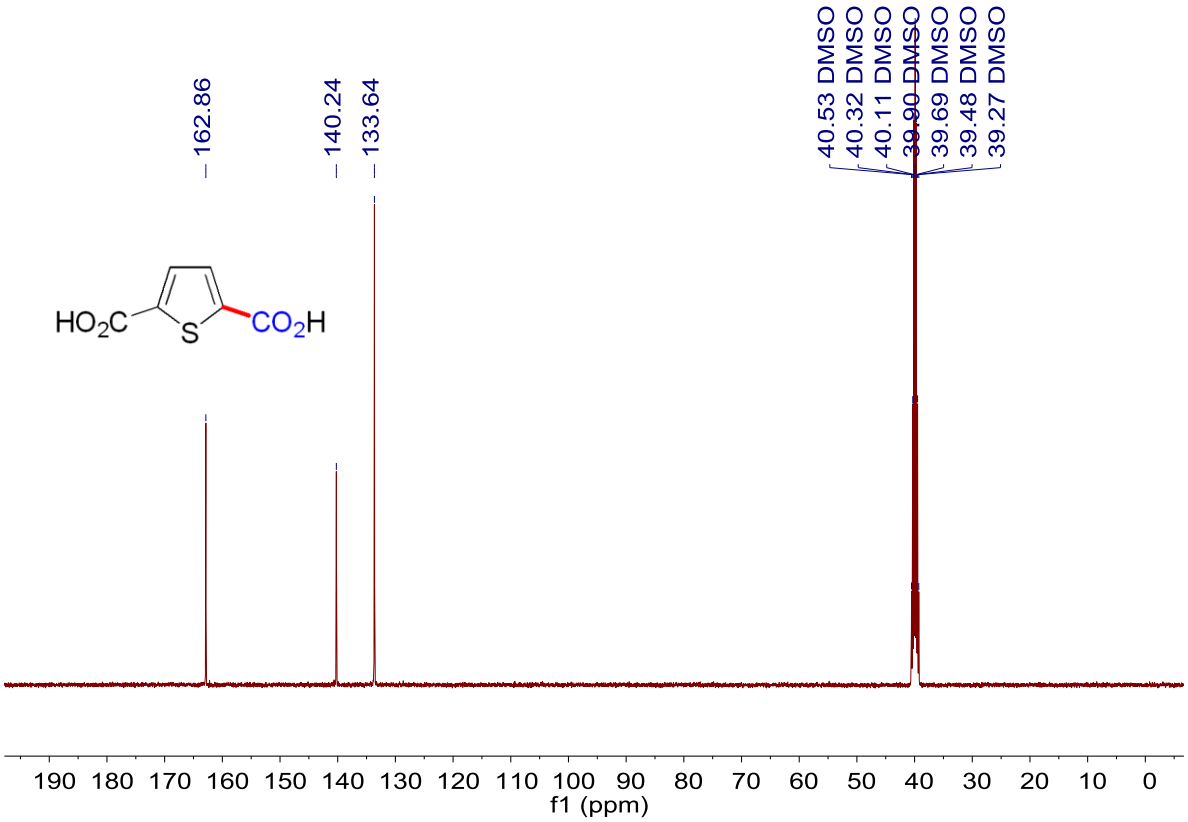

References

1 Wang Y, Tang S, Yang G, Wang S, Ma D, Qiu Y. *Angew Chem Int Ed*, 2022, 61: e202207746.

2 Zhao B, Pan Z, Pan J, Deng H, Bu X, Ma M, Xue F. *Green Chem*, 2023, 25: 3095-3102.

3 Liao LL, Wang ZH, Cao KG, Sun GQ, Zhang W, Ran CK, Li Y, Chen L, Cao GM, Yu DG. *J Am Chem Soc*, 2022, 144: 2062-2068.

4 Gaussian 16, Revision C.01, M. J. Frisch, G. W. Trucks, H. B. Schlegel, G. E. Scuseria, M. A. Robb, J. R. Cheeseman, G. Scalmani, V. Barone, G. A. Petersson, H. Nakatsuji, X. Li, M. Caricato, A. V. Marenich, J. Bloino, B. G. Janesko, R. Gomperts, B. Mennucci, H. P. Hratchian, J. V. Ortiz, A. F. Izmaylov, J. L. Sonnenberg, D. Williams-Young, F. Ding, F. Lipparini, F. Egidi, J. Goings, B. Peng, A. Petrone, T. Henderson, D. Ranasinghe, V. G. Zakrzewski, J. Gao, N. Rega, G. Zheng, W. Liang, M. Hada, M. Ehara, K. Toyota, R. Fukuda, J. Hasegawa, M. Ishida, T. Nakajima, Y. Honda, O. Kitao, H. Nakai, T. Vreven, K. Throssell, J. A. Montgomery, Jr., J. E. Peralta, F. Ogliaro, M. J. Bearpark, J. J. Heyd, E. N. Brothers, K. N. Kudin, V. N. Staroverov, T. A. Keith, R. Kobayashi, J. Normand, K. Raghavachari, A. P. Rendell, J. C. Burant, S. S. Iyengar, J. Tomasi, M. Cossi, J. M. Millam, M. Klene, C. Adamo, R. Cammi, J. W. Ochterski, R. L. Martin, K. Morokuma, O. Farkas, J. B. Foresman, D. J. Fox, Gaussian, Inc., Wallingford CT, 2016.

5 Bajdich M, García-Mota M, Vojvodic A, Nørskov J K, Bell A T. *J Am Chem Soc*, 2013, 135: 13521-13530.

6 Luo X, Wu B, Li J, Wang Y, Tang X, Li C, Shao M, Wei Z. *J Am Chem Soc*, 2023, 145: 20665-20671.

7 Lu T, Chen F. *J Comput Chem*, 2012, 33: 580-592.